Mechanisms of Osmotically-Induced T-tubule Remodeling in Mouse Cardiomyocytes

by

Keita Uchida

A dissertation submitted in partial fulfillment
of the requirements for the degree of
Doctor of Philosophy
(Molecular and Integrative Physiology)
in the University of Michigan
2018

Doctoral Committee:

Associate Professor Anatoli N. Lopatin, Chair
Professor Héctor H. Valdivia, University of Wisconsin-Madison, Co-chair
Professor Daniel E. Michele
Professor Mark W. Russell

Keita Uchida

kuchida@umich.edu

ORCID ID: 0000-0001-8458-9796

ACKNOWLEDGEMENTS

There are countless people to thank without whom the successful completion of this thesis work would not have been possible. First and foremost, I would like to thank my mentors Hector Valdivia and Anatoli Lopatin. Hector is a consummate gentleman who shows limitless generosity toward his mentees. I cannot thank him enough for introducing me to amazing new ideas and people who have broadened my world. Anatoli has been there for me from day one, personally assisting me with the technical work, and this dissertation work would not have been possible without his excellent hands-on teaching. Anatoli also performed the computational work in Chapter 2. Anatoli has always held my written and experimental work to the highest standards and his unattainably lofty expectations of me have driven me to become a better scientist. Both men epitomize integrity in science and are role models to me.

Next, I would not be here if not for Scott Pletcher and Lori Isom recruiting me to MIP and PIBS, respectively. PIBS provided an incredibly supportive environment to transition into graduate school and allowed me to meet a close-knit group of supportive friends (PIBS and friends!) who have drawn me out of the lab over the past five years. In MIP, the leadership of Bishr Omary (and now Santiago Schnell) made the department feel like home and created a welcoming environment that remains receptive of our exceedingly biophysical work. Of course, the department would not function without the

tireless work of the MIP administrators, particularly Michele Boggs who has always helped me with any problem without hesitation. Finally, I would like to thank Sue Moenter for gently pushing me to take active leadership roles within the department. Thank you all for creating such a fantastic training environment!

Next, I would like to thank Dan Beard, Santiago Schnell, Brian Carlson, Malcolm Low and other members of the Systems and Integrative Biology training grant for funding me for two years and for believing that their trainees can master differential equations, code in Matlab, and decipher mathematical modeling papers. This training has undoubtedly reduced the anxiety I felt when applying mathematical equations to my work and has opened an entirely new approach to research.

I would like to thank my committee members, Dan Michele and Mark Russell, for their helpful scientific advice and for presenting alternative viewpoints while we try to put our work into context. Also, thank you for occasionally reining in Anatoli's expectations.

Last but not least, I would like to thank all of the supportive friends and family, including my fellow lab members, whose enthusiasm and encouragement have helped me achieve my scientific endeavors. I would like to thank the Valdivia lab for welcoming me into their group and always providing insightful comments from the other side of campus (and dyad). Also, I would like to thank the past and present members of the Lopatin lab, in particular Ian Moench, Greta Tamkus, and Azadeh Nikouee who contributed to the work presented in Chapters 3 and 4. Science is undeniably difficult to tackle alone and none of this would have been possible without everyone's contribution.

TABLE OF CONTENTS

ACKNOWLEDGEMENTS ii

LIST OF TABLES vi

LIST OF FIGURES vii

ABSTRACT ix

Chapter 1 Introduction 1

1.1 Form follows function: Overview of excitation-contraction coupling in cardiomyocytes 1

1.2 T-tubular structure 3

1.3 Alterations in t-tubule structure during pathophysiological conditions 6

1.4 Study of t-tubules in *vitro* 13

1.5 Scope and aims of this dissertation 18

Chapter 2 Diffusional and electrical properties of t-tubules are governed by their constrictions and dilations 21

2.1 Acknowledgements 21

2.2 Abstract 21

2.3 Introduction 22

2.4 Materials and Methods 25

2.5 Results 29

2.6 Discussion 40

2.7 Supporting Material 49

Chapter 3 T-tubule constrictions promote t-tubule sealing 77
3.1 Acknowledgements 77
3.2 Introduction 77
3.3 Materials and methods 79
3.4 Results 79
3.5 Discussion 86
Chapter 4 Small membrane permeable molecules protect against osmotically induced sealing of t-tubules in mouse ventricular myocytes 100
4.1 Acknowledgements 100
4.2 Abstract 100
4.3 Introduction 101
4.4 Materials and Methods 103
4.5 Results 107
4.6 Discussion 115
Chapter 5 Conclusions, ongoing projects, and future directions 129
5.1 Summary of key findings 129
5.2 Mechanisms of detubulation 130
5.3 T-tubular structural stability 136
5.4 Physiological Implications 141
BIBLIOGRAPHY 147

LIST OF TABLES

Table 2.1. Specific gravity and viscosity measurements 56

LIST OF FIGURES

Figure 2.1 Schematics of the dextran diffusion assay 57
Figure 2.2 Properties of time-varying fluorescence observed in cardiomyocytes 58
Figure 2.3 Relative amplitude of slow time-dependent component 59
Figure 2.4 Effects of detubulation on the amplitude of slow component of dextran diffusion 60
Figure 2.5 Distribution of dextran diffusion time constants in normal cells 61
Figure 2.6 Cell swelling restricts t-tubule diffusion 62
Figure 2.7 Computer modeling of radial (2D) diffusion of dextran. 63
Figure 2.8 Computer modeling of 3D diffusion of dextran. 64
Figure 2.9 Effects of dilations and constrictions of TTs on the kinetics of dextran diffusion. 65
Figure 2.10 Efficient flow of bath solution around the cell is critical for correct measurement of t-tubular diffusion. 66
Figure 2.11 Effects of the movement of the dye application pipette on dextran fluorescence. 67
Figure 2.12 Experimental setup for the measurements of spot spread function 68
Figure 2.13 Effect of position of recording spot on dextran fluorescence 69
Figure 2.14 Dependence of t-tubular time constants on washout flow rate. 70
Figure 2.15 Dependence of t-tubular time constants on position of recording spot. 71
Figure 2.16 Effects of Neuraminidase A 72
Figure 2.17 Effects of mild hyposmotic stress on dextran diffusion 73
Figure 2.18 Computer modeling of radial (2D) inward-going diffusion of dextran 74
Figure 2.19 Computer modeling of outward-going diffusion of dextran and effects of spot recording. 75
Figure 2.20 Effects of local application of dextran. 76

Figure 3.1 Hyperosmotic stress is sufficient to seal t-tubules 94
Figure 3.2 Threshold for hyposmotic detubulation 95
Figure 3.3 Hyposmotic stress dose-dependently restricts diffusion in t-tubule lumen ... 96
Figure 3.4 Magnitude of dextran trapping is not determined by magnitude of osmotic shock 97
Figure 3.5 The magnitude of dextran trapping strongly correlates with the preceding t-tubular constriction 98
Figure 3.6 WGA treatment leads to slow t-tubular diffusion and augments the amount of t-tubular sealing following hyposmotic stress 99
Figure 4.1 Effects of post-shock acute application of DMSO on t-tubular sealing. 122
Figure 4.2 Effect of timing of DMSO application on dextran trapping. 123
Figure 4.3 Electrophysiological effects of DMSO application. 124
Figure 4.4 Effects of DMSO on myocyte dimensions. 125
Figure 4.5 Protective action of DMSO occurs exclusively upon removal of osmotic stress 126
Figure 4.6 SMPM reduce dextran trapping when present upon washout of hyposmotic 0.6 Na solution. 127
Figure 4.7 Effects of high concentration of DMSO and formamide on hyposmotically-induced sealing of t-tubules 128

ABSTRACT

T-tubules are invaginations of the surface sarcolemma that form a complex, interconnected network and are distinctive structures of adult ventricular cardiomyocytes. T-tubules are intimately linked to the intracellular sarcoplasmic reticulum to form structures called dyads, which house proteins critical for excitation-contraction coupling. Disruption of the t-tubule network, particularly t-tubule loss, causes contractile dysfunction and has been extensively characterized in various cardiovascular diseases. Multiple studies have correlated mechanical stress associated with cardiovascular diseases with t-tubule remodeling but the underlying causal mechanism remains unknown.

The overall goal of this thesis is to study the function of t-tubules and the factors that contribute to their remodeling. This thesis tests the central hypothesis that sub-microscopic t-tubular structures (constrictions and dilations) regulate the diffusional properties and stability of t-tubules in response to osmotic stress.

Generally, t-tubules have been modeled as cylindrical tubes and although constrictions and dilations within t-tubules have been well documented, the contributions of these sub-microscopic structures to cardiac physiology has been largely unrecognized. A novel fluorescence based assay was developed to characterize the diffusional properties of cardiac t-tubules, which depend on the fine t-tubular structure. Quantitative measurements of dextran diffusion in t-tubules combined with computational modeling revealed that t-tubular constrictions and dilations make significant contributions to the

apparent diffusion coefficient of molecules within the t-tubular lumen and to the electrical properties of t-tubules.

Subsequent experiments demonstrated that osmotic detubulation is a threshold phenomenon and provided quantitative insights into the mechanism of detubulation. A series of conditions were developed to induce t-tubular constrictions through osmotic stress and chemical modifications. Next, I tested the hypothesis that t-tubule constrictions predispose t-tubules to seal following osmotic stress. A strong correlation between the diffusional accessibility of t-tubules and the magnitude of t-tubule sealing following osmotic stress was established, suggesting that constrictions and dilations strongly modulate the stability of t-tubules.

Finally, we found that the concentration gradient of small membrane permeable molecules (SMPMs) across the membrane could strongly affect the susceptibility of t-tubules to detubulation. We proposed that the “bilayer-couple hypothesis”, which describes the formation of membrane curvature due to membrane area asymmetry across the membrane, can effectively explain the modulatory roles of SMPMs. These results support the notion that the sub-microscopic structure of t-tubules play a key role in determining their stability in response to osmotic stresses.

Overall, we have identified a number of critical factors that regulate t-tubular stability and determine the response of t-tubules to stress. The results presented in this dissertation demonstrate the functional and structural significance of sub-microscopic t-tubular structures. Furthermore, the contribution of sub-microscopic t-tubular structures must be taken into account when developing future models of t-tubular remodeling.

CHAPTER 1 INTRODUCTION

1.1 Form follows function: Overview of excitation-contraction coupling in cardiomyocytes

The human heart beats billions of times throughout a typical lifespan. This robust, synchronized activity is achieved through the concerted effort of millions of cardiomyocytes that respond to a propagating action potential. Cardiomyocytes have a complex structural organization to ensure that the cell can contract forcefully in response to the action potential. Adult cardiomyocytes are large cells, roughly 100 μm long and 20 μm in diameter, and are densely packed with repeating arrays of myofilaments— the contractile machinery of myocytes— and mitochondria that provide energy for the contraction. A network of membrane structures exists within the cardiomyocyte to ensure the synchronous contraction of the myofilaments throughout the cell. At the z-line, the surface membrane invaginates inward toward the center of the cell and forms long narrow tunnels called the transverse tubules (t-tubules). The t-tubule lumen forms a physical connection with the extracellular solution and allows for the diffusion of small molecules and the propagation of the action potential into the interior of the cell. Longitudinally or obliquely oriented tubules may interconnect with t-tubules to form a complex network. In this dissertation, all tubules will be referred to as t-tubules regardless of the orientation for simplicity. Within the cell, regions of the t-tubule membrane closely appose the sarcoplasmic reticulum (SR) membrane and form a specialized structure called dyad. The

SR forms a mesh-like intracellular compartment that surrounds the myofilaments and stores the Ca^{2+} necessary for contraction. This structural organization allows for rapid and synchronous transduction of electrical signals in the t-tubular membrane into mechanical contraction of the myofilaments via a process known as excitation-contraction coupling (ECC).

ECC is an expansive field of study and the short summary here understates the intricacy of the physiological processes that occur with each heart beat (for a more detailed description, see (Bers, 2001)). Briefly, an action potential (AP) propagates down the t-tubule membrane into the cell to initiate ECC. Depolarization of the t-tubular membrane opens L-type Ca^{2+} channels (LTCC) that are concentrated at the dyad on the t-tubular membrane. Opening of the LTCC causes a small amount of Ca^{2+} to enter the cell and rapidly increases the local dyadic Ca^{2+} concentration. Binding of the dyadic Ca^{2+} to the ryanodine receptors (RyR2) on the SR membrane opens RyR2, which release a large amount of stored SR Ca^{2+}. This process called Ca^{2+}-induced Ca^{2+} release rapidly and synchronously raises the global intracellular $[Ca^{2+}]$ ($[Ca^{2+}]_i$). This cellular Ca^{2+} transient activates myofilaments and allows the myocyte to contract. The following decline in $[Ca^{2+}]_i$ is primarily due to re-sequestration of Ca^{2+} through the SR Ca^{2+} ATPase (SERCA) and partly through the extrusion of Ca^{2+} out of the cell through the Na^+/Ca^{2+} exchanger (NCX), thereby allowing the myocyte to relax.

Furthermore, signaling pathways that modulate ECC are also specifically localized within t-tubule membranes. The receptors that initiate the biochemical signaling pathways that augment ECC in response to adrenergic stimulation (Nikolaev et al., 2010), reactive oxygen species or nitric oxide (Jian et al., 2014; Prosser et al., 2011) and other signaling

pathways including the angiotensin II receptor (Gao et al., 2014) and endothelin I receptor (Robu et al., 2003) are preferentially localized within the t-tubule network.

1.2 T-tubular structure

Much of what we know about the organization of membrane domains and intracellular organelles in striated muscle is derived from the works of many electron microscopists from the second half of the 20th century. After multiple iterations from many electron microscopists (Peachey, 1965; Porter and Palade, 1957), Fawcett and McNutt elegantly summarized the information gleaned from the 2-D images into an abstracted drawing depicting the important structures present within a cardiac myocytes (Fawcett and McNutt, 1969). This drawing shows the cross section of the myocyte that is packed full of myofilaments with mitochondria sandwiched between them. Large, nearly cylindrical membrane tunnels representing t-tubules extend into the cell at the z-lines and are connected to a mesh of SR membranes that extends throughout the sarcomere. This image of the cardiomyocyte has since been reproduced and adapted in many forms and has become a standard textbook model to understand cardiomyocyte structure (See (Katz, 2010)). Although the simplified diagrams are excellent tools to explain the link between cardiomyocyte structure and function (Bers, 2001; Fawcett and McNutt, 1969), these drawings are oversimplifications of the actual cardiomyocyte structure and lack much of the important quantitative details necessary to fully appreciate t-tubule function. In contrast to the single large t-tubule depicted in these images, a robust network of t-tubules pervades the myocyte to ensure a synchronized contraction.

In humans, t-tubules form spoke-like structures that extend toward the center of the cell (Jayasinghe et al., 2012). In addition to the predominant transversally oriented

tubules, there are some interconnecting tubules but these are relatively sparse (~0.17 branch points per square μm). T-tubules are present throughout the entire length of the cell and remarkably, ~ 55% of the total sarcolemmal membrane is devoted to forming these structures (Ohler et al., 2009). However, the diameters of individual t-tubules are quite small and therefore, the overall t-tubular luminal volume only accounts for ~8% of the total intracellular volume (Ohler et al., 2009). With this extensive t-tubule network, the majority (~64%) of the intracellular space lies within 250 nm of the extracellular boundary demarcated by the surface or t-tubule membranes (Jayasinghe et al., 2012). Although these data are obtained from a limited number of healthy human donor hearts, they provide quantitative details of human t-tubules.

The structure of t-tubules has been better studied in other species, revealing the significant quantitative differences in t-tubular structure among mammals. Rabbit cardiomyocytes have t-tubules that are organized similar to that of humans. However, rodents (mice and rats) have t-tubules that form noticeably more interconnections with each other (both arcing transversally and longitudinally from z-line to z-line), forming a dense, complex network of t-tubules within the cell. These longitudinal or axial tubules between the z-lines form nearly 40% of the total t-tubule network in rats (Soeller and Cannell, 1999). Most of the branches are short but some can extend over multiple sarcomeres with the average length around 7 μm (Soeller and Cannell, 1999). As a result, rat cardiomyocytes have a ~4-fold increase in the t-tubule density, and correspondingly ~4-fold increase in the number of branch points where t-tubules intersect, compared to human cardiomyocytes (Jayasinghe et al., 2012). This dense network ensures that nearly the entire intracellular space (~94%) lies within 250 nm of the surface or t-tubule

membrane in rats (Jayasinghe et al., 2012). This extensive t-tubular network represents roughly 30-65% of the total surface membrane area (Pasek et al., 2008) but only occupies ~1-4% of the total cellular volume (Kong et al., 2017; Soeller and Cannell, 1999). This discrepancy in the t-tubular luminal volume between rats and humans is largely due to the difference in the diameters of individual t-tubules. Rats have significantly narrower t-tubules.

The structure of individual t-tubules also shows considerable species variation. T-tubules are generally narrow, with average diameter ~350 – 500 nm in humans and in rabbits (Jayasinghe et al., 2012; Kong et al., 2017; Savio-Galimberti et al., 2008), and are considerably narrower in small rodents (~250-300 nm in rats (Jayasinghe et al., 2012) and ~170 nm in mice (Kong et al., 2017)). Comparison of a singular t-tubular "diameter" can be misleading since the size of the t-tubule is heterogeneous along their length. Constrictions and dilations of the t-tubule lumen is a ubiquitous feature of normal t-tubules across multiple species (Kong et al., 2017; Pinali et al., 2013). This is especially evident in rabbit cardiomyocytes where t-tubule diameters can vary 7-fold ranging from ~100 nm to ~700 nm (Kong et al., 2017). Interestingly, there appears to be some regularity to the locations of narrower t-tubular segments suggesting that the heterogeneity in t-tubule diameter is not entirely due to random variability. Narrowing of t-tubules was found to be located every ~1.9 μm along the length of the t-tubule (Savio-Galimberti et al., 2008). At these constrictions, the cross-sectional area decreased by ~2-fold demonstrating a significant bottleneck within the t-tubule. Due to the inherently small size of mouse t-tubules, even normal t-tubules cannot be easily resolved in live mouse cardiomyocytes by standard light microscopy techniques, making the observation of t-tubular constrictions

a challenge. However, dilations have been observed at the intersections of transverse and axial tubule segments of fixed mouse ventricular myocytes (Forbes et al., 1984). Recent work has confirmed this observation using both super-resolution microscopy and electron tomography (Wong et al., 2013). Currently, the exact location, composition, and function of these t-tubular constrictions and dilations are unknown.

1.3 Alterations in t-tubule structure during pathophysiological conditions

Beginning in the early 2000s, it became increasingly clear that t-tubule structure is dramatically altered in various disease states. Physiological cardiomyocyte t-tubule loss was first observed, to the best of my knowledge, in a canine model of tachycardia-induced dilated cardiomyopathy (He et al, 2001). Since then, a flood of publications have reported on the state of the t-tubular network in a variety of disease states. These are well summarized in multiple excellent reviews (See (Guo et al., 2013; Louch et al., 2010)) and tables (see online table IV from Wagner et al. (Wagner et al., 2012)).

There is considerable variability in the degree and magnitude of t-tubule remodeling depending on the model used. It remains unclear whether t-tubule remodeling is a consequence or contributor to the progression to heart failure and evidence for either case can be found in the literature (Louch et al., 2006; Wei et al., 2010). T-tubular remodeling is highly context dependent and likely has a complex reciprocal cause and effect relationship with disease progression. Overall, it is generally accepted that there is reorganization of t-tubule networks associated with a moderate degree of t-tubule loss during pathophysiological conditions in various heart failure models. Additionally, with the recent use of higher resolution 3D imaging techniques, it is becoming increasingly clear

that t-tubules dilate as cardiovascular disease progresses (Seidel et al., 2017b; Wagner et al., 2012).

In humans, the appearance of dilated or vacuolated t-tubules has been consistently observed during cardiovascular diseases (Crossman et al., 2017; Kaprielian et al., 2000; Kostin et al., 1998; Louch et al., 2004; Maron et al., 1975; Schaper et al., 1991; Seidel et al., 2017a). The sizes of these dilated t-tubules are difficult to characterize due to their varying geometries (Crossman et al. report an average diameter of ~436 nm although Maron et al. report t-tubule vacuoles that are up to 2.5 μm in diameter). Notably, with the improvement in 3-dimensional confocal imaging, large complex sheet-like t-tubule structures have been observed in human cardiomyocytes (Seidel et al., 2017a). These structures can extend longitudinally and radially inward, which may explain the appearance of longitudinal t-tubules in 2-dimensional images. The authors note, however, that these t-tubule sheets were observed using conventional confocal imaging and do not have the necessary spatial resolution to distinguish sheets from a network of densely interconnected tubules. Recent work in a porcine model of myocardial infarction revealed that t-tubules form dilated and highly branched structures when viewed using serial SEM images (Pinali et al., 2017). These structures may potentially appear as sheets when processed (especially after applying dilation/erosion functions) and higher resolution imaging is necessary to fully elucidate the structure of these dilated t-tubules.

The general trend of t-tubule loss that is observed in model organisms is questionable in human myocytes. Some groups have reported clear t-tubular loss and a decrease in the t-tubule density in isolated cardiomyocytes and tissue sections from explanted failing hearts with diverse etiologies (ischemic, idiopathic, dilated, and

hypertrophic cardiomyopathies) (Kostin et al., 1998; Lyon et al., 2009; Maron et al., 1975; Seidel et al., 2017a). However, other groups did not observe changes in the t-tubular density within the cardiomyocytes although the organization of t-tubules appears disrupted (Louch et al., 2004; Ohler et al., 2009). There are many possible explanations (for example, limited sample sizes, heterogeneity in disease severity, pharmacological interventions, etc.) in the discrepancy between the multiple human studies. In many cases, it is unclear which region of the explanted heart the cells are isolated from. T-tubule remodeling can display significant regional heterogeneity in the left ventricular myocardium in animal models and it is possible that this may underlie the different reports (See work by Sachse's group on cardiac resynchronization therapy: (Li et al., 2015; Sachse et al., 2012)). Nonetheless, it has been suggested that it is not necessarily the loss of t-tubules that is important but rather the relation of the t-tubule system to the underlying Ca^{2+} release units (Cannell et al., 2006). In nearly all cases, there is a significant increase or a convincing trend towards increased distance between the RyR to the sarcolemmal membrane. This disconnection of the Ca^{2+} release units from the sarcolemma has significant functional consequences.

1.3.2 Functional consequences of t-tubule loss

Even before t-tubule loss was documented in heart failure models, Gomez et al. demonstrated that ECC is disrupted in cardiomyocytes isolated from the failing hearts of hypertensive rats (Gomez, 1997). Simultaneous measurements of the inward $I_{L,Ca}$ and intracellular Ca^{2+} transients revealed that the ability of the calcium influx from the LTCC to elicit Ca^{2+} release from the SR was reduced in these myocytes. At the time, there were hints that t-tubular structural changes may occur in hypertensive hearts and the authors

speculated that the increased distance between the LTCC and RyR2 may underlie this phenomenon. A few years later, Heinzel et al. convincingly demonstrated that the presence of t-tubules determined Ca^{2+} release kinetics (Heinzel et al., 2002). By taking line scans of electrically stimulated Ca^{2+} release before and after membrane staining, the authors showed that locations of delayed calcium release corresponded to regions without t-tubular staining while the regions of rapid Ca^{2+} release were clearly marked by a membrane specific dye Di-8-ANEPPS. More recent work has followed up on this initial study and demonstrated that t-tubule loss in disease states exacerbates the delay in Ca^{2+} release specifically at regions where t-tubules are absent (Heinzel et al., 2008). These RyRs that are not associated with t-tubular membranes have been referred to as “orphans” and their presence reduces the synchrony of Ca^{2+} release throughout the cell and ultimately results in a slower rise in global Ca^{2+} transient (Gomez et al., 2001; Song et al., 2006).

Contractility is inevitably affected by the disturbance in calcium transient. In hypertrophy and heart failure, the T-tubule power index- a parameter that quantifies the organization or regularity of the t-tubule network- correlates with the contractile function of the heart as measured by ejection fraction (Wei et al., 2010). However, a variety of additional factors in diseased states may contribute to the reduced contractility and the direct effect of t-tubule loss on cellular contractility is difficult to assess under pathophysiological conditions. Ferrantini et al. used an *in vitro* method to artificially remove t-tubules through a process called “detubulation” (Ferrantini et al., 2014). Detubulated rat ventricular trabeculae display a dramatic increase in the time to peak of intracellular $[Ca]_i$, reduced the calcium transient amplitude, and significantly reduced force

generation. Importantly, atrial trabeculae, which have ~10-fold sparser t-tubules than ventricular myocardial cells (Smyrnias et al., 2010), did not show significant changes in contractility following a similar detubulating stress, suggesting that the reduction in contractility in this study can be largely attributed to the magnitude of t-tubule loss.

Interestingly, complete t-tubule loss may not be necessary for these functional defects in ECC to manifest in cardiomyocytes. Sacconi et al. performed elegant studies using a custom made random access multiphoton microscope to record optical APs simultaneously from segments of surface and t-tubular membranes. Using this unique system, the authors demonstrate that, in detubulated cardiomyocytes and in cardiomyocytes from failing hearts, t-tubules that are still physically connected to the surface membrane can fail to produce an AP following electrical stimulation (Sacconi et al., 2012). Furthermore, these t-tubules that do not conduct APs are associated with delayed calcium release similar to regions that lack t-tubules (Crocini et al., 2014). The authors speculated that t-tubular “stenosis” or changes in the interconnection of t-tubules (either through increasing the effect t-tubular length or decreasing the space-clamp conditions of the t-tubular network) may underlie the AP propagation failure. These data demonstrate that milder t-tubular remodeling that is observed during pathophysiological conditions can have functional consequences.

1.3.3 Pathological stresses that result in t-tubule remodeling

A dizzying number of changes occur during hypertrophy and heart failure and the field is still at the outset of identifying the factors responsible for t-tubule remodeling. That being said, there are at least two well-established changes during pathophysiological conditions that show a clear correlation with t-tubular remodeling. First, the expression

level of the cytoskeletal protein junctophilin 2 (JP2), a transmembrane protein that resides on the SR membrane and is thought to form a direct connection with the t-tubular membrane, decreases during heart failure and the magnitude of t-tubule loss correlates strongly with the decline in JP2 expression (Wei et al., 2010). Overexpression of JP2 has been shown to increase the average size of the dyads and, presumably due to the presence of these stabilized t-tubule structures, these mice are markedly protected against t-tubule loss during pressure overload-induced heart failure (Guo et al., 2014). Furthermore, knockdown of JP2 causes t-tubules to become more susceptible to undergo t-tubule loss in pathological conditions (Guo et al., 2017; Wei et al., 2010). Despite the strong correlation between t-tubular organization and JP2 expression, it remains unclear whether the loss of JP2 directly results in t-tubule remodeling or merely makes the t-tubule more susceptible to other stresses that disrupt the t-tubular structure.

Second, mechanical stress strongly modulates t-tubular structure. This relationship between mechanical stress and t-tubule remodeling has been studied using vastly different models. In a myocardial infarction model, Frisk et al. demonstrated that there is a regional gradient of wall stress- the amount of tension applied to the ventricular wall- with the greatest stress applied to the surviving myocardium proximal to the infarcted region (Frisk et al., 2016). The proximal region also displayed the greatest t-tubular disorganization while regions with lower wall stress displayed only partially disrupted t-tubules. As a proof of concept, the authors went on to culture papillary muscles under low or high pre-load conditions corresponding to the wall stress observed in normal myocardium and in the proximal region, respectively. There was marked t-tubule disarray in the muscle contracting against the high load at 0.5 Hz for 48 hours in culture but not in

the low load condition, demonstrating a direct link between mechanical stress and t-tubular remodeling.

A similar relationship is observed in dog hearts with dyssynchronous heart failure. In this model, ablation of the left bundle branch results in delayed activation of the lateral wall of the left ventricle relative to the anterior wall. As a result, the lateral wall experiences a significant increase in stress compared to the rest of the left ventricle. T-tubule remodeling occurs in the lateral myocardium but not in the anterior myocardium, indicating that t-tubule remodeling is again dependent on the local mechanical stress (Sachse et al., 2012). This link between mechanical stress and t-tubule loss leads to the straightforward assumption that removal of mechanical stress is beneficial for the t-tubule network. This indeed appears to be the case as removal of the excessive mechanical stress using cardiac resynchronization therapy (i.e. biventricular pacing to resynchronize the activation of the LV and RV) largely restored the t-tubule structure (Sachse et al., 2012).

The link between mechanical stress and t-tubular structure is further strengthened in a series of papers by Ibrahim et al. (Ibrahim et al., 2012a; Ibrahim et al., 2012b; Ibrahim and Terracciano, 2013) using a heterotopic abdominal heart transplant model to fully remove the mechanical stress from failing hearts after myocardial infarction. In this model, the aorta of the donor heart (either the sham-operated or failing heart) is connected to the aorta of the recipient rat and the pulmonary artery is connected to the recipient inferior vena cava so the donor heart is back perfused and largely unloaded. After this mechanical unloading, a remarkable recovery of the t-tubule network is observed in the failing hearts (Ibrahim et al., 2012b). The results from the cardiac resynchronization therapy and

heterotopic abdominal heart transplant models demonstrate that t-tubules may recover if the initial mechanical stress is removed. However, complete removal of mechanical stress does not appear to be entirely beneficial. Control hearts atrophied after undergoing heterotopic abdominal heart transplantation and also displayed t-tubule disruption (Ibrahim et al., 2010). These studies led to the suggestion that mechanical load regulates t-tubule structure through a Goldilocks-esque relationship with too little or too much mechanical stress resulting in t-tubular loss (Ibrahim and Terracciano, 2013). However, despite this strong correlation, it remains unclear how the mechanical stress translates into t-tubule structural changes.

There is some evidence to suggest that t-tubule structure may be stretch dependent. During the cardiac cycle, the cell must lengthen while maintaining a constant volume and membrane surface area. This necessitates that the cell shrinks radially in response to stretch and swell in response to a contraction. As for the surface area, the myocytes has a robust reservoir of “slack” membrane to accommodate rapid changes in the required surface area for a given geometric shape. Kohl et al. has suggested that this extension/relaxation of the slack membrane can affect the t-tubular opening radius although quantitative data on this is limited (Kohl et al., 2003). In rabbit hearts fixed during contraction, t-tubules are longer and have greater luminal volume whereas t-tubules tend to be shorter and smaller in volume when hearts are fixed while volume loaded (McNary et al., 2012). This study suggests that t-tubules may undergo continuous changes in size and shape during the cardiac cycle.

1.4 Study of t-tubules *in vitro*

1.4.1 Detubulation as a model of t-tubule remodeling

T-tubules can be rapidly disrupted through a process called detubulation *in vitro*. The detubulation process typically involves exposure of the myocyte to a strong osmotic stress that results in the functional uncoupling of the t-tubular membrane from the outer surface membrane. Initially, detubulation in cardiomyocytes was thought to be caused by the rapid transient cell swelling following removal of high concentrations (~1.5 M) of membrane permeable formamide (Kawai et al., 1999). This idea was likely derived from early studies of glycerol-induced detubulation of frog skeletal muscle t-tubules that suggested that the increase in myocyte diameter during cell swelling stretched t-tubules to the point that they detached from the surface membrane (Gallagher and Huang, 1997). However, we now know that detubulation occurs during cell shrinking, not cell swelling (Moench et al., 2013). During hyposmotic detubulation, adult mouse left ventricular myocytes are swollen in Tyrode solution made hyposmotic by reducing the [NaCl] to 60% of normal isosmotic Tyrode solution (0.6 Na). T-tubules remained intact during cell swelling. However, upon removal of 0.6 Na solution, detubulation was observed coincident with cell shrinking.

How cell shrinking causes detubulation remains an open question. Understanding how these geometric changes in the cardiomyocyte translates to modulation of t-tubule structure may provide hints into how t-tubules respond to mechanical stress. This may be especially true during high levels of wall stress when cardiomyocytes are excessively stretched and therefore, undergo greater radial compression.

1.4.2. Fluorescence-based approaches to study t-tubule integrity

Various approaches are available to confirm functional uncoupling of the t-tubular membrane following detubulation. Following detubulation, the t-tubule lumen becomes

inaccessible from the extracellular solution and the intracellular space will appear dark when cells are bathed in a solution containing a fluorescent marker (Brette et al., 2002). Additionally, the t-tubular membrane become inaccessible to membrane binding dyes such as Di-8-ANEPPS. These observations have led to the conclusion that the detubulation procedure causes t-tubules to “pinch off” from the surface membrane (i.e. complete structural detachment). The efficacy of membrane binding dyes to label the t-tubular membrane can reveal the organization of the t-tubular network and provide a measure of t-tubular integrity.

Conversely, any extracellular marker present within the t-tubular lumen before detubulation will subsequently become ‘trapped’ within the t-tubules. By labeling t-tubular membranes before detubulation or by trapping an extracellular marker, it becomes possible to observe the structure of the t-tubules following detubulation. Detubulation results in the formation of large, dilated t-tubules that can be >1 μm in diameter. These vacuole-like structures are apparent throughout the entire cardiomyocyte and typically align in orderly rows, likely along the z-lines. Overall, detubulation is able to recapitulate some aspects of t-tubule remodeling (specifically regional t-tubule loss and t-tubule dilation) that are observed in pathophysiological conditions.

1.4.3. Electrophysiological measures of t-tubule integrity

In addition to the fluorescent measures described above, electrophysiological approaches can be used to detect t-tubular integrity. Formamide detubulation can nearly completely remove the electrical contribution from the t-tubular membrane. The whole-cell membrane capacitance, which is a product of the total surface membrane and the specific capacitance, decreases by ~26-32% following formamide detubulation in rats and

mice (Despa et al., 2003; Kawai et al., 1999). The decrease in membrane capacitance in detubulated cells suggests that t-tubules are either fully disconnected from the surface membrane or severely constricted such that they become highly resistant to electrical propagation, thereby reducing the electrically accessible surface membrane area. However, membrane capacitance alone is not a particularly quantitative measure of the extent of t-tubule loss. Membrane capacitance is strongly dependent on cell size, which can vary >4 fold in cardiomyocytes, and so the capacitance measurements must be normalized to the cell volume (or cross sectional area) (Satoh et al., 1996). In addition, the relative contribution of the t-tubule membrane to the whole cell membrane capacitance is still unknown. Typically, the specific capacitance is assumed to be constant (1 $\mu F/cm^2$) throughout the sarcolemmal membrane (Schneider, 1970). However, the high cholesterol content of the t-tubular membrane has been postulated to reduce the specific capacitance of the t-tubular membrane (Pasek et al., 2008) suggesting that there may be unequal contribution of the surface and t-tubular membranes to the whole cell capacitance. Indeed, there is a large discrepancy between the membrane fraction in t-tubules estimated by optical microscopy (~65%) and by the decline in membrane capacitance following detubulation (~30%). Until the specific capacitance of the t-tubular membrane can be directly measured, the contribution of the t-tubular membrane to the whole cell capacitance will remain an open question.

Detubulation has predominantly been used to extensively characterize the localization of many ionic currents that contribute to the ventricular action potential (See Table 1 in Brette and Orchard's review for an excellent summary of t-tubular localization of cardiac ion channels: (Brette and Orchard, 2007)). ECC proteins such as the LTCC

and NCX are highly concentrated in the rat t-tubular membrane compared to the surface membrane. It should be noted that although many ion channels are concentrated in the t-tubules, there are no ion channels that are exclusively present on the t-tubular membrane and absent on the surface membrane. Additionally, the t-tubular density of these ion channels is highly species dependent and this information may be lacking for some species. Recent work has demonstrated that, in contrast to rat ventricular myocytes, mouse ventricular myocytes show predominantly surface membrane localization of NCX (Gadeberg et al., 2017b). This demonstrates that there are remaining gaps in our understanding of t-tubular ion channels and highlights the importance of performing comprehensive and quantitative measurements of ionic currents and their localization in ventricular myocytes of various species. Finally, these t-tubular ion channels are imperfect measures of t-tubular remodeling similar to membrane capacitance.

The inward 'tail current' through Kir2 channels ($I_{K1,tail}$) is unique in that it is currently the only known ionic current that is entirely dependent on potassium accumulation within the lumen of intact t-tubules. During prolonged depolarizing voltage steps, outward potassium currents in the t-tubular membrane cause potassium to accumulate in the lumen, which depolarizes the Nernst potential for potassium. It is estimated that the Nernst potential for potassium can depolarize by 20 mV to ~-60 mV in t-tubules following a 200 ms depolarizing step to +10 mV (Clark et al., 2001). Upon repolarization to the resting membrane potential (-75 mV), two separate pathways dissipate the accumulated potassium. One, some potassium will diffuse out through the t-tubule network into the extracellular space. Two, the accumulated potassium will enter the cell through open Kir2 channels. Normally, there is very little I_{K1} current at the resting membrane potential since

the Nernst potential for potassium is near the resting membrane potential and therefore, the driving force for potassium is low. However, a stronger driving force is generated when potassium has accumulated in the t-tubular lumen, generating the $I_{K1,tail}$- an inward I_{K1} current that decreases in amplitude over time as the t-tubular luminal potassium dissipates. The $I_{K1,tail}$ is completely absent in mice expressing the Kir2.1 subunit with a dominant-negative mutation (AAA-TG) and is abolished in normal cardiomyocytes following formamide detubulation, confirming its I_{K1} and t-tubular origins, respectively (Cheng et al., 2011). The kinetics of the $I_{K1,tail}$ current can indicate potassium diffusion in the t-tubular lumen. As such, differences in $I_{K1,tail}$ current kinetics may elucidate subtle alterations in t-tubule structure, provided that I_{K1} current remains constant. Unfortunately, prolonged measurements of $I_{K1,tail}$ current in whole-cell voltage-clamped cardiomyocytes displays a gradual loss of the current in a temperature and time dependent manner, which may reflect the loss of t-tubular integrity by cell-dialysis.

1.5 Scope and aims of this dissertation

In summary, cardiac t-tubules are essential for proper ECC and despite the known disruption in the organization and sub-microscopic structure during cardiovascular disease states, little is known about the mechanisms that lead to t-tubular remodeling. In addition, the literature supports the existence of complex t-tubular structures characterized by sub-microscopic dilations and constrictions. The function of these structures is unknown and remains difficult to study due to their small size. The overall goal of this thesis is to study the function of t-tubules and the factors that contribute to their remodeling. This thesis tests the central hypothesis that sub-microscopic t-tubular structures (constrictions and dilations) regulate the diffusional properties and stability of

t-tubules in response to osmotic stress. Although the experiments presented are *in vitro* studies performed on isolated cardiomyocytes, the findings presented in this thesis provide important fundamental facts about t-tubule physiology and will likely be helpful for many investigators interested in t-tubule structure.

Before the start of this project, few tools were available to observe subtle changes in t-tubular structure. Much of the membrane labeling techniques could only distinguish between intact and completely sealed t-tubules. This simple binary measure is clearly insufficient to study transitions from intact to sealed t-tubules. As mentioned above, $I_{K1,tail}$ current is a useful measure for K^+ diffusion in the t-tubule network but the process of patching in the whole-cell configuration resulting in the dialysis of intracellular components was known to disrupt t-tubule structure. Chapter 2* will describe the development of a novel fluorescence-based assay to quantitatively measure changes in the t-tubular diffusional properties of live, intact cardiomyocytes. This assay is the only known tool available to obtain repeated measurements of t-tubular diffusional accessibility on the same cardiomyocyte and allows for observations of rapid t-tubular structural changes. By comparing the data obtained from this assay with simulations using a finite-elements based model, we came to the surprising conclusion that diffusion within the t-tubules is heavily dependent on the heterogeneity in t-tubular diameter. Constrictions and dilations within the t-tubule lumen are major determinants of the diffusional mobility of solutes and electrical propagation within the t-tubule network.

Using the newly developed dextran diffusion assay, I then tested the hypothesis that prior t-tubule remodeling predisposes the t-tubules to seal following a strong detubulating stress. Chapter 3 describes the strong correlation between the diffusional

accessibility of t-tubules and the magnitude of t-tubule sealing following osmotic stress. This study highlights the notion that, in addition to the known effects on ECC, sub-microscopic t-tubular structures can profoundly affect the stability of t-tubules in response to osmotic stress and may provide insight into the link between mechanical stress and t-tubule remodeling that is observed *in vivo*.

Chapter 4* describes the effects of various SMPMs on preventing or promoting detubulation. The observation that SMPMs can protect against osmotic detubulation when transiently applied during cell shrinking, or conversely promote detubulation when high concentrations of SMPMs are removed, demonstrated that the concentration gradient of SMPMs across the membrane plays an important modulatory role in detubulation. We proposed that the "bilayer-couple hypothesis", which describes the formation of membrane curvature due to membrane area asymmetry across the membrane, can effectively explain the seemingly bipolar effects of SMPMs. Although the results obtained with these SMPMs are unlikely to directly lead to therapeutic options to prevent t-tubular remodeling, they offer valuable insight into the physical properties of t-tubular membranes and the structures they fold into during t-tubule sealing.

Finally, Chapter 5 will summarize the results from the preceding three chapters and propose hypothetical mechanisms underlying detubulation in cardiomyocytes. In addition, the predominantly biophysical results presented within this thesis will be discussed within the context of physiological relevance.

* Chapters 2 and 4 have been previously published and are reproduced with minor edits in this dissertation.

CHAPTER 2 DIFFUSIONAL AND ELECTRICAL PROPERTIES OF T-TUBULES ARE GOVERNED BY THEIR CONSTRICTIONS AND DILATIONS

2.1 Acknowledgements

This chapter has been previously published in the *Biophysical Journal* (Uchida and Lopatin, 2018) and is reproduced here with minor edits. The chapter includes computer modeling data obtained by Anatoli Lopatin. This work was supported by the National Institutes of Health (HL127023 to ANL and T32-GM008322 to KU), and the American Heart Association (17PRE33350049 to KU).

2.2 Abstract

Cardiac t-tubules (TTs) form a network of complex surface membrane invaginations that is essential for proper excitation-contraction coupling. Although electron and optical microscopy studies provided a wealth of important information about the structure of TTs, assessing their functional properties remains a challenge. In this study, we investigated the diffusional accessibility of TTs in intact isolated adult mouse ventricular myocytes using a novel fluorescence-based assay. In this approach, a small part of TTs is first locally filled with fluorescent dextran and then its diffusion out of TTs is monitored after rapid removal of extracellular dextran. In normal cells, diffusion of 3 kDa dextran is characterized by an average time constant of 3.9 ± 1.2 seconds with the data ranging from 1.8 to 10.5 seconds. The data are consistent with essentially free diffusion of dextran in TTs although measurable contribution of binding is also evident. TT fluorescence is abolished in cells treated with high concentration of formamide or after

hyposmotic stress. Importantly, the assay we use allows for quantitative, repetitive measurements of subtle dynamic changes in TT structure of the same cell that are not possible to observe with other approaches. In particular, dextran diffusion rate decreases two-to-three fold during cell swelling suggesting significant structural remodeling of TTs. Computer modeling shows that diffusional accessibility and electrical properties of TTs are primarily determined by the constrictions and dilations of individual TTs and that, from a functional perspective, TTs cannot be considered as a network of cylinders of the same average diameter. Constriction/dilation model of cardiac TTs is in a quantitative agreement with previous high resolution microscopy studies of TT structure and alternative measurements of diffusional and electrical time constants of TTs. The data also show that the apparent electrical length constant of cardiac TTs is likely several-fold smaller than that estimated in earlier studies.

2.3 Introduction

T-tubules (TTs) are narrow plasma membrane invaginations that form a complex network in cardiac myocytes (Forbes et al., 1984; Ogata and Yamasaki, 1990; Soeller and Cannell, 1999). They house critical calcium handling proteins and form intimate connections with the sarcoplasmic reticulum called dyads that are essential for proper excitation-contraction coupling (Bers, 2002). TTs are most prominent in ventricular myocytes (Smyrnias et al., 2010) and the overall appearance of the TTs remains essentially constant throughout the adult life. However, a number of studies have demonstrated that TTs are significantly disrupted or even lost in a variety of cardiac diseases ((Guo et al., 2013) for review). In these pathological conditions, TT remodeling

results in various functional defects including dyssynchronous calcium release and impaired contractility (Oyehaug et al., 2013).

Recent work demonstrated that in failing hearts individual TTs may display action potential propagation failure while remaining connected to the outer sarcolemma (Sacconi et al., 2012). This is consistent with a straightforward idea that the affected TTs are characterized by significant local constrictions of their lumens which present a barrier for propagation of membrane potential. However, in live cells observation of local constrictions of TTs, or changes in their local diameter, would be a challenging, if not practically impossible, task even with the use of super-resolution optical microscopy (diameter is ~170-200 nm in mouse cardiomyocytes (Kong et al., 2017; Wagner et al., 2012), and the sizes are typically smaller in fixed tissues when measured using electron microscopy (Ogata and Yamasaki, 1990)).

However, TT constrictions, as well as dilations, in turn should be reflected in the changes of diffusional accessibility of TTs prompting the development of tools capable of accessing this property of t-system. In fact, a number of diffusion-based tools have already been employed in TT studies. In most of them, diffusional accessibility of TTs was derived from electrophysiological measurements of some relevant parameters: (*a*) time course of blockage of t-tubular ion channels by extracellular agents (Christe, 1999), (*b*) kinetics of so-called I_{K1} tail current (Cheng et al., 2011; Clark et al., 2001), or (*c*) changes in specific ionic currents and membrane potential in response to fast changes of extracellular solutions (Shepherd and McDonough, 1998; Swift et al., 2006; Yao et al., 1997). However, in all cases a number of inherent experimental limitations, such as necessity of intracellular dialysis during whole-cell electrophysiological recordings or

uncertainties in the interpretation of indirect data, precluded a robust and strongly quantitative assessment of diffusional properties of TTs.

An alternative, and essentially non-invasive, way of assessing diffusional properties of TTs employs the use of fluorescent molecules. The earliest reports of this approach date back to the 1960s when Endo (Endo, 1964, 1966) used Lissamine Rhodamine B 200 to show that TT lumens are connected to the extracellular space in skeletal muscle. Other investigators have adapted this technique to study changes in diffusional properties of skeletal muscle TTs in response to osmotic shock (Kerr et al., 2013), and this general approach has recently been extended for cardiac myocytes using Fluorescence Recovery After Photobleaching (FRAP) microscopy by Scardigli et al. (Scardigli et al., 2017) to estimate the electrical length constant of TTs.

In this paper, we provide detailed description of a novel robust assay allowing for the dynamic quantitative measurement of TT diffusional properties by observing the movement of fluorescent dextrans in the TT network of live intact cardiomyocytes, and demonstrate its capabilities in detecting subtle changes in the TT structure in response to acute osmotic challenges. Similar to previous reports and the study by Scardigli et al. (Scardigli et al., 2017), the data show that TTs present a significant barrier for diffusion of small molecules. Importantly, quantitative computer modeling shows that the kinetics of dextran diffusion in TTs is primarily determined by the irregularity of TT diameter along their length and not by their average diameter, the density of TTs, or the overall complexity (tortuosity) of t-tubular network. The simulated data are quantitatively consistent with previous alternative measures of diffusional properties of TTs and show, in particular, that

the apparent electrical length constant of cardiac TTs was likely overestimated by several-fold in earlier studies (Kong et al., 2017; Pasek et al., 2008; Scardigli et al., 2017).

2.4 Materials and Methods

Animals

All experiments involving mice were carried out in accordance with the Guide for the Care and Use of Laboratory Animals (8th edition; The National Academic Press, Washington, DC, USA) and protocols were approved by the veterinary staff of the University Committee on Use and Care of Animals at the University of Michigan. Both male and female C57BL/6 mice were included in this study. The average ages of the male and female mice were 17.2 ± 1.72 and 16.7 ± 2.4 weeks, respectively (p = NS).

Solutions (mM)

Modified Tyrode (Tyr): 137 mM NaCl, 5.4 mM KCl, 0.5 mM $MgCl_2$, 0.3 mM $CaCl_2$, 0.16 mM NaH_2PO_4, 3 mM $NaHCO_3$, 5 mM HEPES, and 10 mM glucose, pH = 7.35.

Myocyte storage solution (C solution): 122 mM NaCl, 5.4 mM KCl, 4 mM $MgCl_2$, 0.16 mM NaH_2PO_4, 3 mM $NaHCO_3$, 15 mM HEPES, 10 mM glucose, 5 mM mg/mL of bovine serum albumin, and 1.38 mg/mL taurine, pH = 7.35.

Hyposmotic Tyrode (0.6 Na): prepared as Tyr but with 60% of NaCl (82.2 mM). Hyposmotic (0.7 Na) solution was prepared by mixing 0.6 Na and Tyr solution (3:1 ratio), pH = 7.35.

All solutions were filtered using a 0.22 µm filter and pH adjusted with NaOH.

Chemicals

We used HEPES (EMD Chemicals, Inc., Darmstadt, Germany); KCl, $NaHCO_3$, and NaH_2PO_4 (Mallinckrodt, Bedminster, NJ); 3 kDa and 10 kDa tetramethylrhodamine dextrans in anionic, lysine fixable form, Wheat Germ Agglutinin, and Alexa Fluor 633 conjugate (Thermo Fisher Scientific, Waltham, MA). Purified neuraminidase was from Clostridium perfringens, Collagenase (Type 2; Worthington Biochemical, Lakewood, NJ). All other chemicals and reagents were from Sigma-Aldrich.

Isolation of ventricular myocytes

Myocytes were isolated from the hearts essentially as described in the study by Moench and Lopatin (Moench and Lopatin, 2014) and used for experiments within 1-8 hours post-isolation.

Viscosity measurements

Measurements of kinematic viscosity were performed using calibrated Cannon-Manning semi-micro (size 25) viscometer (Cannon Instrument Co., State College, PA) according to the manufacturer instructions in a water bath at 24.6^{o}C. Specific gravity was determined using a 2.00 mL Gay-Lussac bottle (Cole-Parmer, Vernon Hills, IL) and the weight was measured using an AG64 Analytical Balance (Mettler Toledo, Columbus, OH). All viscosity measurements are obtained in duplicates and specific gravity measurements were obtained in triplicates. The measured values are presented in **Table 2.1**.

Confocal imaging

Confocal imaging was performed in Microscopy and Image Analysis Laboratory (University of Michigan, Ann Arbor, MI) on an Olympus FV-500 microscope using 60x 1.4 NA oil objective. Images of myocytes were manually outlined and mean intracellular fluorescence of trapped dextran per unit area calculated using *ImageJ* software (http://imagej.nih.gov). Further data analysis, e.g. correction for background fluorescence, was performed in Microsoft Excel (Microsoft, Redmond, WA).

Dextran trapping assay

Dextran trapping assay was performed essentially as described in earlier publications (Moench et al., 2013; Uchida et al., 2016). In brief, 3 kDa dextran was added to a suspension of isolated ventricular myocytes during the swelling phase in hyposmotic 0.6 Na solution in order to fill TTs with this fluorescent marker. Cells were then returned to Tyr solution, still containing dextran, and finally extracellular dextran was washed out using normal Tyr. The cells were further washed and stored in C solution on ice prior to confocal imaging. Control myocytes were treated identically except that they were exposed to Tyr solution instead of 0.6 Na solution.

Dextran diffusion assay

Direct testing of diffusional accessibility of TT network relies on measuring the movement of an appropriate molecular marker. Accordingly, in our approach, TTs are first filled with fluorescent dextran by external application and then, after its quick removal from extracellular solution, dextran diffusion out of TTs is monitored by recording its fluorescence from a small intracellular spot using wide-field fluorescent microscopy (**Fig. 2.1**). To obtain a clean TT fluorescence signal and eliminate potential contamination by

extracellular fluorescence, cells are lifted and placed in a rapid stream of bath solution. A typical spot recording from a TT system obtained using this approach is depicted in **Fig 2.2**. While the principle of this assay is conceptually simple, its practical implementation in live cardiac myocytes is not straightforward and requires addressing a number of technical and computational issues in order to make it a reliable quantitative method. In particular, justification of the fluorescence recording from a spot rather than at specific point(s) of TTs is addressed later in the computer modeling part of the *Results* (Chapter 2.4) section. Detailed description of the assay is provided in Chapter 2.6 *Supporting Material.*

Computer modeling.

Computer modeling studies of dextran diffusion in TTs and electrical properties of TTs were performed using Finite Element Method implemented in COMSOL Multiphysics 5.3 software (COMSOL, Inc., Burlington, MA) installed on a PC computer (Intel® Core™ i7, 4 GHz CPU; 32 GB RAM, 64-bit Windows 10 OS). Mesh parameters were chosen to minimize the total number of elements (up to 1-1.5 million free tetrahedral elements plus up to ≈100,000 triangular elements), yet to achieve a good approximation of the narrowest regions (e.g. 20 nm TT constrictions). As an example, a calculation of 50 sec diffusion in TT network as in **Fig. 2.9 [3]** would take ≈15 minutes, and the times are significantly smaller for less complicated geometry.

Statistics

The data (mean ± standard error) in each experimental series are from at least two heart preparations. Statistical significance was determined using a two-sample t-test

assuming equal variances and considered significant if $p < 0.05$. In figures *, **, and *** correspond to p values of 0.05, 0.01 and 0.001, respectively. A use of standard deviation, instead of standard error, is indicated wherever it is appropriate.

2.5 Results

Validation of t-tubular dextran diffusion assay

The relatively small amplitude of the presumable t-tubular component of fluorescent signal and the potential contribution of various technological parameters to the quantitative measurements of true t-tubular diffusion of dextran(s) make validation of the assay a necessity.

It follows from the data in **Fig. 2.2** that the time constant of presumable t-tubular component is in the range of few seconds. Therefore, to ensure that TTs are maximally filled with dextran, in all experiments the application time was set significantly above this value, at 30 seconds, as was the duration for washout of the dye.

Amplitude

If the slower component of dextran fluorescence originates from TTs, then its amplitude should correspond to that produced by other relevant approaches. Dextran trapping assay provides one way of addressing the question (see *Materials and Methods* and **Fig. 2.3**). In brief, cardiomyocytes were detubulated using hyposmotic shock (Moench et al., 2013) in the presence of the same concentration of extracellular dextran as in the diffusion assay, and the fluorescence of dextran trapped in TTs was measured using dextran diffusion setup (spot illumination, same recording parameters etc). Confocal images in **Fig. 2.3B** show detubulated cells with dextran trapped in numerous

sealed TTs throughout the cell (**Fig. 2.3B*i***), whereas cells not exposed to hyposmotic stress do not retain t-tubular dextran (**Fig. 2.3B*ii***). The data in **Fig. 2.3C** show that the amplitude of time-dependent fluorescence is significantly higher than background control values (e.g. cell autofluorescence) but also significantly smaller than that expected from sealed TTs filled with dextran (≈25% of that in detubulated cells). However, the latter formal discrepancy is easily resolved considering that the local application of dextran leads to a standing gradient of dextran inside the cell and thus a lower concentration at the recording spot (see **Fig. 2.20**).

Notably, the steady-state values of fluorescence after dextran withdrawal are greater than that for cell autofluorescence alone. This suggests a small (and relatively stable over the time used to measure the diffusion of dextran), practically insignificant, membrane binding or internalization of dextran.

One of the most important features of dextran diffusion assay is that it allows for long-term dynamic measurements of diffusional accessibility of TTs on the same cell as various experimental protocols proceed. The data in **Fig. 2.4A&B** show representative traces of dextran fluorescence before (dashed line) and after (solid line) application and later removal of hyposmotic (0.6 Na) or hyperosmotic (1.5 M formamide) solutions known to lead to nearly complete detubulation (Kawai et al., 1999). Quantification of the data (**Fig. 2.4C**) shows that treatment with formamide (15 min) and 0.6 Na (7 min) solutions reduced the TT fluorescence amplitude by 88.3 ± 4.0 % (n=4) and 84.5 ± 4.1 % (n = 6), respectively. Milder hyposmotic stress (0.7 Na) led to partial detubulation and a variable response indicative of a threshold level stress (see **Fig. 2.17** and *effects of mild osmotic stress on dextran diffusion* in Chapter 2.6).

An important observation highlighting the sensitivity of the assay is that cells that have been perfused with normal Tyr solution for 15 minutes display a 23.2 ± 11.8% *increase* in the TT fluorescence amplitude (n = 5), which is reflected in the corresponding increase in the normalized amplitude for control cells in **Fig. 2.4C**.

Kinetics

We first performed a number of tests to estimate the potential contribution of a number of experimental variables to the kinetics of dextran diffusion. In particular, experiments showed that variations in washout flow rates and positions of recording spot have no appreciable effect on the measured time constants (**Figs. 2.14** and **2.15**). To test whether the fluorescence decline observed with the diffusion assay is not an artifact due to photobleaching, cardiomyocytes with dextran trapped in sealed TTs were exposed to light with intensity typical for all our experiments. Under this condition, the fluorescence declined with a time constant of 169 ± 18 seconds (n=3) strongly suggesting that photobleaching effects are too small to affect the time course of diffusion-dependent fluorescence in any appreciable manner.

In order to further test that fluorescence kinetics reflects mostly free dextran diffusion (as opposed to, e.g., membrane binding) we performed experiments using larger, 10 kDa, dextran and solutions with different viscosities.

The effective Stokes radii of polydisperse 3 kDa and 10 kDa dextrans were estimated to be 13.4 and 23.5 Å (Venturoli and Rippe, 2005), respectively, which translates to ≈1.75 fold difference. Experiments showed that the time constant of fluorescence for 10 kDa dextran increased ≈2.2 fold, from 4.9 ± 0.4 sec (n=7) to 10.9 ±

1.2 sec (n=9, p<0.001), for 3 kDa and 10 kDa dextrans, respectively. These data are in a good quantitative agreement with the increase in dextran size (free diffusion is inversely proportional to the effective radius).

Next, the viscosity of the surrounding media was modified using either 5 % (w/v) non-fluorescent 40 kDa dextran or 2% polyvinylpyrrolidone (PVP). Viscosities of these two solutions were ≈2.2 fold and ≈1.5 fold larger, respectively, than that of normal Tyr solution (Table S1). We found that addition of 40 kDa dextran led to a 1.6 ± 0.1 fold increase, from 4.4 ± 0.3 sec (n=16) to 7.2 ± 0.4 sec (n=11, p<0.001), in the time constant of diffusion of 3 kDa fluorescent dextran. Similarly, addition of PVP led to a 1.5 ± 0.2 fold increase, from 3.4 ± 0.3 sec (n=11) to 5.1 ± 0.6 sec (n=9, p<0.01), in the diffusion time constant. These data, again, are in a good quantitative agreement with the expected change in free diffusion constant (inversely proportional to viscosity).

The above data, however, still cannot fully exclude the effects of some other potential contributors to the measured apparent diffusion constant of dextran. For example, dextran diffusion can be significantly slowed by the presence of extracellular matrix (e.g. collagen (Crossman et al., 2017)) or binding to glycocalyx. In particular, dense collagen matrix may increase the 'tortuosity' of diffusion pathway at the molecular level (by creating longer, less 'straight', diffusion pathways). However, this increase would clearly be very incremental, especially in our experimental settings where collagen component of extracellular matrix is likely mostly removed by crude collagenase during isolation of cardiomyocytes. However, some components of glycocalyx may still remain intact. Accordingly, we have measured diffusion rates of dextran in cardiomyocytes treated with 0.25 U/mL neuraminidase A. The data in **Fig. 2.16** show that further removal

of significant part of remaining glycocalyx does not lead to acceleration of dextran diffusion. In contrast, diffusion rates become smaller likely reflecting structural remodeling of TTs due to changes in membrane stability.

Overall, the data in this section strongly argue that the time-dependent fluorescence originates from TTs and that the time constant of its decline primarily (see *Discussion*) reflects the diffusion of dextran out of the TT network.

Variability of dextran diffusion in individual cardiomyocytes

The time constant of dextran fluorescence varies significantly from cell to cell (**Fig. 2.5**). On average, the time constant, τ^{exp}_{dex}, is 3.9 ± 1.3 (SD) seconds (n = 131 cells; median value = 3.7 seconds). The distribution of these time constants is not fully Gaussian; it displays a peak at ≈3.5 seconds as well as a clear 'tail' at larger time constants beyond 5 seconds. Approximately 7% of normal cells show time constants above 6 seconds and the largest time constant was 10.5 seconds. Since the time constant of diffusion is strongly dependent on the size (and the shape) of the cell (see *Discussion*), we speculate that significant part of this variability may arise from the variation in the cell size. In this regard, as shown in Chapter 2.6 *Supporting Material*, technical limitations of the approach do not significantly affect the TT diffusion time constant. Importantly, the average time constants for male and female mice were essentially the same: 3.8 ± 0.65 and 4.0 ± 0.65 seconds (p = NS), respectively. Furthermore, there was no correlation between the time constant and the age of the adult mice used in this study (11-19 weeks, R^2=0.02).

Hyposmotic cell swelling restricts t-tubule diffusion

In order to further investigate the potential contribution of dextran binding to the measured time constants of its diffusion in TTs, single-cell time series recordings of dextran diffusion were performed at 1 min intervals before and during cell swelling in hyposmotic 0.6 Na solution. Cell swelling alone would not be expected to affect dextran binding to a presumable target in TTs, and we have previously shown that TT sealing does not occur during hyposmotic swelling (Moench et al., 2013). Performing single-cell recordings significantly reduces the contribution of cell-to-cell variability to the measured parameters and greatly helps to infer dynamic, real-time changes in TTs structure in response to acute stress. As shown in **Fig. 2.6A**, after 5 min of swelling in hyposmotic solution (~13% change in cell width (Moench and Lopatin, 2014)), the same cell displays a significantly reduced peak amplitude and a significant increase in the time constant of dextran fluorescence consistent with decreased volume of TTs and development of TT constrictions, respectively. The time course of TT remodeling is characterized by the time constant ~3.2 minutes (single exponential approximation) with the measured time constant of dextran diffusion (relative diffusion time constant in **Fig. 2.6B**) reaching a final value that is 2.4 ± 0.6 fold greater than the initial time constant. It is important to note that the magnitude of a change in the diffusional time constant (200-300%) cannot be explained by ~13% change in cell width and corresponding increase in the diffusional distance (diffusion time constant ~(cell radius)^2; ≈$(1.13)^2$≈1.28 or <30% increase). Overall, the data demonstrate a remarkably dynamic change in TT diffusional accessibility that likely reflects nanoscale changes in TT structure such as constrictions (see below).

Modeling free diffusion in cardiac TTs

Measuring diffusion of small molecules in cardiac TTs can provide unique important information about their structure and function. However, conclusions reached in this type of experimentation would strongly depend on specific interpretation of the data, and thus appropriate modeling studies would be of great importance. While there are known analytical solutions for free diffusion in simple geometries (e.g. cylinder), either appropriate approximations or numerical calculations are necessary to model diffusion in more realistic cases (e.g. cells containing cardiac TTs). Therefore, we used finite element computer modeling (COMSOL 5.3) to calculate relevant parameters of free dextran diffusion in various 2D and 3D geometries of TTs.

In this work we study outward-directed diffusion of dextran. However, essentially identical results are obtained from considering a situation when a diffusible molecule is applied to the whole cell and its inward-directed diffusion is characterized (**Fig. 2.18**) thus allowing for quantitative comparison of the data obtained previously (Scardigli et al., 2017).

Cardiac myocytes can be well approximated as long cylinders which allows for modelling only radial diffusion. While modeling is easily scalable to essentially any relevant parameter we, nevertheless, chose realistic dimensions of cardiac cell radius (≈10 μm), TT diameter (50-200 nm), and free diffusion coefficient of 3 kDa dextran (D^{free} =150 μm^2/sec; (Kihara et al., 2013; Scardigli et al., 2017)). TTs were arranged in 2D or 3D rectangular array and spaced at 2 μm, a geometry which fits well with the rat and mouse TTs.

First, let's assume that a cell is loaded with a molecule which is then allowed to diffuse through the cytoplasm and membrane without restrictions of any kind like in the bulk surrounding solution (**Fig. 2.7A[1]**). As expected, the concentration of the molecule

in the center of the cell follows a time course characterized by a delay phase (reflecting a 'propagation of the wave front' of concentration; **Fig. 2.7B▼**) followed by quasi-exponential (Scardigli et al., 2017) decrease in the concentration with the time constant $\tau_{dex}^{free} \approx 0.11$ sec.

Surely, the time course of diffusion out of the center of cell is affected if the molecule is allowed to freely diffuse only through a TT network. Indeed, **Fig. 2.7[2]** shows that if TTs are modelled as a rectangular array of 200 nm diameter cylinders, τ_{dex} is increased ≈2 fold, to ≈0.20 sec. This would be interpreted by an observer as ≈2-fold decrease in the apparent diffusion coefficient of a molecule, D'_{dex} in our case.

Fig. 2.7 also highlights an expected, but essential, finding which helps to better understand the key factors underlying the kinetics of apparent diffusion in TTs. Specifically, a 4-fold decrease in diameter (to 50 nm) or a 2-fold increase in the density of TTs has no practical influence on the time course of diffusion ($\tau_{dex} \approx 0.22$ sec and $\tau_{dex} \approx 0.21$ sec, respectively).

In our experimental approach we measure outward-directed diffusion of dextran using spot recording (*vs* point recording) of fluorescence (~concentration). In order to test whether the two approaches are quantitatively comparable, we also modelled diffusion in a configuration that better matches our experiments. The data in **Fig. 2.19** show that the time constant of dextran diffusion is essentially independent of the position of recording point (Scardigli et al., 2017) (**Fig. 2.19; A&B**), and is essentially the same if calculated for a spot region (**Fig. 2.19; C&D**). The data are also not significantly affected by the position of the recording spot (**Figs. 2.15A** and **2.19C&D**).

Next, we tested whether the local application of dextran used in our approach would lead to appreciably different parameters of dextran diffusion. As expected, local application of dextran leads to significant reduction in its average concentration in the recording spot (**Fig. 2.20**), which is in a quantitative agreement with experimental data in **Fig. 2.3C**. Importantly though, the time constant of dextran diffusion (fluorescence integrated over the recording spot) is not affected by local application: $\tau_{dex\ global} = \tau_{dex\ local} = 0.20$ sec (**Fig. 2.20D**).

A better estimation of t-tubular diffusion can be made by taking into account the 3D nature of the t-tubular network. In particular, in rat and mouse myocytes TTs are characterized by the presence of extensive axial connections (Kong et al., 2017; Soeller and Cannell, 1999) which should be taken into consideration even though the overall diffusion in a model proceeds in radial direction. One would expect that diffusion from the center of the cell should be slowed due to extra time necessary for diffusion out of axial TTs.

Accordingly, we next modelled TTs as 3D rectangular array of cylinders of the same diameter and confirmed that, indeed, diffusion time constant is increased by ≈50% when compared with that using 2D or 3D modeling in the absence of axial TTs ($\tau_{dex\ no\ axial\ tubules} = 0.21$ sec *vs* $\tau_{dex\ with\ axial\ tubules} = 0.31$ sec; **Fig. 2.8**). However, the calculated time constant is still not even near to the experimentally measured values (1.8 to 10.5 seconds). Importantly, and consistent with 2D modeling data, neither the density nor the diameter of TTs in 3D models had any significant effect on diffusion kinetics (data not shown).

In each simulation using cylindrical TTs, the diffusion time constants are more than 13-19 times smaller than the experimentally determined average value τ^{exp}_{dex} (see below

for cell size/shape correction). It is also clear at this juncture that no matter how dense or complex (within reasonable limits) the network of TTs is, the time course of diffusion to or out of the center of the cell, and thus the apparent diffusion coefficient, will not be significantly affected as long as this modelled network is composed of cylinders with the same diameters.

It follows from the above that the model must be extended to include other important features of TTs. In particular, it is well established that TTs are characterized by the presence of dilated and constricted regions (Kostin et al., 1998; Maron et al., 1975; Ogata and Yamasaki, 1990; Pinali et al., 2013; Pinali and Kitmitto, 2014; Schaper et al., 1991). Diffusion through such TTs differs quite dramatically from that in a cylinder with a similar overall (average) diameter, and this difference surely depends on the sizes of those dilations and constrictions. **Fig. 2.9** shows that including experimentally meaningful dilations and constrictions to TTs leads to dramatic slowing of apparent dextran diffusion and, finally, brings the diffusion time constant to that observed experimentally.

We have considered two alternative architectures of TTs. One was dominated by dilations, and the other was dominated by short running constrictions (**Fig. 2.9A**). We found that including 300 nm (radius) dilations along with 2-fold reduction in the diameter of the remaining TTs (100 nm) leads to >6-fold deceleration of apparent diffusion, with the time constant changing from $\tau_{dex\ no\ dilations}$ =0.31 sec to $\tau_{dex\ with\ dilations}$ =2.0 sec. Alternatively, introduction of short running 20 nm (diameter) constrictions to otherwise same TTs (200 nm diameter) leads to an equally dramatic, >7-fold deceleration of diffusion with the time constant $\tau_{dex\ with\ constrictions}$ =2.3 sec. Diffusion time constant depends on the cell size (Scardigli et al., 2017) and shape, and therefore the modeling or

experimental data must be scaled appropriately for comparison purpose. The cell width of mouse ventricular myocytes measured in a separate experiment was 31.9 ± 1.4 μm (SE; n = 31). Ventricular myocytes, however, are not cylinders and are characterized by the ratio width/depth ≈2 (Gerdes et al., 1994; Satoh et al., 1996). Accordingly, ventricular myocytes can be modelled as cylindrical ellipsoids with major and minor radii ≈16 μm and ≈8 μm, respectively. Comparing diffusion in 10 μm cylindrical cell with that in cylindrical ellipsoid with the above parameters leads to a scaling factor k≈1.1, which means that the time constants derived from modeling 10 μm cylindrical cell can be essentially directly (≈10% difference) compared to that in ventricular myocytes.

The data in **Fig. 2.9B** show that the cell size corrected time constants, $\tau^{corr}_{dex\ with\ dilations}$=2.2 sec and $\tau^{corr}_{dex\ with\ constrictions}$=2.5 sec, for just constrictions or just dilations alone, are very close to experimentally measured time constant of dextran diffusion, τ^{exp}_{dex}=3.9 ± 1.2 sec (SD).

Modeling electrical properties of cardiac TTs

The same modeling approach used for characterization of dextran diffusion can be easily extended to study electrical properties of TTs. In particular, instead of applying extracellular dextran one can apply an electric potential and quantify the time course of membrane potential change in the center of the cell. In this study we have assumed specific membrane capacitance C_m=1 μF/cm^2, membrane resistivity ρ_m =7 kΩ·cm^2 (as in reference (Kong et al., 2017)) and resistivity of external solution ρ_i =100 Ω·cm (*vs* ≈83 Ω·cm in reference (Scardigli et al., 2017)), the values close to experimentally determined ones. With these parameters, the calculated time constant of propagation of membrane potential, τ_{Vm}, was 10.1 μsec for cylindrical TTs presented in **Fig. 2.9[1]**, and it was

increased ≈10-fold, to 102 μsec, in the presence of short running 20 nm diameter TT constrictions as presented in **Fig. 2.9[3]**.

Since the speed of electrotonic propagation is ~$r_i C_m$, even a 10-fold decrease in ρ_m did not have any appreciable effect on τ_{Vm} (≈2% and ≈8% change for +/- constrictions models, respectively; data not shown).

The steady-state length constant of TTs is also affected dramatically by the presence of constrictions and, in contrast to the speed of propagation, is strongly dependent on the membrane resistivity (~$(\rho_m)^{1/2}$). A common way of characterizing the length constant is to consider an infinitely long tube with desired or known parameters. Accordingly, for a single 200 nm diameter TT with 20 nm constrictions spaced every 2 μm, similar to that in the 3D model of the whole t-system, numerically calculated length constant, λ, was ≈68 μm, and a 10-fold decrease in membrane resistivity to 0.7 kΩ·cm^2 reduced λ to ≈22 μm.

As we will show in *Discussion,* both diffusional and electrical time constants in the presence of constrictions (and/or dilations) of TTs are in very good quantitative agreement with experimental data obtained by alternative means, thus strongly suggesting that the irregularity of TT diameter is the major contributor to the diffusional and electrical properties of TTs.

2.6 Discussion

Dextran diffusion assay

In this paper, we describe a novel technique for quantitative dynamic measurements of diffusional accessibility of cardiac TTs to small molecules in individual

live intact ventricular myocytes, and apply it for studying basic functional properties of TTs.

During development of the assay we have performed a number of experiments and computer modeling simulations to assure the quantitative robustness of the diffusion measurements. In particular, we have considered potential contribution of fluorophore bleaching, flow rates of relevant solutions, and the effects of spot illumination/recording. Perhaps the most important finding was the magnitude of the contribution of solution flow between the cell and the floor of the chamber. Therefore, lifting the cell up using a holding pipette (**Fig. 2.1A** and **Fig. 2.10**) was a critical step in avoiding significant artifacts (Uchida and Lopatin, 2016) in the estimation of true diffusion kinetics in TTs.

The data show that the assay is also very sensitive with regard to measuring the time constant of dextran diffusion in the same cell over long periods of time which, in part, is due to the relatively low intensity of excitation light leading to reduced phototoxicity. For example, in all single cell time-controlled experiments (e.g. as in **Fig. 2.4** and **Fig. 2.17**) the 'control' data (normalized to that 10-15 minutes before) already display measurable, but otherwise invisible, changes in TTs structure due to a silent response of the cells to a change in the extracellular environment (storage solution *vs* bath solution).

It was not very surprising to find dramatic changes in the amplitude of dextran fluorescence in detubulated cells (**Fig. 2.4**). However, the observation of significant changes in diffusion kinetics during cell swelling highlights the dynamic and robust, but otherwise silent, remodeling of TTs occurring before TT sealing (detubulation is induced by removal of osmotic stress (Moench et al., 2013)). Notably, these changes occur on the

time scale of seconds to minutes, rather than the weeks required for TT remodeling to become evident in pathophysiological models (Wei et al., 2010).

The time constant of dextran diffusion varies significantly from cell to cell (**Fig. 2.5**), but the average value is very close to that obtained by Scardigli et al. (Scardigli et al., 2017) for rat ventricular myocytes using FRAP microscopy approach (4.9 sec *vs* 3.9 sec for mouse myocytes in our study). Close inspection of the data in **Fig. 2.5** shows the presence of a second (smaller) component. This could be indicative of the existence of two types of cells with either different general architecture of TTs or different group size (the time constant is dependent on the cell size (Scardigli et al., 2017), ~(radius)^2). Since the relative variation in the size (width) of the cells is close to that of the time constant of diffusion, it seems that the spread in kinetics of diffusion can be at least in part explained by cell size variation. Alternatively, the second group of cells may represent 'overdigested' cells similar to neuraminidase A treated cells (**Fig. 2.16**). These hypotheses, however, will need to be tested in future experiments.

The origin of small apparent diffusion coefficient in cardiac TTs

Quantitative modeling shows that the measured average time constant of dextran diffusion, τ^{exp}_{dex}=3.9 sec, is significantly larger than that predicted for a free diffusion in/out of a bulk cytoplasm of a r_{cell} =10 μm cylindrical cell, τ^{free}_{dex}=0.11 sec. τ_{dex} is strongly dependent on the cell size (Scardigli et al., 2017) and the shape, and this should be taken into account for a quantitative comparison of experimental and computer modeling data (e.g. in **Fig. 2.9C**). However, as mentioned in *Results,* the scaling factor between the data obtained in modeling a 10 μm radius cylindrical cell and those corresponding to mouse

ventricular myocytes is only k≈1.1, and therefore essentially no (minor) adjustments are necessary for comparison purpose (will be ignored below).

Accordingly, it follows from the data in **Fig. 2.7B** that the apparent diffusion in TTs of myocytes is ≈35 times slower than it would be in the free solution (τ^{free}_{dex}=0.11 sec *vs* τ^{exp}_{dex}=3.9 sec). The latter in turn translates to an apparent t-tubular coefficient of diffusion of only D'_{dex}≈4 μm^2/sec *vs* D^f_{dex} ≈150 μm^2/sec in free solution. The modeling data in **Fig. 2.7** and **Fig. 2.8** also clearly show that this dramatic and unexpected discrepancy cannot be explained using a TT network made of collection of cylindrical elements of the same diameter. In particular, in the presence of only radial TTs τ_{dex}=0.21 sec, and in the presence of both radial and axial TTs τ_{dex}=0.31 sec (**Fig. 2.8**), which is ≈13-19 fold smaller than τ^{exp}_{dex}=3.9 sec.

It is reasonable to suggest though that dextran diffusion in TTs may not be free and its kinetics may be strongly or fully dominated by dextran binding to the membrane (e.g. glycocalyx or some components of extracellular matrix (Crossman et al., 2017)). The small size of TTs, and thus relatively high surface to volume ratio, would further support the above hypothesis. However, there are several pieces of experimental evidence that strongly argue against the significant contribution of membrane binding to the diffusion kinetics of dextran.

(a) If binding is involved, then it may contribute to the time course of diffusion as another component with different time constant since it is unlikely that free diffusion and binding would accidentally proceed with the same kinetics. The data, however, are well approximated by single exponential function. It should be noted though that the above argument will not be correct if membrane binding/unbinding kinetics of dextran is fast (τ_{on}/

τ_{off} constants significantly smaller than τ_{dex}). It has been shown by Bers and Peskoff (Bers and Peskoff, 1991) that in this case the apparent diffusion of dextran will simply be slowed by a factor of $1+2k/r_t$, where k describes binding according to $[dex]_{bound}=k[dex]_{free}$ and r_t is the TT radius. In particular, Bers and Peskoff (Bers and Peskoff, 1991) estimated that diffusion of Ca^{2+} in 200 nm diameter cylindrical TTs can be decelerated 5 fold due to Ca^{2+} binding. Unfortunately, we are not aware of any relevant binding data for the 3 kDa dextran used in our work which could be easily converted to the needed coefficient k.

In order to address the binding question experimentally, we have treated cardiac myocytes with neuraminidase A to further remove glycocalyx which can be considered as one of the most significant contributors to non-specific binding. However, the data in **Fig. 2.16** essentially ruled out this possibility.

The contribution of glycocalyx to the accessibility of TTs for small particles was studied by Parfenov et al. (Parfenov et al., 2006). The authors showed that in rat ventricular myocytes only particles less than 11 nm can enter the TTs, and that reducing the amount of glycocalyx by application of neuraminidase increased that threshold to only 16 nm. While no data on the kinetics of the diffusion of particles were provided the results are strongly supportive of the existence of very narrow constrictions of TTs where they operate by size exclusion mechanism.

(b) If dextran binding is indeed a contributing factor, then its apparent diffusion is unlikely to be affected by osmotic stress. However, hyposmotic swelling leads to dramatic (2-3 fold) decrease in the rate of dextran diffusion in the TT network (**Fig. 2.6**). We consider this finding as one of the most compelling evidence against significant effect of dextran binding to its diffusion rates. In particular, it is hard to come up with a solid

mechanistic explanation of how essentially non-specific membrane binding of dextran can be affected by osmotically-induced membrane stretch. Since under these conditions the overall (macroscopic) tortuosity of the TT network is not expected to change, an alternative explanation is required to accommodate the 2-3 fold increase in the diffusional time constant. In this regard, these data provide strong experimental support for significant structural nanoscopic remodeling of TTs diffusion pathway, e.g. development of tight constrictions (below).

(c) Changes in dextran size and viscosity of extracellular solution (see *Results*) lead to appropriate and quantitatively expected changes in τ_{dex} due to corresponding changes in free D^{f}_{dex}. However, it should be noted, again, that membrane binding cannot be easily excluded just based on this data.

(d) Perhaps the strongest support for essentially free diffusion of dextran in TTs comes from the data on diffusion of K^+ ions which may be considered as the least binding agents. Electrophysiological measurements showed that in mouse ventricular myocytes the time constant of diffusion of K^+ out of t-tubules $\tau_K \approx 120$ ms (Clark et al. (Clark et al., 2001)). The measured τ_K can be translated to τ_{dex} using the ratio of diffusion coefficients for K^+ and 3 kDa dextran in water, $D^{free}_{K} \approx 2 \cdot 10^3$ μm^2/sec (Friedman and Kennedy, 1955) and $D^{free}_{dex} = 150$ μm^2/sec (Kihara et al., 2013; Sandrin et al., 2016), respectively, leading to calculated $\tau_{dex} \approx 1.7$ sec which is close to a lower range of measured values (τ^{exp}_{dex}) in our study. The latter is consistent with the existence of a relatively minor binding of dextran to some, yet unknown, TT substrate. Unfortunately, the cell size was not reported in the study by Clark et al. (Clark et al., 2001), and the size of the cells used in our diffusion

experiments could potentially be somewhat biased to larger values leading to larger τ_{dex}^{exp}.

Diffusion of K^+ in TTs has been characterized in other studies (Swift et al., 2006; Yao et al., 1997) using electrophysiological approach combined with fast application of solutions. While the data in mentioned reports showed significantly slowed apparent diffusion of K^+ in TTs, quantitatively, the data in the Clark et al. (Clark et al., 2001) study can be considered most reliable because the employed approach does not rely on the technologically complicated perfusion systems, which may be prone to various artifacts.

Overall, assuming all the variables mentioned above, the data strongly support essentially free diffusion of dextran in TTs although some relatively minor contribution of binding cannot be fully excluded.

Accordingly, the next most plausible explanation of very large τ_{dex}^{exp} would be the presence of dilated and constricted regions along otherwise relatively 'straight' individual TT segments. Inclusion of such features in a model produces dramatic effects and brings the model closer to reality (**Fig. 2.9**). First, both dilations and constrictions slow apparent dextran diffusion. Second, it has been known for a long time that TT dilations and constrictions are common features of the t-system in normal and pathological states (Kostin et al., 1998; Maron et al., 1975; Ogata and Yamasaki, 1990; Pinali et al., 2013; Pinali and Kitmitto, 2014; Schaper et al., 1991), and it is quite surprising that they have not been taken into account in earlier quantitative studies addressing functional properties of TTs (e.g. electrical length constant). For example, optical microscopy studies of live ventricular myocytes showed that in rabbit and rat TTs diameter may vary ≈5-fold. In mouse, variation in TTs diameter is apparently smaller, ≈3-fold (Kong et al., 2017; Wagner

et al., 2012). However, mouse TTs are significantly smaller than those in rabbit (Kong et al., 2017) and even those in rat (Soeller and Cannell, 1999), and thus the variation in mouse TT diameter is likely underestimated because small and short running constrictions can simply be missed due to limited resolution. Inspection of electron microscopy and super resolution images of fixed tissues and cells indeed confirms the presence of very narrow regions of TTs, down to 50 nm and likely to even smaller diameters (Forbes et al., 1984; Pinali et al., 2013; Wong et al., 2013). The data in **Fig. 2.9B** show that TT dilations and constrictions of relevant sizes are dominant factors underlying slow apparent diffusion of dextran (and other small agents).

Electrical properties of TTs

One of the goals of microscopic and diffusional studies of TTs is to get a better understanding of their electrical properties which are difficult to assess directly due to their small size and intracellular location. A recent study in rat cardiomyocytes using an alternative diffusional approach estimated the electrical length constant of TTs to be λ≈290 μm (Scardigli et al., 2017). A similar value, λ≈240 μm, was derived from light microscopy imaging data for mouse TTs in another recent study (Kong et al., 2017). Both values are close to the earlier estimation of the length constant λ ≈226 μm (Pasek et al., 2008), and support the idea of a reliable electrotonic conduction at distances comparable within the size of cardiac myocytes.

However, there is one common step in all mentioned studies which leads to significant, at least several-fold, overestimation of the electrical length constant – the assumption that t-system can be approximated as a network of cylinders of the same average diameter. The latter justifies the use of some form of classical formula, e.g. $\lambda =$

$\sqrt{\frac{d_t R_m}{4R_i}}$, where d_t is average diameter of TTs, and R_m and R_i are membrane and bath solution resistivities, respectively. It is clear though that this formula cannot be used for tubes of variable diameter, and thus it cannot be applied to TTs containing dilations and constrictions.

The modeling data in our study show that the effects of dilations and constrictions of TTs on their electrical properties are similar in magnitude to the effects on t-tubular diffusion. The results are also quantitatively consistent with available data. In particular, Cheng et al. (Cheng et al., 2011) showed that the electrical time constant of mouse TTs τ^{exp}_{Vm}≈200 µsec. This value is very far from τ_{Vm}=10.1 µsec expected from cylindrical TTs with a diameter similar to the average value in mouse (200 nm *vs* 170 nm (Cheng et al., 2011)). In contrast, in the presence of short running 20 nm diameter constrictions the τ_{Vm} was increased 10-fold to τ_{Vm} =102 µsec. Assuming a number of experimental and modeling variables (cell size, magnitude of dilations and constrictions etc) involved in the analysis this is a strong quantitative match to the experimentally measured time constant τ^{exp}_{Vm}≈200 µsec.

Accordingly, and in contrast to previous studies, the numerically calculated length constant for a TT with a variable diameter - 200 nm cylinders with 20 nm constrictions spaced every 2 µm - is only ≈68 µm. This is >3-4 fold smaller than earlier estimates (Kong et al., 2017; Pasek et al., 2008; Scardigli et al., 2017). As mentioned in the study by Kong et al. (Kong et al., 2017), this steady-state value should be reduced by a factor of 2, to λ^{AP}≈34 µm, if one would take into account characteristic frequencies associated with action potential. The above estimations assume the resting state, and therefore, it is likely

that the length constant is even smaller during electrical activity of the cell or in any other situation where membrane resistivity may be reduced (e.g. due to activation of K_{ATP} channels in ischemic conditions or due to accumulation of interstitial or t-tubular K^+ during excessive activity leading to increased I_{K1} conductance).

2.7 Supporting Material

Technical implementation of dextran diffusion assay

Mechanical setup

Cells are first placed onto a custom-made perfusion chamber commonly used for electrophysiological recordings. The bath chamber is constantly perfused with Tyr solution using a peristaltic pump (by pumping air to the container with solution). The solution level in the perfusion chamber is regulated using a syringe needle connected to a vacuum.

One of the major challenges in our approach is to remove extracellular dextran fast enough, so the relatively small dextran fluorescence originating from a small volume of TTs (≈<3% of whole cell volume) can be well resolved using a wide field (non-confocal) microscope where the out of focus extracellular fluorescence has significant contribution to the useful signal. However, the bulk perfusion flow is not fast enough to remove extracellular dextran quickly, especially from the areas of restricted flow.

Therefore, to ensure proper flow of solutions all around the cell, individual cardiomyocytes are lifted ≈10 μm above the surface of the chamber using a holding pipette, so the cell can retain a stable position in a stream of local flow of Tyr solution produced by the washout pipette (see below). This approach turned out to be absolutely

essential to prevent artifacts arising from restricted flow between the cell and glass (**Fig. 2.10***)*.

Myocyte holding pipettes were crafted from borosilicate glass capillaries (OD: 1.5 mm, ID: 1.1 mm, BF 150-110-10: Sutter Instruments, Novato, CA) using Micro Forge MF-830 (Narishige, Japan). The long taper pipettes were carefully broken and the tips fire-polished to produce an opening of ≈30 µm (OD). The holding pipettes were filled with normal Tyr solution. A negative pressure in the capillary, usually in the range of -20 cm H_2O, was applied and monitored using Flex-Tube U-Tube Manometer (Dwyer, Michigan City, IN). The pipettes were mounted vertically onto a pipette holder controlled by MHW-3 hydraulic micromanipulator (Narishige, Japan) attached to MC-35A coarse manipulator (Narishige, Japan).

Washout pipettes were made of borosilicate glass capillary (OD: 1.0 mm, ID: 0.5 mm; BF 100-50-10; Sutter Instruments, Novato, CA), attached to a mechanical micromanipulator (MC-35A; Narishige, Japan) and the pipette opening positioned upstream of the recording region. Solution flow rate was regulated by hydrostatic pressure (≈50 cm H_2O) and turning flow On and Off was controlled either manually using stopcocks or through the use of electronically controlled solenoid valves. The solution flow rate in the washout pipette was ~240 µL/min for normal (*vs* more viscous) Tyr solution.

Dye application pipettes were pulled from the same glass capillaries as those used for holding pipettes but had tip diameters ≈3 µm. In most experiments pipettes were filled with Tyr solution containing 1 mg/mL of 3 kDa fluorescent dextran. Pipette solutions were filtered using PVDF 0.22 µm, 13 mm diameter syringe filters (CellTreat, Pepperell, MA). A positive pressure of ≈80 cm H_2O was constantly applied to the pipette to create a steady

stream of solution. The pipette was mounted onto P-621.2CD piezoelectric XY stage (Physik Instrumente L.P., Auburn, MA) controlled by E-621 Piezo Servo-Controller (Physik Instrumente L.P., Auburn, MA), so it could be moved axially as well as laterally for up to 100 µm in each dimension. The piezoelectric stage was also angled at ≈70° and the pipette aimed about upstream to the flow of the solution from the washout pipette. Movements of piezoelectric XY stage were achieved using a combination of same manipulators used for movements of holding pipettes. Movements of the application pipette beyond ≈50 µm in each dimension during local washout perfusion led to nearly complete suppression of background fluorescence (**Fig. 2.11**).

Optical setup

Illumination to the Nikon TE300 inverted microscope was provided by a HBO 100 W/2 Mercury short-arc lamp (Osram, Munich, Germany) powered by Mercury-100 W short arc DC power supply (Chiu Technical Corporation, Kings Park, NY).

The excitation light path consisted of a 100 µm diameter pinhole (allowing for spot illumination), focusing lens (not in the schematics; this lens is a part of original microscope setup), 540/25 bandpass excitation filter (all filters and mirror are from Chroma Technology Corporation, Bellows Falls VT), two neutral density filters (allowing for adjustments of light intensity), a home-made shutter, and a DM565LP dichroic mirror to excite tetramethylrhodamine labeled dextrans. A Nikon Apo 60x 1.40 NA oil λS objective was used to focus the excitation light on the specimen and to collect the emission light.

The emission light path consisted of a 580/25 bandpass filter and a 200 µm diameter pinhole located ‘confocally’ with the excitation pinhole. Emitted light was

collected by an 814 Photomultiplier Detection System (PDS; Photon Technology International, Birmingham, NJ) and the signals were digitized with the Digidata 1322A (Molecular Devices, Sunnyvale, CA) using Clampex 8.2 software (Molecular Devices, Sunnyvale, CA). For most of cell recordings, the signals were low-pass filtered by the PDS using 50 ms time constant and digitized at 50 Hz. For some test recordings, the time constant on PDS was set to 5 ms and signals sampled at 500 Hz (see *Performance of local application and washout of fluorescent dextran in cell free conditions* below).

To minimize potential photobleaching of the fluorophore and cell photodamage in all experiments the power of excitation light was minimized by setting the photomultiplier voltage to ≈800 V (high) while engaging appropriate neutral density filters to avoid saturation of the signal.

In order to estimate the dimensions of the recording spot a 175 nm (diameter) fluorescent bead (PS-Speck Microscope Point Source Kit, Thermo Fisher Scientific Inc., Waltham, MA) was attached to a small mica chip held by glass pipette using negative suction and scanned in X and Z (Y) directions using piezoelectric translational stage P-621.2CD (Physik Instrumente L.P., Auburn, MA) (**Fig. 2.12**). The size of the spot at the half of the maximal signal intensity was ≈3.5 μm x 3.5 μm x 5 μm. The spot is large enough to cover several sarcomeres, thus enclosing significant number of individual TTs, and yet it is quite small allowing to significantly minimize the unwanted fluorescence from traces of extracellular dextran.

Performance of local application and washout of fluorescent dextran in cell free conditions

To test the efficiency of the dye application and washout, the application pipette was positioned ≈5 μm above the surface of the chamber (in the absence of any cells), dextran solution was applied against the flow of Tyr solution from the washout pipette, and the recording spot site was positioned right above the top surface of the chamber. To ensure a more efficient removal of applied dextran, the dye application pipette was moved 100 μm (maximum allowed) in both the Z (vertical) and X (along the washout flow) directions. Under this conditions decline in recorded fluorescence was well fit by exponential function with the time constant of 40.7 ± 2.4 ms (n = 23).

Performance of local application and washout of fluorescent dextran using cardiomyocytes

Once proper flow of the washout pipette is confirmed, a cell is lifted with the holding pipette and positioned directly downstream of the washout pipette opening. The tip of the dye application pipette is positioned ≈10 μm above the surface of the myocyte to ensure that the hydrodynamic force produced by flowing solution does not significantly displace the cell (conversely, the cell would not shift when the dye pipette is retracted).

To maximize the TT fluorescence relative to the extracellular contamination, the recording spot must be positioned in the center of the cell. In order to achieve this, the flow from the washout pipette is temporarily paused allowing dextran solution to fully surround the cell, and the position of the recording spot is adjusted to achieve the lowest possible fluorescence signal which would correspond to the vertical position closest to the middle of the cell (**Fig. 2.13A&B***)*.

At this stage, despite the relatively small size of the recording spot located mostly inside the cell the remaining fluorescence is still dominated by the fluorescence of extracellular dextran because of the relatively small volume of TTs which are now filled with the dye.

Once the recording spot is appropriately positioned and the washout flow restored, the retraction of the dye application pipette leads to fast decline of fluorescence (**Fig. 2.2B**). However, in the presence of cardiomyocytes the signal is now better characterized by two exponential components, a large amplitude fast component with time constant <50 ms (similar to that in cell-free tests), and a smaller and slower component likely originating from t-tubular diffusion which can be well fit using time constant of ≈4 seconds (**Fig. 2.2C**). Note: for experimental data, the slow (TT) component of fluorescence decline was estimated using single exponential fit starting from 0.88–1.38 sec from the zero time (withdrawal of application pipette) which closely corresponds to the full amplitude of the slow component. In contrast, for modeling data (both inward going and outward going diffusion), the starting time corresponded to that when concentration declined or raised to 50% of the original value. It can be shown that the latter approach provides the best estimation of diffusion coefficient using the first term of the analytical solution of diffusion equation (20). Using earlier fitting time leads to ≈10% underestimation of the diffusion coefficient (data not shown).

Effects of mild osmotic stress on dextran diffusion

Application of both, 1.5 M formamide and 0.6 Na, osmotic stresses results in nearly complete loss of TTs and corresponding dramatic decrease in the amplitude of dextran fluorescence (**Fig. 2.4**), which in turn precludes *precise* measurements of diffusion

kinetics through the remaining TTs. To test whether diffusion assay is sensitive enough for detecting subtler changes in TTs structure cardiomyocytes were treated with a moderately hyposmotic 0.7 Na solution (~200 mOsm). As expected, the average amplitude of dextran fluorescence was decreased by 11.6 ± 18.5% (**Fig. 2.17A**, *p*=NS; n = 11), and the corresponding time constant was increased by 37.6 ± 21.0% (**Fig. 2.17B**, *p*=0.14).

The data demonstrate great cell-to-cell variability as one would expect for an effect close to some threshold state. Importantly, careful inspection of individual responses shows that some cells display essentially unchanged amplitude of dextran fluorescence and, yet, significantly increased time constant (**Fig. 2.17C**). This data strongly argue against any significant contribution of glycocalyx and extracellular matrix to the diffusion of dextran (**Fig. 2.16**) and, instead, are strongly consistent with a hypothesis that in these cells osmotic shock may lead to the development of relatively tight but short running constrictions of TTs, so that the volume of TTs (proportional to the amplitude of fluorescence) remains essentially unchanged.

Table 2.1. Specific gravity and viscosity measurements

(mean ± STDEV where available)

Solution	**Specific Gravity (g/ mL)**	**Kinematic Viscosity (cSt)**	**Dynamic Viscosity (cP)**	**n**
Normal Tyr	1.0170 ± 0.0002	0.908 ± 0.005	0.924 ± 0.005	6
5% 40 kDa dextran	1.0355 ± 0.0002	1.970 ± 0.010	2.040 ± 0.010	3
2% PVP	1.0212 ± 0.0004	1.377 ± 0.003	1.407 ± 0.003	3

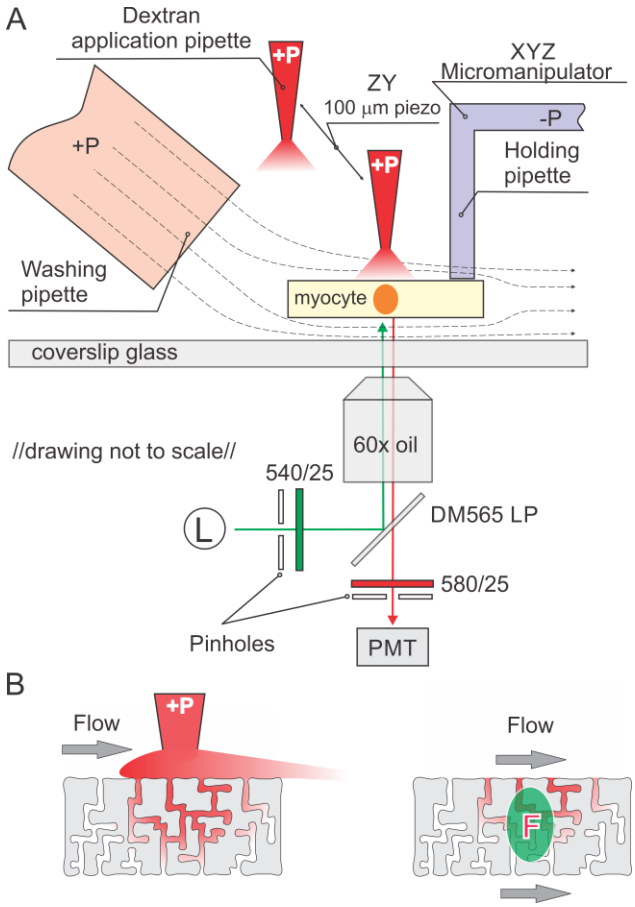

Figure 2.1 Schematics of the dextran diffusion assay

(A) Mechanical and optical setup for local application of dextran and spot recording of t-tubular fluorescence. ***(B)*** Principle of local application and recording of fluorescent intracellular (t-tubular) dextran.

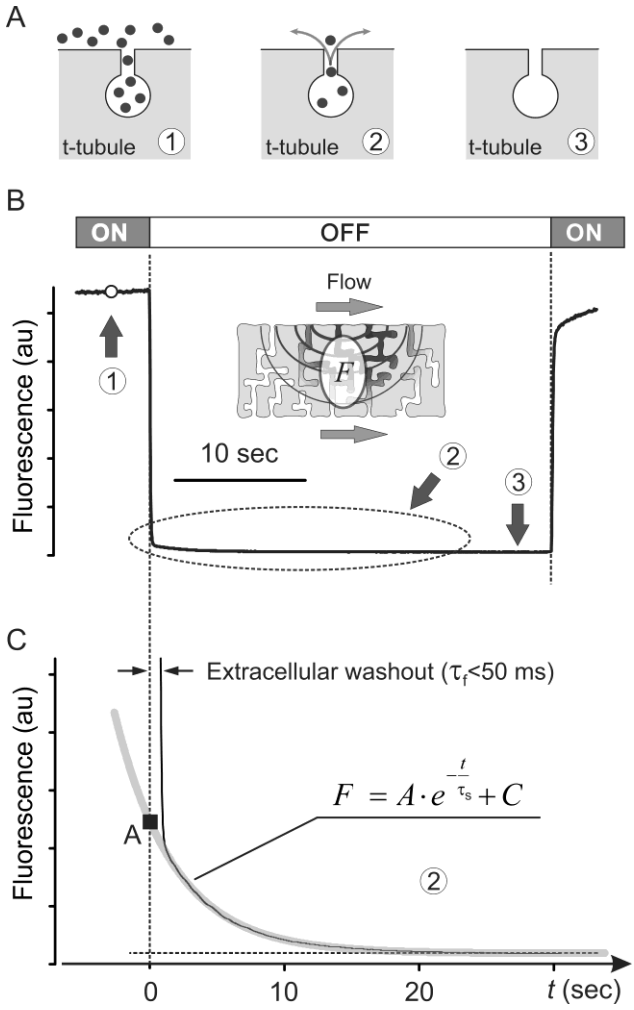

Figure 2.2 Properties of time-varying fluorescence observed in cardiomyocytes

(A) Major steps in the application and diffusion of fluorescent dextran (●). ***(B)*** Representative low magnification trace of dextran (3 kDa) fluorescence obtained with the diffusion assay. ***(C)*** Expanded scale of region (2) in *B* highlighting the presence of additional slow (≈4 sec) component of fluorescence due to the presence of TTs. The data (black thin line) were fit using single exponential function (gray thick line), where the *A* (■) is the amplitude of the slow component at time of withdrawal of the application pipette, τ_S is the time constant and *C* is the baseline fluorescence. τ_f is the estimated time constant of fast large amplitude component of fluorescence.

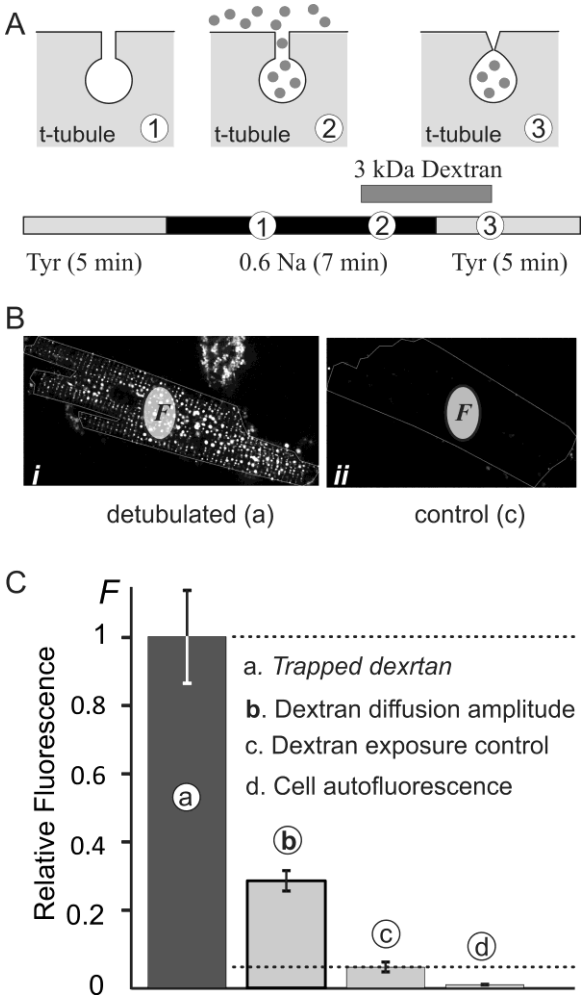

Figure 2.3 Relative amplitude of slow time-dependent component

(A) Detubulation protocol used to estimate the maximal fluorescence of t-tubular dextran. ***(B)*** Representative confocal images of detubulated *(i)* and control cell *(ii)* exposed to dextran but not subjected to stress). The fluorescence *(F)* was recorded from the indicated spot using the diffusion assay setup. ***(C)*** Quantification of the data. The amplitude of the slow time-dependent component measured using diffusion assay (**b**) is about 25% of maximal value (a) and significantly higher than that in cells not subjected to stress (but exposed to dextran; c) or cell autofluorescence (d).

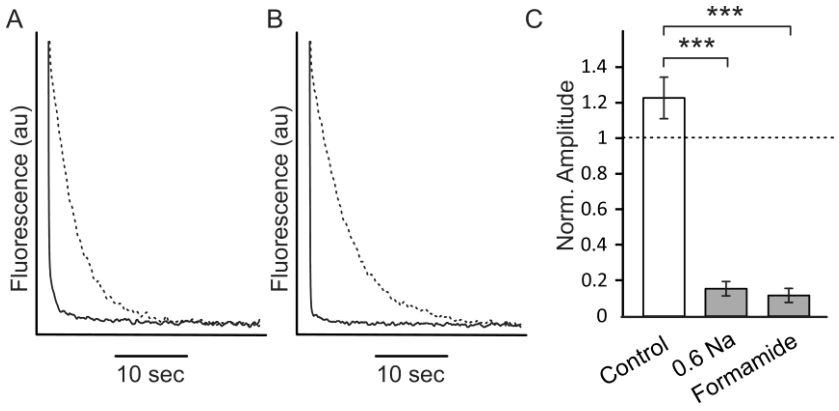

Figure 2.4 Effects of detubulation on the amplitude of slow component of dextran diffusion

(A and B) Representative fluorescence recordings from the same cell before (dotted lines) and after osmotic stress induced by application of hyposmotic 0.6 Na solution *(A)* or 1.5 M formamide *(B)*. ***(C)*** Quantification of the data. Control data correspond to timed recordings from normal cells exposed to Tyr solution for the duration of detubulation procedure (≈15 min). All data were normalized to that recorded at zero time. ≈20% increase in normalized amplitude (≈1.2) for control cells reflects a slow increase in the amplitude of dextran fluorescence, likely originating from slow remodeling of TTs during cells transition from storage solution to bath Tyr solution.

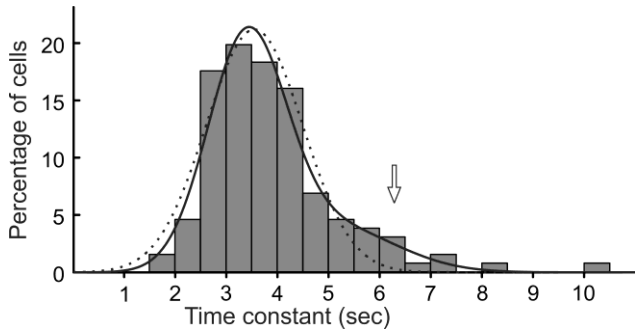

Figure 2.5 Distribution of dextran diffusion time constants in normal cells

Diffusion of 3 kDa dextran was measured in control Tyr solution from 131 cells and time constant was estimated using a single exponential fit. A histogram depicting the frequency of observed TT diffusion time constants is plotted along with fitted curves using a one-component Gaussian function $f(x) = \frac{1}{\sigma \cdot \sqrt{2\pi}} e^{-\frac{1}{2}\left(\frac{x-\mu}{\sigma}\right)^2}$ (dotted line) and a two-component Gaussian function $f(x) = \frac{A}{\sigma_1 \cdot \sqrt{2\pi}} e^{-\frac{1}{2}\left(\frac{x-\mu_1}{\sigma_1}\right)^2} + \frac{1-A}{\sigma_2 \cdot \sqrt{2\pi}} e^{-\frac{1}{2}\left(\frac{x-\mu_2}{\sigma_2}\right)^2}$ (solid line). $\mu = 3.55$; $\sigma = 0.94$; $\mu_1 = 3.39$; $\sigma_1 = 0.76$; $\mu_2 = 5.07$ $\sigma_2 = 1.23$.

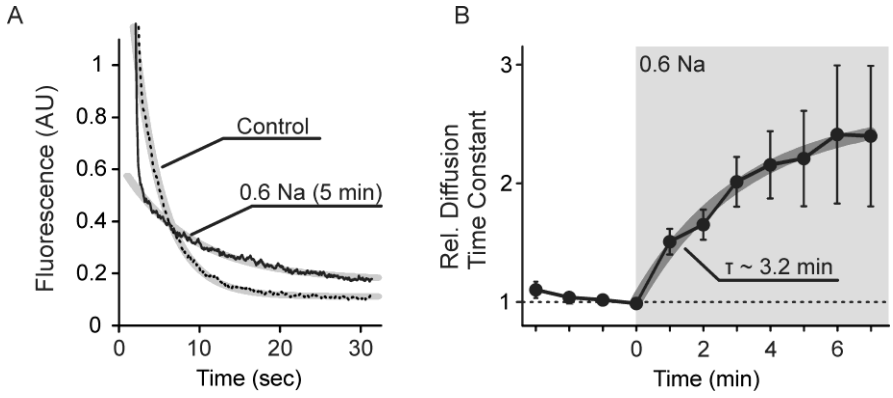

Figure 2.6 Cell swelling restricts t-tubule diffusion

(A) Representative traces from a single cell before (control, dashed line) and after 5 minutes treatment with 0.6 Na hyposmotic solution (solid line). The single exponential fits (grey highlight) for both traces are overlaid. *Note: the nearly vertical portion of the 0.6 Na trace that is not fit with the exponential function represents the washout component that is cropped out in the control trace.* ***(B)*** Normalized changes in time constant of dextran diffusion during exposure to 0.6 Na solution (n = 5-7 cells). Time constants are normalized to those measured immediately before application of 0.6 Na solution (time = 0 min).

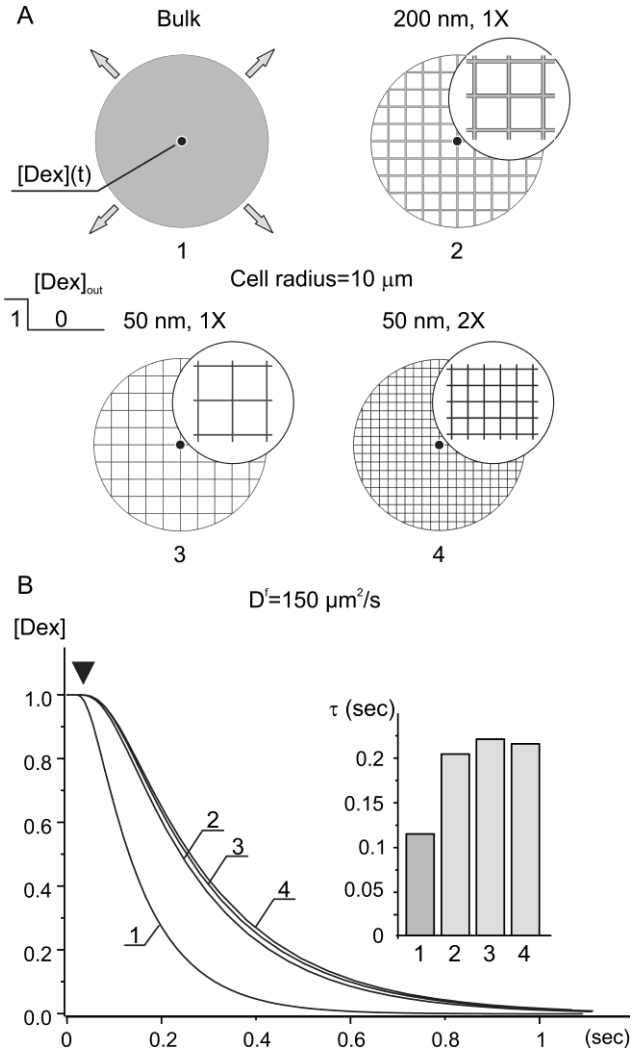

Figure 2.7 Computer modeling of radial (2D) diffusion of dextran.

(A) Cell is modelled as a cylinder with r_{cell}=10 μm, and axial symmetry allows for considering only radial diffusion. TTs are initially filled with dextran which is then allowed to diffuse in outward direction. Dextran concentration is calculated in the center of the cell as function of time assuming D^{free} =150 μm^2/s. TTs are modelled as a rectangular network of cylinders with indicated diameters. (1) free diffusion inside the cell allowed; (2-3) free diffusion is allowed in 200 nm and 50 nm TTs spaced at 2 μm and (4) 50 nm TTs spaced at 1 μm. ***(B)*** The time course of dextran concentration at the cell center is characterized by delay phase (▼) followed by quasi-exponential decrease with the time constants for corresponding TTs geometries (as indicated in *A*) shown in *Insert*.

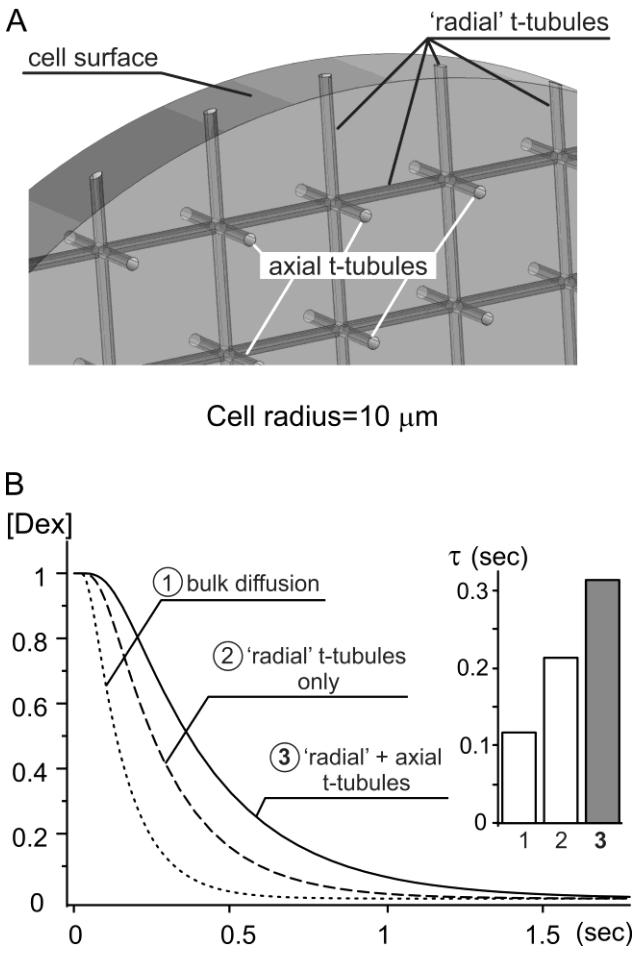

Figure 2.8 Computer modeling of 3D diffusion of dextran.

(A) TTs are modelled as 3D rectangular network of cylinders including axial elements. Axial periodicity of cardiac myocytes allows for modeling only one sarcomere segment: segment width=2 μm; r_{cell}=10 μm; D^{free} =150 μm^2/sec; 200 nm diameter TTs are spaced at 2 μm. ***(B)*** Time course of dextran concentration in the center of the cell for indicated geometries of TTs is compared to that of free bulk diffusion. 3D diffusion kinetics in the presence of radial TTs is identical to that obtained in 2D simulations (Fig. 7). The presence of axial TTs leads to ≈50% deceleration of dextran diffusion.

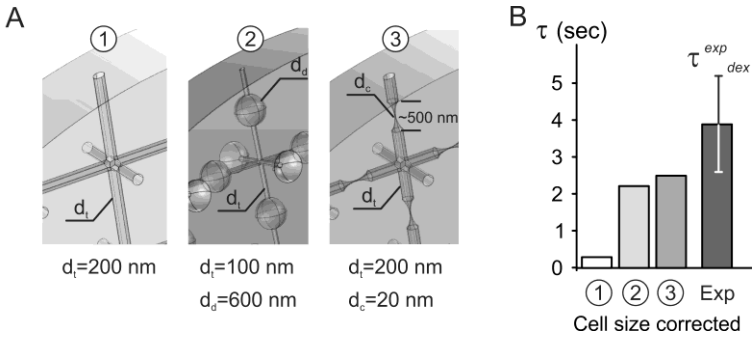

Figure 2.9 Effects of dilations and constrictions of TTs on the kinetics of dextran diffusion.

(A) TT dilations and constrictions are modelled using parameters as indicated, including segment width=2 µm, r_{cell}=10 µm, D^{free} =150 µm^2/sec, and TTs are spaced at 2 µm. ***(B)*** The presence of dilations and constrictions leads to >6-7 fold increase in the time constant of dextran diffusion (3 and 2 *vs* 1). The calculated time constants are 10% corrected for the measured cell size and compared to the experimentally measured time constant.

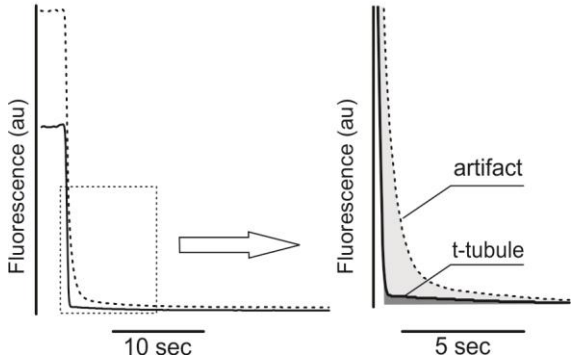

Figure 2.10 Efficient flow of bath solution around the cell is critical for correct measurement of t-tubular diffusion.

Fluorescence signals were obtained from a single cell with the holding pipette attached. *(Left)* The dashed trace presents the signal obtained when the cell is attached to the chamber surface. Raising the cell >10 µm above the chamber surface using holding pipette (Fig. 1; Main text) leads to significant changes in recorded fluorescence (solid line). *(Right)* Enlargement of the traces to the *Left* highlighting the magnitude of fluorescence due to slow washout of fluorescent dextran from the restricted space between the cell and the floor of the chamber.

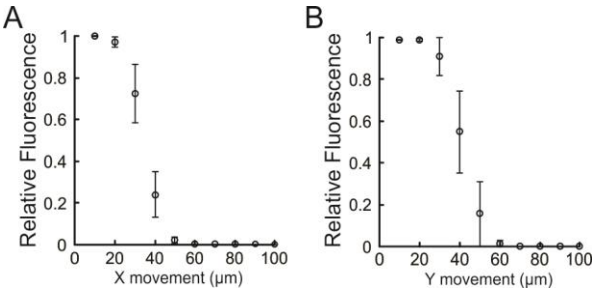

Figure 2.11 Effects of the movement of the dye application pipette on dextran fluorescence.

(A) and (B) The steady state fluorescence of dextran from a recording spot was measured as a function of pipette position in 10 µm increments using the settings (e.g. solution flow rates, pressures etc) similar to that employed in experiments with cells.

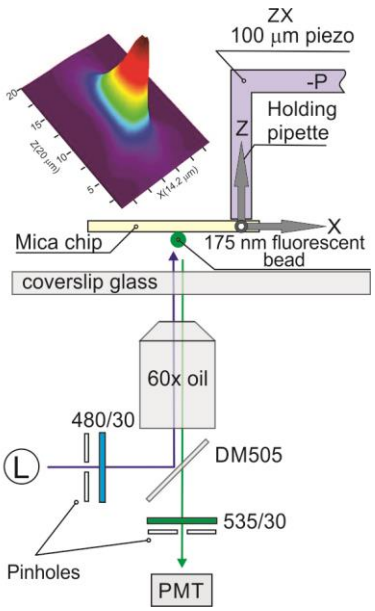

Figure 2.12 Experimental setup for the measurements of spot spread function

Insert: Estimated spot spread function profile.

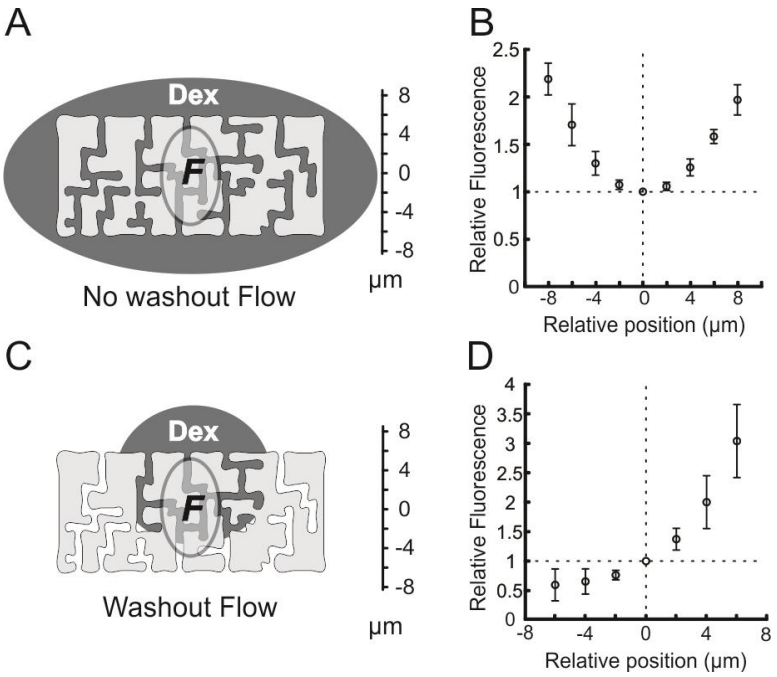

Figure 2.13 Effect of position of recording spot on dextran fluorescence

(A) Cartoon depicting dextran distribution when the washout flow is stopped. The oval (***F***) represents the recording spot. ***(B)*** The fluorescence was measured at different vertical (Z) positions of the recording spot in 2 µm increments with positive values corresponding to regions above the cell. Position is relative to that corresponding to minimum fluorescence, and the data are normalized to the minimal value. ***(C)*** Cartoon depicting the dextran distribution with local bath perfusion engaged (Fig. 1; Main text). ***(D)*** Total fluorescence was measured and presented as described in *B*.

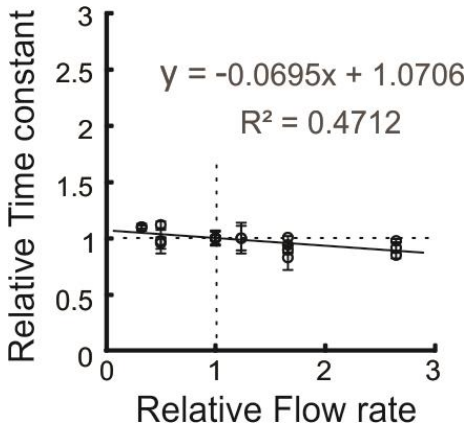

Figure 2.14 Dependence of t-tubular time constants on washout flow rate.

The flow rate was adjusted by modulating the hydrostatic pressure applied to the washout pipette (Fig. 1; Main text) while measuring time constant of the same cell. Time constants are normalized to that recorded at normalize normal flow rate (i.e. =1), and the flow rates are normalized to normal flow rate (=1) as well.

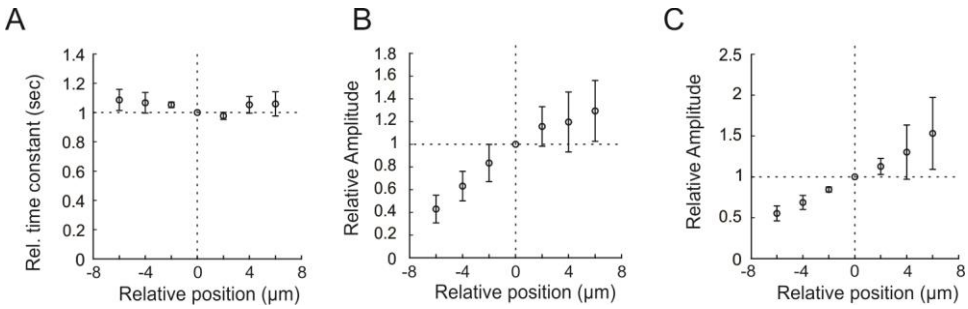

Figure 2.15 Dependence of t-tubular time constants on position of recording spot.

Sequential measurements of dextran diffusion were performed on the same cell (n = 3) as the position of the recording spot was adjusted as described in **Fig. 2.13**. Relative changes in t-tubular time constant (A), in the amplitude of the TT component (B) and in the steady-state value of the t-tubular component (C) as a function of focal plane height as a function of spot position.

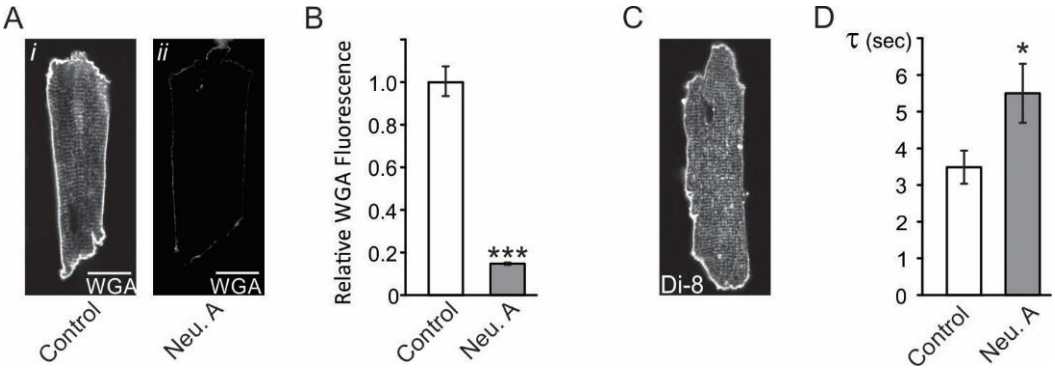

Figure 2.16 Effects of Neuraminidase A

(A) Representative confocal images of cardiomyocytes labeled with fluorescent WGA (Wheat Germ Agglutinin; Alexa Fluor 633, Thermo Fisher Scientific) following a 1 hour incubation with *(i)* no Neuraminidase A (control) and *(ii)* 0.25 U/mL Neuraminidase A (Worthington Biochemical Corp, Lakewood, NJ) in C solution at 36 °C. Scale bars: 20 µm. ***(B)*** Quantification of intracellular (i.e. t-tubular) WGA fluorescence in control cells and in cells following Neuraminidase A treatment (n = 31 and 30 cells, respectively). ***(C)*** Representative confocal image of cardiomyocyte treated with the Neuraminidase A as described above and labelled with Di-8-ANEPPS shows an intact TT network. ***(D)*** Quantification of TT diffusion time constant in control cardiomyocytes and cells after Neuraminidase A treatment (n = 10 each).

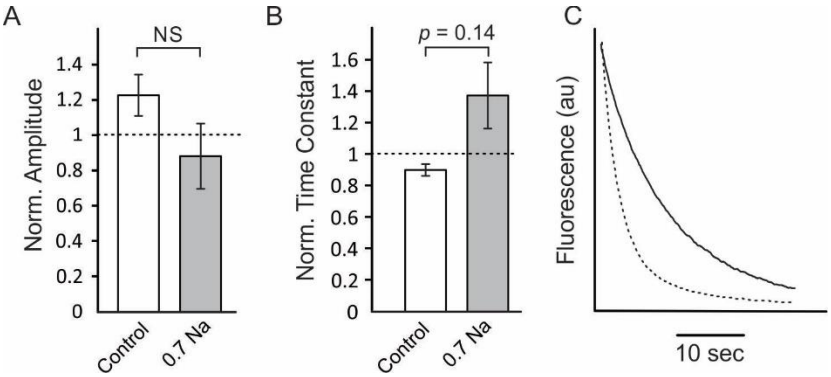

Figure 2.17 Effects of mild hyposmotic stress on dextran diffusion

(A) Quantification of the changes in the t-tubular fluorescence amplitude and ***(B)*** diffusion time constant after timed control measurements and after hyposmotic shock with 0.7 Na solution. ***(C)*** Example of recordings from a cell that displayed significant deceleration in diffusion kinetics (solid line *vs* dashed line for control) after exposure to 0.7 Na solution.

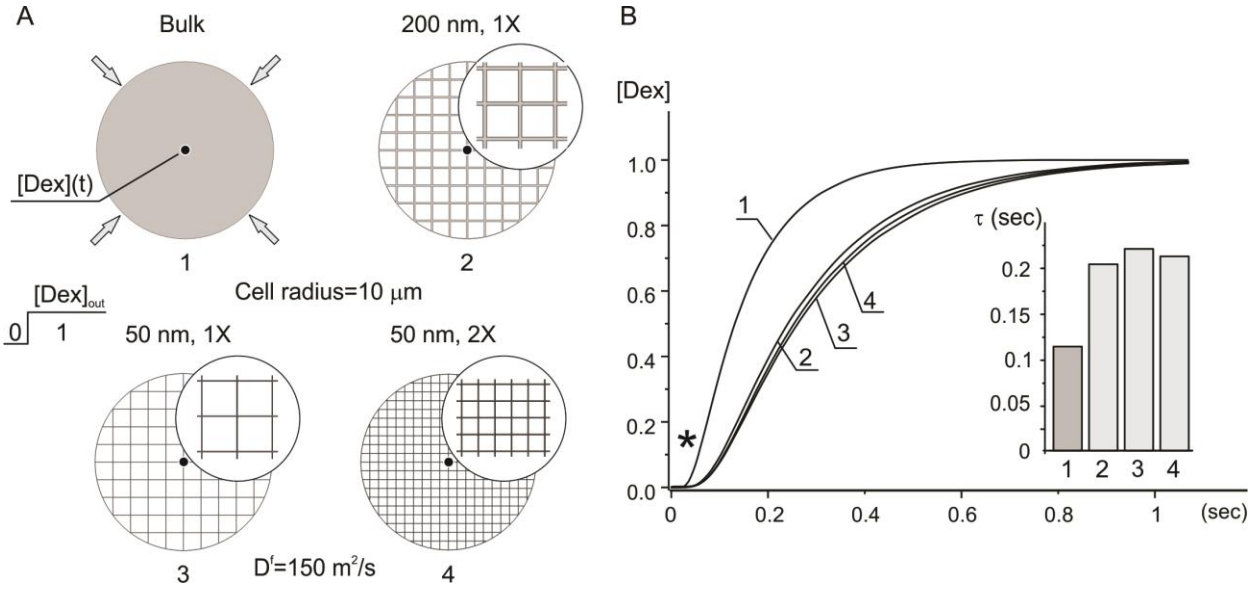

Figure 2.18 Computer modeling of radial (2D) inward-going diffusion of dextran.

(A) Cell is modelled as a cylinder with rcell=10 μm, and axial symmetry allows for considering only radial diffusion. Dextran is applied from outside and its concentration calculated in the center of the cell as function of time assuming Dfree =150 μm2/sec. TTs are modelled as a rectangular network of cylinders with indicated diameters. (1) free diffusion inside the cell allowed; (2-3) free diffusion is allowed in 200 nm and 50 nm TTs spaced at 2 μm and (4) 50 nm TTs spaced at 1 μm. ***(B)*** The time course of dextran concentration at the cell center is characterized by delay phase (*) followed by quasi-exponential increase with the time constants for corresponding TTs geometries (as indicated in A) shown in Insert.

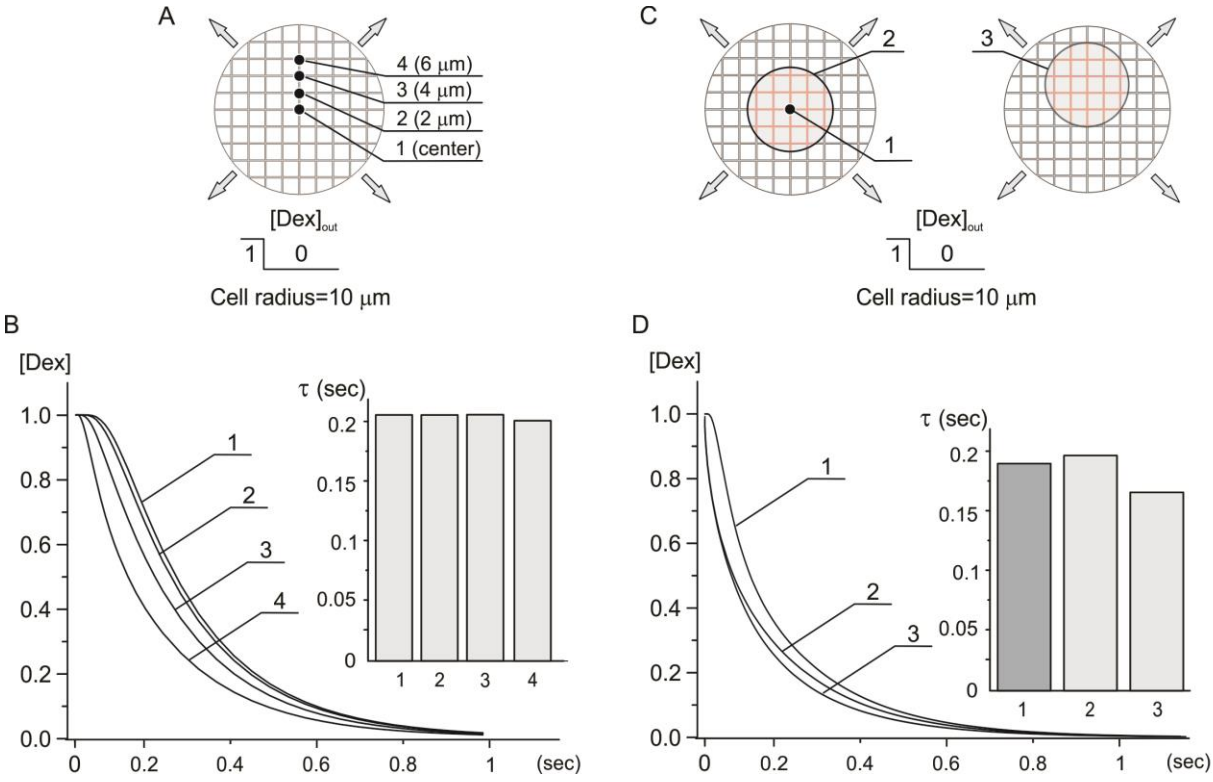

Figure 2.19 Computer modeling of outward-going diffusion of dextran and effects of spot recording.

(A) Dextran is allowed to freely diffuse in outward direction from prefilled cylindrical TTs and the calculated time course of its concentration at the indicated positions is presented in *B*. ***(B; Insert)*** The time constant of dextran diffusion is essentially independent of the position of recording point. ***(C)*** Dextran is allowed to freely diffuse in outward direction from a spot of prefilled cylindrical TTs and the calculated time course of its average (within the spot) concentration at the indicated positions of the spot is presented in *D* along with that using point recording at the cell center. ***(D; Insert)*** The time constant of dextran diffusion is essentially independent of the mode of recording. *Insert:* calculated time constants. D^{free} =150 μm²/sec; 200 nm diameter TTs are spaced at 2 μm.

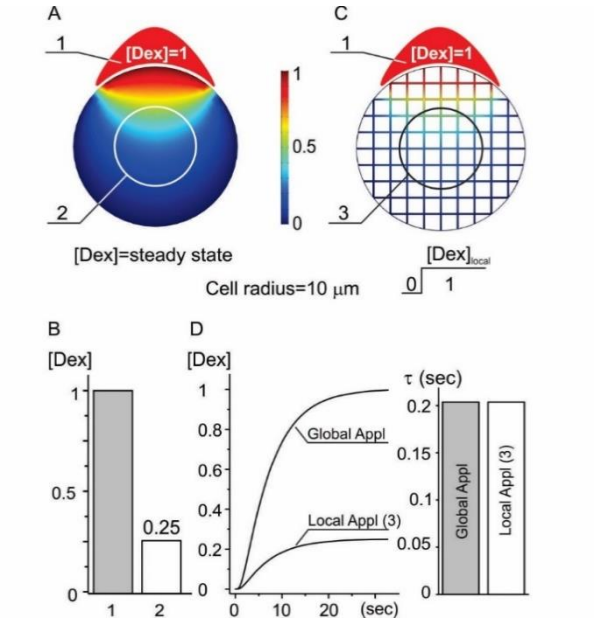

Figure 2.20 Effects of local application of dextran.

(A) Steady state local application of dextran leads to its characteristic gradient distribution inside the cell. Dextran is allowed to freely diffuse within the cell while its outside concentration beyond application area is set to zero. ***(B)*** Averaged concentration of dextran in the recording spot (2) is ≈25% of the applied concentration (1). ***(C)*** Locally applied dextran is allowed to freely diffuse through TTs while its outside concentration beyond application area is set to zero. ***(D)*** Comparison of local and global application of dextran. The time course of dextran concentration in the recording spot (3; in *C*) is identical in both modes of application.

CHAPTER 3 T-TUBULE CONSTRICTIONS PROMOTE T-TUBULE SEALING

3.1 Acknowledgements

This chapter represents a manuscript in preparation and includes data contributed by Azadeh Nikouee and Greta Tamkus (dextran trapping experiments). This work was supported by the National Institutes of Health (HL127023 to ANL and T32-GM008322 to KU), and the American Heart Association (17PRE33350049 to KU).

3.2 Introduction

The properties of biological membranes determine how they respond to external forces. The elastic modulus, the ratio of the applied force and the resulting deformation (expansion or compression), of cell membranes is high (Diz-Munoz et al., 2013; Hochmuth et al., 1973). This value indicates that membranes are highly resistant to mechanical compression or expansion. On the other hand, the low bending stiffness (Diz-Munoz et al., 2013; Hochmuth et al., 1996) reflects the flexible nature of membranes. These two parameters dictate that membranes behave as incompressible/non-expandable sheets that readily fold/unfold. Indeed, when artificial bilayers are exposed to mechanical or osmotic forces, ruffled or reservoir membranes will passively unfold to match the required surface area and, conversely, will spontaneously form protrusions when the membrane is compressed (Staykova et al., 2013; Staykova et al., 2011).

Cells undergo significant shape and volume changes that necessitate dramatic alterations in the cell surface area (Morris and Homann, 2001). Large amounts of

membrane reservoirs in the form of caveolae (Sinha et al., 2011), membrane folds (Dulhunty and Franzini-Armstrong, 1975), or intracellular vesicles (Gauthier et al., 2011) can dynamically incorporate into, or are sequestered from, the surface membrane to accommodate the demand for membrane surface area following shape and volume changes. However, these reservoir membranes can passively mis-fold following the removal of hyposmotic stress (Kosmalska et al., 2015). In particular, vacuole-like dilations (VLDs), which are large surface membrane balloons created by extracellular fluid bulging into the cytoplasm, can form following removal of hyposmotic stress in fibroblasts and neurons (Kosmalska et al., 2015; Reuzeau et al., 1995). In these studies, VLDs formed specifically on the bottom membrane of the cell which contacts the culture substrate suggesting that the interaction between the membrane and an extracellular scaffold is necessary. Recent work from our lab has demonstrated that a similar removal of hyposmotic stress in cardiomyocytes can cause t-tubule sealing and the formation of dilated t-tubules (Moench et al., 2013). This similarity between osmotic detubulation and VLD formation suggests that both phenomena may be mechanistically related and understanding the forces induced by cell shrinking may provide insights into how certain membranes aberrantly form into vacuolar structures.

Here, we modified previous detubulation methods to demonstrate that cell shrinking is sufficient to detubulate cardiomyocytes. T-tubule stability was assessed by titrating the amount of osmotic stress and ‘stress-testing’ cardiac t-tubules to the point of sealing. Using this approach, we found that detubulation is a threshold phenomenon and the minimum necessary requirements for detubulation in live adult mouse cardiomyocytes were quantified. Furthermore, the formation of dilated t-tubules was strongly promoted by

the presence of t-tubular constrictions. Overall, the data suggest that the mechanism of osmotic detubulation is consistent with the formation of VLD reported in other cell types and is highly dependent on the geometry of sub-microscopic t-tubular structures.

3.3 Materials and methods

Detailed descriptions of the animals, solutions, chemicals, myocytes isolation, dextran trapping assay, confocal imaging, dextran diffusion assay, and data analysis are presented in Chapter 2.3. The cardiomyocyte cell width measurements are performed as described in Chapter 4.3.

The strength of hypo- and hyperosmotic NaCl solutions are indicated as the [NaCl] relative to isosmotic Tyrode solution. For example, a hyperosmotic solution containing twice the NaCl concentration of isosmotic Tyrode solution is denoted 2.0 Na.

3.4 Results

Hyperosmotic stress is sufficient to detubulate mouse cardiomyocytes

We began by testing whether hyperosmotic stress alone, without cell swelling, is sufficient to seal cardiac t-tubules. To test this hypothesis, a modified dextran trapping assay was performed using hyperosmotic solutions prepared by the addition of excess NaCl. Hyperosmotic solutions were applied to cardiomyocytes in the presence of fluorescent dextran, which was removed prior to the removal of hyperosmotic stress. In doing so, this protocol specifically tested for t-tubule sealing during cell shrinking and not during the cell swelling that occurs when hyperosmotic stress is removed. A cardiomyocyte detubulated using previously described 0.6 Na hyposmotic stress was included as a control. As **Fig 3.1A&B** shows, application of hyperosmotic NaCl stress

was sufficient to cause dextran to become trapped within the t-tubule lumen in a dose-dependent manner. Using a 2.0 Na hyperosmotic solution resulted in a nearly uniform trapping of dextran throughout the t-tubule network of the cardiomyocyte, similar to that observed with hyposmotic 0.6 Na detubulation. Moderate hyperosmotic stresses (1.5 Na) resulted in 'patchy' patterns of dextran trapping suggesting that some t-tubules within the network fully seal while other t-tubules remain open. Remarkably, there was essentially no trapping with hyperosmotic 1.25 Na solution suggesting that a threshold stress is necessary for detubulation (**Fig 3.1B**).

Qualitatively similar results were obtained with solutions made hyperosmotic by the addition of sucrose (**Fig 3.1C**). With relatively low concentrations (100 mM) of sucrose, cardiomyocytes show little dextran trapping consistent with our previous findings (Moench et al., 2013). However, when greater concentrations of sucrose are used, hyperosmotic sucrose solutions also detubulate cardiomyocytes in an osmolarity dependent manner that also displays a threshold response. Oddly, in contrast to NaCl, the maximal amount of trapped dextran peaks at ~65% of the trapping observed with hyposmotic stress even with 0.5 M sucrose suggesting that an additional factor may inhibit t-tubule sealing with sucrose. Indeed, when the magnitude of dextran trapping is plotted against solution osmolarity, dextran trapping with sucrose is right shifted compared to that observed with NaCl, suggesting that sucrose is protective against t-tubule sealing. (**Fig 3.1D**). Overall the results confirm that hyperosmotic cell shrinking is sufficient to induce t-tubule sealing in a dose dependent manner.

Estimation of threshold for hyposmotic detubulation

The unexpected finding of a threshold phenomenon for hyperosmotic detubulation suggested that perhaps hyposmotic detubulation would also display a threshold response. Therefore, a series of experiments using hyposmotic stresses were performed to measure the presumed threshold value.

Similar to hyperosmotic detubulation, hyposmotic detubulation also shows a dose dependence that displays a clear threshold phenomenon (**Fig 3.2**). We began by simply modulating the duration of the hyposmotic 0.6 Na stress prior to detubulation. The top panel of **Fig 3.2A** plots the magnitude of the dextran trapping as a function of the duration of the 0.6 Na stress from 1 to 7 minutes. The plot clearly shows a dependence of t-tubule sealing on the duration of the hyposmotic stress. When a single exponential function was fitted to the data (grey highlight), the x-intercept of the fitted curve did not lie at zero time, again indicating that a certain threshold is required for dextran trapping. Rather, the fitted curve intercepted the X-axis at 0.69 minutes, demarcating the minimum exposure time to 0.6 Na stress necessary before dextran trapping is practically observed.

Using the threshold duration calculated above, we next determined the corresponding cell width observed during 0.6 Na swelling. Cardiomyocytes exposed to 0.6 Na solution will swell with kinetics that can be accurately estimated with a single exponential function (time constant ~1 min, **Fig 3.2B**; bottom panel). At the threshold time of 0.69 min (dashed vertical line), cardiomyocyte width is estimated to be increased by 6.6%. This result is consistent with the threshold observed during the hyposmotic dose response experiments. As shown in **Fig 3.2C**, increasing the magnitude of hyposmotic stress causes a corresponding increase in cell swelling (measured at 7 minutes) and in dextran trapping. Note how cardiomyocytes exposed to 0.8 Na solution increase in width

by only ~6%, slightly below the estimated threshold value, and display barely detectable dextran trapping (~3% of control 0.6 Na trapping). However, cardiomyocytes exposed to 0.7 Na solution increase in cell width by ~9.5%, well beyond the threshold, and display obvious dextran trapping (~48% of control 0.6 Na trapping). Overall, the results demonstrate that detubulation with both hypo- and hyperosmotic stress displays threshold phenomena.

Water flow during detubulation

Osmotic volume changes have been extensively studied in cardiomyocytes. Based on hydraulic conductivity measurements, volume changes in cardiomyocytes likely occur predominantly by water permeation through the lipid bilayer (Suleymanian and Baumgarten, 1996). Cell width provides an accurate estimation of total volume changes because (1) the cell length remains largely unaffected by osmotic stress (Drewnowska and Baumgarten, 1991) and (2) the cell width to vertical thickness ratio remains constant through a range of osmotic stresses (Ogura et al., 2002). Furthermore, regulatory volume decrease or increase are negligible at room temperature (Suleymanian and Baumgarten, 1996). In effect, the cardiomyocyte can be treated as a cylindrical, nearly-perfect osmometer.

Let’s assume a model cylindrical cardiomyocyte 100 μm in length and 20 μm in width. This cell has an initial volume of 125.7 pL and a t-tubular luminal volume of 3.8 pL based on estimates that ~3% of the total cell volume in cardiomyocytes is occupied by the t-tubular lumen (Soeller and Cannell, 1999). If this cell experiences a threshold hyperosmotic shock that causes a 6.6% reduction in the cell width, the cell volume will decrease by 16.1 pL to 109.6 pL based on geometric considerations alone. Assuming

that the hydraulic conductivity of the cell is homogeneous throughout the entire cell membrane and that 35% of the total cell membrane lies within the t-tubular network (note, 35% is near the lower limit of the estimated cell membrane fraction within t-tubules (Pasek et al., 2008)), approximately 5.6 pL of water will move into the t-tubular lumen. This is a remarkable amount of water that can enter the t-tubule network (~150% of the initial t-tubule luminal volume) before t-tubular structural remodeling becomes apparent.

Of course, water flow into the t-tubule lumen does not happen instantaneously. Cardiomyocyte volume changes in response to hyperosmotic steps can be approximated with an exponential decay with time constants ~1 min (Suleymanian and Baumgarten, 1996; Uchida et al., 2016). For simplicity, let's estimate that the total volume change occurs over 60 seconds at constant flow rate. This results in water flowing into the t-tubule lumen at a rate of ~0.09 pL/s. If we make the assumption that the t-tubule network consisted of a collection of tubes of equal diameters, then we can estimate the linear flow rate through t-tubular openings. The number of t-tubule openings can be approximated as 0.3 openings/μm^2 of surface membrane (not including t-tubular membrane area) (Pasek et al., 2008), resulting in an estimated 3770 cylindrical t-tubules for this cell. In this simplified model, we can estimate a linear flow rate of 0.79 µm/s through the t-tubule openings.

Is this flow rate is even possible within t-tubules? One possibility is that the narrow t-tubule diameter may strongly resist flow. In the scenario above, the flow through a single cylindrical t-tubule is $2.5x10^{-5}$ pL/s. One can estimate the pressure necessary to sustain this flow rate in this tube using Poiseuille's law. Assuming a length of 6.87 µm (Soeller and Cannell, 1999), a constant radius of 100 nm, and the viscosity for water at 25°C (8.9

x 10^{-4} Pa·s), only ~3.9 Pa (0.03 mmHg) of pressure is necessary for this water flow to occur, suggesting that these cylindrical t-tubules provide little resistance to water movement. However, it should be noted that this pressure is inversely dependent on the fourth power of the t-tubular radius. Even a small decrease in t-tubular radius can dramatically increase the resistance to flow. For example, a single 100 nm segment with a diameter of 20 nm can increase the resistance to flow by over 500 Pa. Overall, these simple calculations demonstrate that the resistance to water flow within t-tubules is highly variable depending on t-tubular diameter.

T-tubule constrictions modulate t-tubule sealing

The data above clearly demonstrate an osmolarity dependence for both hypo- and hyperosmotic detubulation. We previously demonstrated using our newly developed dextran diffusion assay that hyposmotic 0.6 Na stress can restrict diffusion in t-tubules (Uchida and Lopatin, 2018), suggesting that t-tubules are likely constricted during cell swelling. This raised the question of whether the state of the t-tubules has any role in determining the t-tubular stability in response to osmotic stress. To test this, a method of inducing graded levels of t-tubular constrictions was developed. Dextran diffusion time constants were measured while cardiomyocytes were perfused with varying hyposmotic stress. As **Fig 3.3A** shows, control cells perfused with normal Tyrode solution displayed a small gradual decrease in the relative time constant, suggesting that the diffusion of dextran becomes slightly faster over time, consistent with our previous observation (Uchida and Lopatin, 2018). Exposure to hyposmotic stress, however, caused a significant increase in the relative time constant in an osmolarity-dependent manner (i.e. diffusion of dextran out of the t-tubular network takes longer when cells are swollen).

Importantly, upon exposure to all levels of hyposmotic stress, the dextran loaded into the t-tubule network dissipated out of the cell with kinetics characterized by a longer time constant than that observed prior to cell swelling. Although cell swelling alone will increase the diffusion time constant by simply increasing the distance for dextran to travel, in all hyposmotic stresses tested, the magnitude of the change in time constant is significantly greater than that expected solely with geometric changes thus indicating the development of t-tubular constrictions. Therefore, the data likely demonstrates graded, hyposmotic stress-dependent development of t-tubular constrictions.

To test the hypothesis that t-tubular constrictions affect t-tubular stability, groups of cardiomyocytes were detubulated using a constant 0.4 Na osmotic gradient (~90 mOsm step) but with some groups pre-exposed to hyposmotic stress for 7 minutes. Surprisingly, a cardiomyocyte exposed to 1.4 Na solution from an isosmotic Tyr shows very sparse dextran trapping while a different cardiomyocyte exposed to the same osmotic gradient but starting in the hyposmotic 0.6 Na solution displays nearly complete t-tubule sealing (**Fig 3.4A**). As shown in **Fig 3.4B**, there is a clear relationship between the magnitude of the prior hypo- osmotic stress and the resulting dextran trapping, suggesting that cell swelling strongly predisposes these t-tubules to undergo sealing during the subsequent hyper- osmotic shock.

Since the diffusional time constant is an estimate of the magnitude of t-tubular constriction, the relative dextran trapping magnitude (from **Fig 3.4B**) was plotted against the normalized time constant 7 minutes after the start of hypo-osmotic stress (from **Fig 3.3B**). As shown in **Fig 3.5**, there is a remarkably strong correlation between the relative diffusion time constant and the resulting dextran trapping. These results demonstrate that

hyposmotic stress strongly predisposes t-tubules to detubulate and suggests that t-tubule constrictions lead to reduced stability.

Membrane dynamics in cells is strongly dependent on the membrane-cytoskeleton adhesion energy. Under excessive stresses, the lipid bilayer can be ‘peeled off’ from the underlying cytoskeleton and become freely responsive to external stresses, such as in the case of membrane blebs. Previous work demonstrated that crosslinking transmembrane proteins with the heterodimer lectin wheat germ agglutinin (WGA) can make the membrane stiffer and resistant against blebbing (Charras et al., 2005; Evans and Leung, 1984). Therefore, we hypothesized that WGA may protect against t-tubule constrictions during hyposmotic stress. Unexpectedly, treatment of cardiomyocytes with high concentrations of WGA (1 mg/mL) in the absence of osmotic stress caused a significant ~2-fold increase in the time constant of dextran diffusion (**Fig 3.6A&B**). Although the mechanism by which WGA slows diffusion in t-tubule lumens is unknown, it served as a useful tool to test whether modulation of t-tubular diffusion corresponds to changes in the propensity for t-tubules to seal. To test this, WGA treated cells were exposed to 0.7 and 0.6 Na hyposmotic detubulation. As shown in **Fig 3.6C**, WGA treated cells display an increase in dextran trapping compared to non-treated cells. These results strengthen the notion that t-tubular diffusional properties strongly correlate with the magnitude of t-tubular sealing following cell shrinking.

3.5 Discussion

In this study, we demonstrated that hyperosmotic stress with NaCl and sucrose is sufficient to induce t-tubule sealing in adult mouse cardiomyocytes (**Fig 3.1**). The quantitative difference between NaCl and sucrose remains unknown although we

speculate that solution viscosity may play a role. Additional studies are necessary to elucidate the difference between these two approaches.

Forces involved in the formation of t-tubule vacuoles

The data above demonstrated that cell shrinking is sufficient for detubulation in cardiomyocytes. During cell shrinking, negative pressure develops within the cell that pulls the membrane inward. This pressure will act uniformly throughout the membrane. However the following observations demonstrate that there is significant heterogeneity in the response of the membrane to the negative pressure: (1) VLD formation is only observed on the bottom membrane of cultured cell that is firmly attached to a substrate (Kosmalska et al., 2015; Reuzeau et al., 1995). (2) Dextran trapping in cardiomyocytes is confined to the t-tubular lumen— dextran fluorescence is not observed along the perimeter of the myocyte indicating that t-tubular membranes respond to the same negative pressure differently than surface membranes even though, presumably, the surface membrane will also have regions of unsupported membranes. At first glance, these observations may suggest that certain membranes are less supported by the underlying cytoskeleton and may be more prone to deformation. However, contrary to expectations, **Fig. 3.6** demonstrated that stabilization of the sarcolemmal membrane with WGA results in greater detubulation. Additional factors must play a role. Here, I will argue that the geometry of the membrane strongly determines the response of these membranes to external forces.

An estimate of the negative pressure necessary to induce detubulation can be obtained from the threshold for dextran trapping. The threshold value that we estimated for dextran trapping is roughly 0.8 Na hyposmotic stress or 1.2 Na hyperosmotic stress.

In perfect osmometers, this osmotic gradient corresponds to a hydrostatic pressure of ~130 kPa. This negative pressure applied to the entire sarcolemmal membrane can have different effects depending on the geometry of the t-tubules. Laplace's law states that the wall stress applied to a thin walled tube is proportional to the pressure applied and inversely proportional to the radius of the tube. Larger diameter t-tubules will experience greater stress (membrane tension) than narrower t-tubules. For example, a 100 nm radius tubule experiencing this pressure will have a linear tension of ~12.8 mN/m. This tension is comparable to the lytic tension of unsupported skeletal muscle sarcolemmal vesicles (Nichol and Hutter, 1996). Yet, lysis of the t-tubule membrane is not observed (dextran fluorescence is confined to discrete, vacuolated t-tubules and does not display a diffuse background staining). In reality, much of the osmotic pressure is dissipated by water flow (i.e. volume change) and the actual tension applied to the membrane is likely much lower. Although the exact magnitude of membrane tension within the t-tubular network remains an open question, heterogeneity in membrane tension must develop due to the variable t-tubular geometries.

Due to the properties of biological membranes discussed in the introduction (Chapter 3.1), heterogeneity in membrane tension results in a redistribution of the membrane (Morris and Homann, 2001). During cell shrinking, the high local membrane tension at dilated t-tubules will be expected to draw more membrane area from the excess reserve membranes available after cell swelling. Increased membrane tension, which increases the area per lipid molecule (Reddy et al., 2012), is predicted to increase water permeability of membranes (Lande et al., 1995; Mathai et al., 2008). Therefore, dilations will continue to grow as intracellular water preferentially flows into these areas. This is

consistent with the observation that cells grown on porous substrates do not develop VLDs (Kosmalska et al., 2015). Furthermore, when hyposmotic stress is relieved in the presence of extracellular dextran, VLDs formed prior to the diffusion of dextran into the VLD lumen. These findings led Kosmlaska et al. to postulate that water accumulation between the cell membrane and the underlying substrate promotes the formation of VLDs (Kosmalska et al., 2015). A similar mechanism has been hypothesized, but not directly tested, in skeletal muscle t-tubules as well (Krolenko and Lucy, 2001; Yeung et al., 2002). It should be noted that the high negative pressure may potentially withdraw extracellular fluid and support the growth of dilated t-tubules, although direct evidence for this is unavailable. T-tubules likely also remain connected in the initial stages of cell shrinking and although the theoretical calculations suggested the resistance to flow within t-tubules may be relatively low, this flow will be rapidly restricted once t-tubules constrict. Further quantitative experiments are necessary to determine whether t-tubule dilations are driven by the accumulation of water originating from intracellular or extracellular solutions.

Overall, the physical laws demonstrate that t-tubule dilations will preferentially expand in response to negative intracellular pressure. Once the available reservoir membranes are exhausted, narrower t-tubules may undergo further constriction to redistribute membrane to the growing vacuoles. In this way, large dilated vacuoles may form in response to negative osmotic pressure while sealing off the t-tubular lumen from the extracellular space.

Fig. 3.4 strongly suggests that osmotic stress alone cannot fully explain the magnitude of dextran trapping. The t-tubule diffusional accessibility was found to strongly correlate with the magnitude of t-tubule sealing (**Fig. 3.5**), suggesting that t-tubule

constrictions play an important role in the sealing process. We speculate that the formation of t-tubule constrictions may exacerbate the difference in t-tubular radii between constricted and dilated t-tubules. As a result, there will be a greater difference in the membrane tension that develops upon cell shrinking, promoting the growth of t-tubular dilations.

Like detubulation, VLD formation is also more efficient following cell swelling rather than through cell shrinking alone (Reuzeau et al., 1995). Exocytosis is prominent in these cells during cell swelling and it has been postulated that VLD formation may coincide with locations of endosome exocytosis (Morris and Homann, 2001; Reuzeau et al., 1995). Perhaps these fused endosomes provide the necessary membrane curvature to nucleate the formation of VLDs in response to the pressures generated during cell shrinking. Overall, the data support the notion that large diameter membrane invaginations are susceptible to undergoing VLD formation following cell shrinking.

Location of t-tubule dilations

Despite the significant role that these nanoscale t-tubular structures play in t-tubule stability, it remains unclear where these structures are located. Some studies have suggested that t-tubules dilate at dyadic junctions. Wong et al. observed dilations of t-tubule lumen at dyadic junctions in a serial block face scanning EM (Wong et al., 2013). This is consistent with a previous study of freeze fracture images where distensions of t-tubules appeared at transverse and axial junctions (Forbes et al., 1984). The junctional SR was seen clearly at one of the junctions suggesting that these distensions may be associated with dyads. In experiments using superresolution 3D dSTORM imaging, dilations were observed at regions where Cav3 and RyR2 staining colocalized and the

authors interpreted this colocalization to further suggest a dyadic location for the t-tubule dilations (Wong et al., 2013). It should be noted, however, that previous reports using confocal microscopy have suggested that Cav3 staining is excluded from dyads (Jayasinghe et al., 2009; Scriven et al., 2005). Thus, t-tubules show regular dilations although their exact localization remains unclear. If t-tubules are dilated at the dyads and are, as we suggested above, more susceptible to undergo vacuolation, then we would expect vacuolated t-tubules associated with the dyad following hyperosmotic stress. Few studies are available on this topic. Cardiomyocytes fixed in hyperosmotic solutions show dilated t-tubules associated with the junctional SR (Page and Upshaw-Earley, 1977). However, the association of vacuolated t-tubules with junctional SR may simply be a consequence of the expansion of distal t-tubule dilations, which brings the vacuole in close proximity to nearby dyads.

Furthermore, care should be taken in interpreting images of fixed cardiomyocytes. Our finding that hyperosmotic solutions are sufficient to induce t-tubule sealing suggests that conventional fixatives such as paraformaldehyde can result in significant fixation artifacts that affect t-tubular morphology. Indeed, preliminary experiments demonstrated that paraformaldehyde containing solutions can cause significant dextran trapping (data not shown), indicating that t-tubules are remodeled by the fixation procedure. Since these osmotic stresses can cause fixation artifacts, t-tubule dilations should ideally be studied in live, intact cells. Unfortunately, few studies have been performed in living cells. In skinned toad skeletal muscle fibers, large 500 kDa dextrans are excluded from longitudinal tubules suggesting that there are constriction points at the junctions of transversally oriented and longitudinally oriented tubules (Edwards and Launikonis, 2008).

Consistent with the hypothetical model of t-tubular vacuolation presented above, stretch of skinned fibers induced vacuolation specifically in longitudinal tubules that are flanked by these junctions. In cardiomyocytes, transverse elements of the t-tubule network were found to be more accessible to 11 nm diameter nanoparticles than longitudinal elements (Parfenov et al., 2006), consistent with the notion of localized constrictions at the intersection between transverse and longitudinal t-tubules. Clearly, further experiments are necessary to clarify the localization of t-tubule constrictions and dilations.

Physiological implications

The data presented may have implications for t-tubular remodeling *in vivo* despite being obtained solely from *in vitro* experiments using osmotic stress. T-tubular remodeling is strongly associated with mechanical stress (Frisk et al., 2016; Ibrahim et al., 2012; Sachse et al., 2012) although the relationship between the two is unclear. Membranes respond to mechanical stretch in a manner similar to that observed with osmotic stress. For example, removal of 6% mechanical strain in cultured fibroblasts passively induced membrane misfolding (Kosmalska et al., 2015). With mechanical stress, however, the misfolded membrane reservoirs did not dilate since there was no need for water confinement. This suggests that removal of excessive mechanical strain can also aberrantly misfold membranes. Notably, cardiomyocyte membranes also passively fold/refold in response to the geometric changes associated with contraction/relaxation (Levin and Page, 1980). T-tubular structure has been demonstrated to undergo significant shape and volume changes in response to stretch (Kohl et al., 2003; McNary et al., 2011; McNary et al., 2012), suggesting that cardiomyocyte membranes are dynamically regulated during the cardiac cycle. In addition, work in skeletal muscle suggests that

intracellular pressure may vary with mechanical stretch or contraction. Rabbany et al. demonstrated that giant barnacle skeletal myocytes generate positive intracellular pressure during isotonic contractions (Rabbany et al., 1994). However, whether negative intracellular pressure can be generated during mechanical stretch remains an open question. The development of t-tubular vacuoles in skeletal muscle during eccentric contractions (Yeung et al., 2002) hint that excessive stretch may create forces that may mimic osmotic detubulation (i.e. negative intracellular pressure). Although additional work is necessary to extend these findings to cardiomyocytes, these studies suggest that the forces necessary for detubulation/VLD formation may be generated in response to excessive mechanical strain, albeit to a much lesser extent than with osmotic stress. However, the data presented demonstrated that t-tubular dilations are likely more susceptible to undergoing further dilations. This leads to the prediction that nanoscale defects will promote subsequent t-tubular remodeling, resulting in the accumulation of structural changes over time. In other words, t-tubular remodeling begets t-tubular remodeling. As a result, excessive mechanical stress may lead to the gradual development of significant t-tubular constrictions and dilations over time. However, considerable quantitative work will be necessary to test these hypotheses.

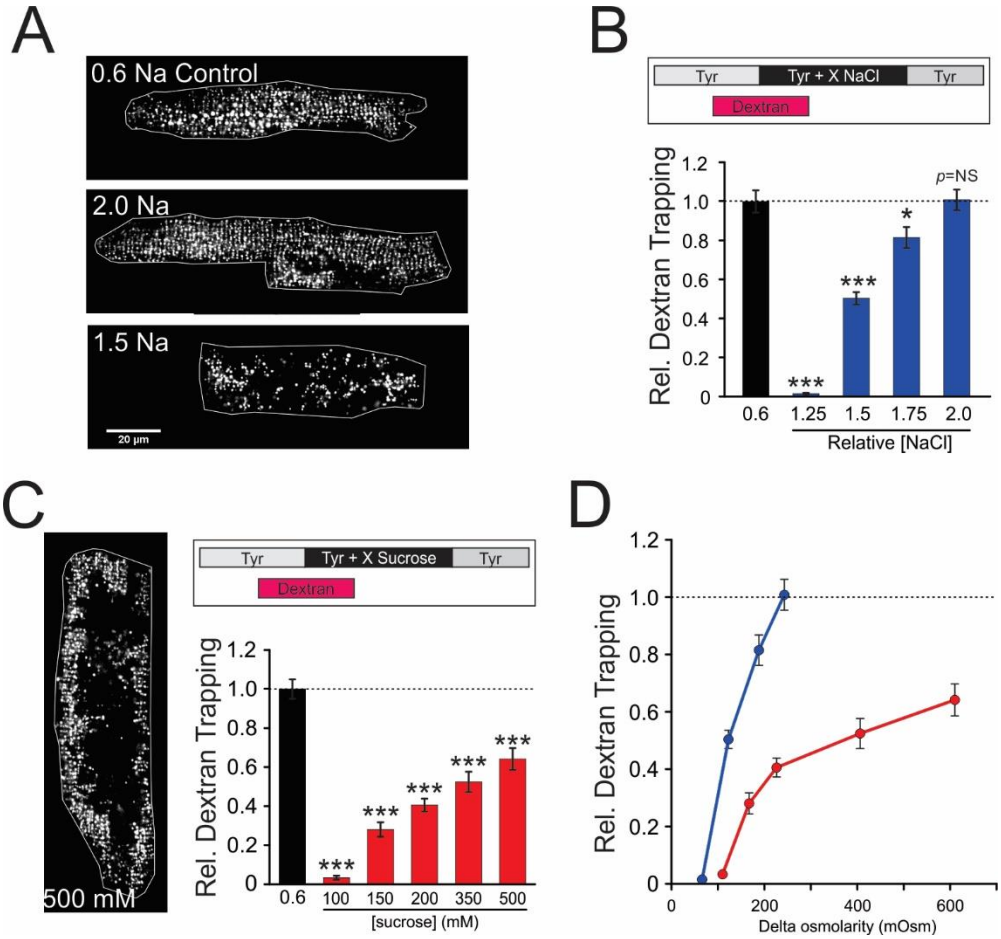

Figure 3.1 Hyperosmotic stress is sufficient to seal t-tubules

(A) Representative images of tetramethylrhodamine-dextran trapped cardiomyocytes using the corresponding hyper-osmotic stresses. Note the fluorescent dilated t-tubular structures apparent in each image. ***(B)*** Quantification of dextran trapping relative to that in cells following hyposmotic detubulation with 0.6 Na solution (n=20-30 cells each). The protocol used to detubulate cardiomyocytes using hyperosmotic NaCl solutions is presented above (Inset). 3 kDa tetramethylrhodamine dextran is added to cells 2 min prior to washout with dextran containing hyperosmotic solutions. The protocol for the control 0.6 Na hyposmotic detubulation is described in Materials and Methods. ***(C)*** Representative image of dextran trapped cardiomyocyte after detubulation using 500 mM sucrose (left). Quantification of dextran trapping relative to that in cells following hyposmotic 0.6 Na detubulation (n=30 cells each). Inset shows the protocol used to detubulate cardiomyocytes using hyperosmotic sucrose solutions. ***(D)*** Alternative depictions of the bar graphs in panels B and D plotted against the measured increase in solution osmolarity. For both NaCl (blue) and sucrose (red) the osmolarity dependence curve displays a sharp osmotic threshold before dextran trapping is observed.

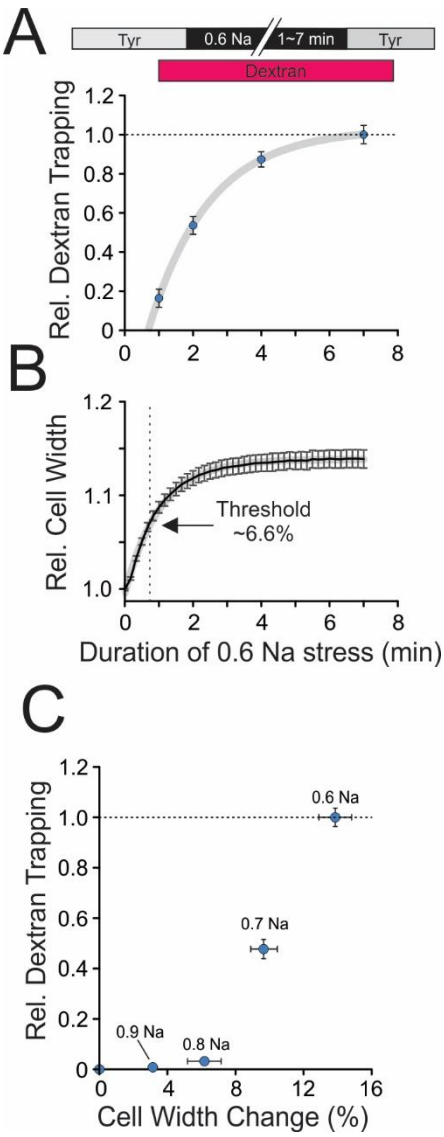

Figure 3.2 Threshold for hyposmotic detubulation

(A) Inset shows the hyposmotic detubulation protocol used. Cardiomyocytes were detubulated by applying 0.6 Na hyposmotic stress for 1, 2, 4, or 7 minutes (n = 20-30 cells each). 3 kDa dextran is present throughout the protocol until after the removal of hyposmotic stress. The magnitude of dextran trapping is dependent on the duration of the preceding hyposmotic stress. The gray line is a single exponential fitting of the data with the equation: [Rel. Dextran trapping] = -1.526*exp(-t/1.767)+1.03; R2 = 0.9999. ***(B)*** The trace shows the change in the cell width over time after perfusion with hyposmotic 0.6 Na solution (n = 7 cells). The time axis is aligned with panel A above. The x-intercept from panel A is presented as a vertical dotted line in panel B. The cell width at threshold time is indicated. ***(C)*** Cells were detubulated using 7 min hyposmotic stress from 0.9 to 0.6 Na (n = 30-50 cells each). The amount of dextran trapping following each hyposmotic stress was quantified. In a separate series of experiments, the change in cell width was measured after 7 minute incubation in the indicated hyposmotic stress (n=3-7 cells). Note, the cell width change for 0.9 Na was estimated from a linear regression obtained from the measured cell width changes for the other solutions. Again, a threshold is apparent around 0.8 Na stress.

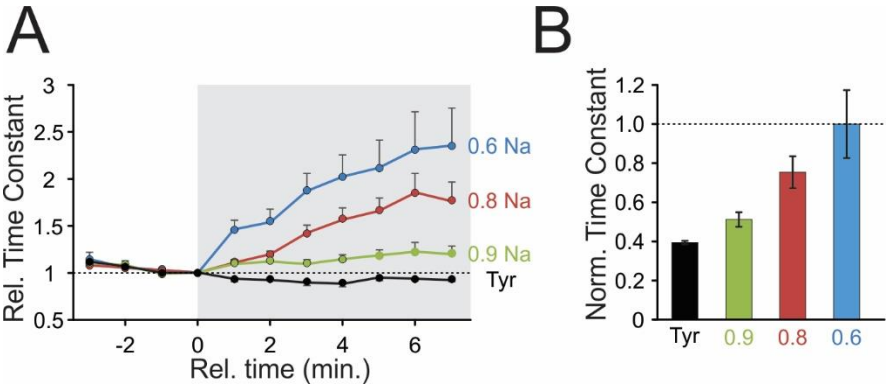

Figure 3.3 Hyposmotic stress dose-dependently restricts diffusion in t-tubule lumen

(A) Quantification of the time constant measured in single cells using the dextran diffusion assay before and during (gray background) exposure to the indicated hyposmotic solution. (n = 7-14 cells each). Perfusion of the hyposmotic solution began at time = 0 min. Diffusion within t-tubules was measured each minute. ***(B)*** The time constant was quantified 7 min after perfusion with hyposmotic solution and normalized to the relative time constant measured with 0.6 Na solution.

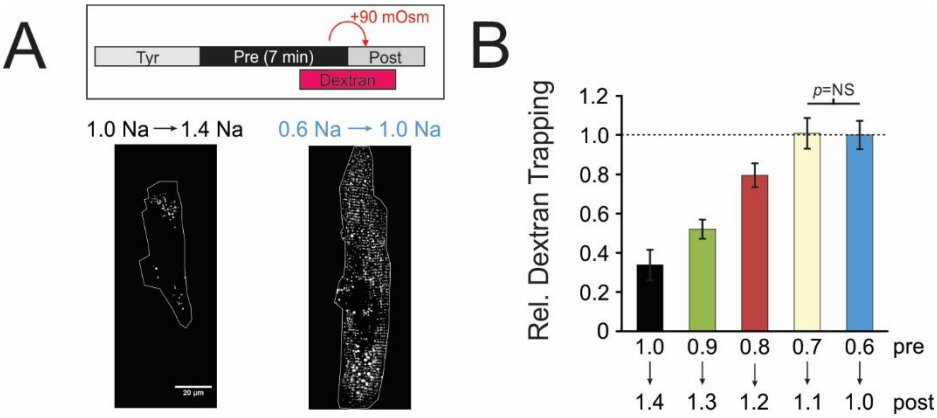

Figure 3.4 Magnitude of dextran trapping is not determined by magnitude of osmotic shock

(A) Modified hyposmotic detubulation protocol is described above (Inset). Cardiomyocytes were treated with various combinations of hyposmotic pre-stress (pre) and post-swelling washout solution (post). In all combinations, there is a constant 0.4 Na (~90 mOsm) osmotic gradient between the pre and post solutions. Representative images of dextran trapped cardiomyocytes from two conditions are shown. The cell on the left began in normal Tyr solution (1.0 Na) and detubulated in hyperosmotic 1.4 Na solution while the cell on the right was pre-exposed to 0.6 Na hyposmotic stress prior to detubulation with 1.0 Na solution. ***(B)*** Quantification of dextran trapping following a constant 0.4 Na (~90 mOsm) osmotic gradient using various combinations of pre/post stress (n=19-22 cells each).

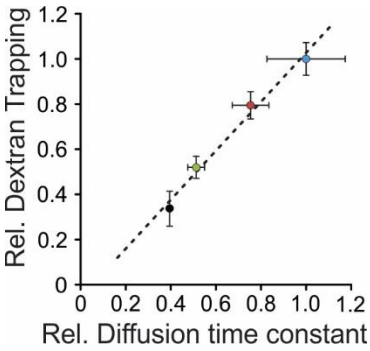

Figure 3.5 The magnitude of dextran trapping strongly correlates with the preceding t-tubular constriction

Correlation of the relative dextran trapping (from Fig. 4B) with the normalized dextran diffusion time constant (from Fig 3B). The relative diffusion time constant provides an estimate of the magnitude of the t-tubular constriction that developed during the hyposmotic pre-stress prior to detubulation. Dotted line is a linear regression with the following equation:

[Rel. Dextran trapping] = 1.0822 * [Rel. Diffusion time constant] - 0.0567; R^2 = 0.9866.

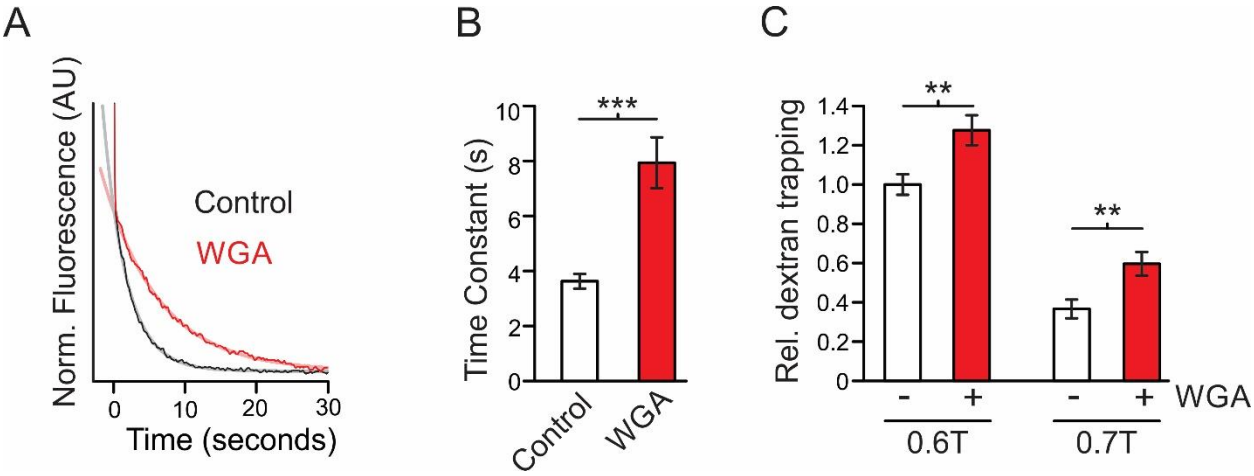

Figure 3.6 WGA treatment leads to slow t-tubular diffusion and augments the amount of t-tubular sealing following hyposmotic stress

(A) Representative fluorescence traces from a cardiomyocyte treated with 0.1 mg/mL WGA for 1 hour at 18°C (red) and a control cardiomyocyte (black).The fluorescence amplitude is normalized to highlight the difference in the fluorescence decay time constant. The grey and pink shaded traces are the single exponential fits for the traces from the control and WGA treated cell, respectively (n = 17 cells each). ***(B)*** Quantification of time constants of dextran diffusion estimated from single exponential fits. ***(C)*** Quantification of dextran trapping in control or WGA treated cells following detubulation with 0.6 Na or 0.7 Na hyposmotic stress (n = 28-30 cells each).

CHAPTER 4 SMALL MEMBRANE PERMEABLE MOLECULES PROTECT AGAINST OSMOTICALLY INDUCED SEALING OF T-TUBULES IN MOUSE VENTRICULAR MYOCYTES

4.1 Acknowledgements

This chapter has been previously published in the *American Journal of Physiology-Heart and Circulatory Physiology* (Uchida et al., 2016) and is reproduced here with minor edits. This chapter includes data obtained with the following collaborators: Ian Moench and Greta Tamkus (dextran trapping experiments), Anatoli Lopatin (cell width measurements and electrophysiological experiments), Azadeh Nikouee (osmolarity measurements), and Olga Zolova (cell isolation). This work was supported by the National Institutes of Health (HL127023 to ANL and T32-GM008322 to KU).

4.2 Abstract

Cardiac t-tubules are critical for efficient excitation-contraction coupling but become significantly remodeled during various stress conditions. However, the mechanisms by which t-tubule remodeling occurs are poorly understood. Recently, we demonstrated that recovery of mouse ventricular myocytes after hyposmotic shock is associated with t-tubule sealing. In this study, we found that the application of Small Membrane Permeable Molecules (SMPM) such as DMSO, formamide and acetamide upon washout of hyposmotic solution significantly reduced the amount of extracellular dextran trapped within sealed t-tubules. The SMPM protection displayed sharp biphasic concentration dependence that peaks at ~140 mM leading to >3-4-fold reduction in

dextran trapping. Consistent with this data, detailed analysis of the effects of DMSO showed that the magnitude of normalized $I_{K1,\ tail}$ current, an electrophysiological marker of t-tubular integrity, was increased ~2-fold when hyposmotic stress was removed in the presence of 1% DMSO (~140 mM). Analysis of dynamics of cardiomyocytes shrinking during resolution of hyposmotic stress revealed only minor increase in shrinking rate in the presence of 1% DMSO, and cell dimensions returned fully to pre-stress values in both control and DMSO groups. Application and withdrawal of 10% DMSO in the absence of preceding hyposmotic shock induced classical t-tubule sealing. This suggests that the biphasic concentration dependence originated from an increase in secondary t-tubule sealing when high SMPM concentrations are removed. Overall, the data suggest that SMPM protect against sealing of t-tubules following hyposmotic stress, likely through membrane modification and essentially independent of their osmotic effects.

4.3 Introduction

T-tubules form an extensive network of interconnected plasma membrane invaginations within cardiomyocytes and may contribute up to ~30-65% to the total surface membrane (Pasek et al., 2008). This network is a central feature of normal adult ventricular cardiac myocytes and contains critical elements underlying efficient excitation-contraction coupling (for reviews: (Brette and Orchard, 2007; Ferrantini et al., 2013)). In healthy cardiomyocytes, t-tubules allow for propagation of action potential deep inside the cell and assure nearly synchronous release of Ca^{2+} from SR and thus spatially and temporally uniform contraction (Brette et al., 2002; Cheng et al., 2011). Numerous studies have shown, however, that the function of t-tubular network becomes compromised during various experimental and clinical conditions, including heart failure (for review:

(Guo et al., 2013)). Disruptions in the t-tubule network, also commonly referred to as t-tubule remodeling, constitute a spectrum of structural changes that range from dilations (Kostin et al., 1998; Louch et al., 2004; Schaper et al., 1991; Wagner et al., 2012) to tight constrictions (Pinali et al., 2013; Sacconi et al., 2012) and loss of t-tubules (for review (Guo et al., 2013), ultimately leading to changes in electrical properties of t-tubules and aberrant Ca^{2+} handling through multiple mechanisms. For example, it has been shown that action potential propagation is impaired in partially constricted t-tubules (Sacconi et al., 2012), which can lead to nonsynchronous SR Ca^{2+} release (Crocini et al., 2014) and ultimately defective contraction (Ferrantini et al., 2014). In more extreme cases, segments of t-tubules can be constricted so tightly that action potential propagation is fully abolished in the regions previously occupied by these segments, further exacerbating the latency in Ca^{2+} release (Crocini et al., 2014). Additionally, we have previously shown that sealed t-tubules remain functionally active albeit being electrically disconnected from the rest of the sarcolemma (Moench and Lopatin, 2014). Importantly, we showed that the process of t-tubular sealing itself is associated with a massive influx of Ca^{2+} trapped in sealed t-tubules which is likely due to depolarization of sealed t-tubules. However, the mechanistic understanding of the causes of t-tubular structural changes still remains unclear, which is in part due to the paucity of appropriate tools to address the problem.

We have recently shown that many essential features of t-tubular remodeling can be reproduced in a model of acute hyposmotic shock (Moench et al., 2013). In particular, we found that constriction of t-tubules occurs nearly exclusively at the time of resolution of hyposmotic stress (i.e. during shrinking of the cell). This led us to a general hypothesis that the aberrant relaxation of the stretched sarcolemmal membrane is a key step

underlying the loss of t-tubular integrity. While this hypothesis does not provide molecular details, it can serve as guide. In particular, membrane stretch and membrane relaxation are surely modulated by numerous factors and processes (e.g. composition of lipids, membrane cytoskeletal interactions).

While testing various pathways that may regulate this relaxation process, we serendipitously discovered that the commonly used solvent DMSO can significantly protect against t-tubular remodeling when applied at relatively low concentration (1%; corresponds to ~140 mM) upon resolution of hyposmotic stress. We also show that other small membrane permeable molecules (SMPM), including the well-known detubulating agent formamide, also display a similar protective effect. At high concentrations, DMSO was also found to resemble formamide as removal of either molecule in the absence of hyposmotic stress resulted in effective t-tubule sealing. These results suggest that SMPM have similar modes of action that can lead to divergent t-tubule effects under different conditions. Detailed analysis of the actions of SMPM on t-tubular sealing strongly suggests that the observed protective effect against hyposmotic shock is likely due to their specific modification of membrane bilayer.

4.4 Materials and Methods

Animals

All experiments involving mice were carried out in accordance with the Guide for the Care and Use of Laboratory Animals (8th edition; The National Academic Press, Washington, DC, USA) and protocols approved by the veterinary staff of the University Committee on Use and Care of Animals at the University of Michigan.

Solutions (mM)

All solutions were filtered using a 0.22 µm filter. Osmolarity was measured using Vapro Osmometer 5520 (Wescor, ELITechGroup, France; mean ± standard deviation).

Modified Tyrode (Tyr): 137 NaCl, 5.4 KCl, 0.5$MgCl_2$, 0.3 $CaCl_2$, 0.16NaH_2PO_4, 3 $NaHCO_3$, 5 HEPES, 10 glucose, pH = 7.35 with NaOH. 273 ± 6 mOsm/L.

Myocytes storage solution (C solution): 122 NaCl, 5.4 KCl, 4 $MgCl_2$, 0.16 NaH_2PO_4, 3 $NaHCO_3$, 15 HEPES, 10 glucose, 5 mg/mL of bovine serum albumin, 1.38 mg/mL Taurine; pH adjusted to 7.35 with NaOH. 289 ± 3.5 mOsm/L.

Hyposmotic Tyrode (0.6 Na): prepared as Tyr but with 60% of NaCl (82.2 mM). 182 ± 4 mOsm/L.

KINT (pipette solution used for patch-clamp experiments): 140 KCl, 2 EGTA, 0.2 $CaCl_2$, 10 HEPES, 5 ATP and pH = 7.35.

Source of the chemicals: Urea - Difco Laboratories; Sucrose - Acros Organics; HEPES – Calbiochem; KCl, $NaHCO_3$, NaH_2PO_4 – Mallincrodt Chemicals, tetramethylrhodamine dextran (3000 MW; Anionic form) - Life Technologies. All other chemicals and reagents were from Sigma or Sigma-Aldrich.

Isolation of ventricular myocytes

Myocytes were isolated from the hearts of adult (~2-6 month old) C57BL/6 mice of either sex essentially as described in Moench and Lopatin (2014) (Moench and Lopatin, 2014) and used for experiments within 1-8 hours post-isolation.

Dextran trapping assay and confocal imaging

10 mg of tetramethylrhodamine dextran was dissolved in 1 ml PBS and used as a stock (stored at -20°C).

Isolated cardiomyocytes were first pre-incubated (~2 min) in Tyr before application of hyposmotic 0.6 Na solution. 1 µL of dextran stock solution (in PBS) was added to 10 µL of cells pelleted by centrifugation in 0.6 Na solution approximately 2 minutes prior to washout of 0.6 Na. Hyposmotic stress lasted 7-9 minutes and was stopped by washing with Tyr containing dextran for 5 min, and extracellular dextran was then washed out using Tyr solution. The cells were further washed and stored in C solution prior to imaging. Control myocytes were treated identically to test cells except that they were exposed to Tyr solution instead of 0.6 Na solution.

Confocal imaging was performed using an Olympus FV-500 microscope (Microscopy and Image Analysis Laboratory, University of Michigan, Ann Arbor). Images were analyzed using ImageJ software (http://imagej.nih.gov) followed by further analysis in Microsoft Excel. Images of myocytes were manually outlined and mean intracellular fluorescence of trapped dextran per unit area calculated. The data were corrected for background fluorescence observed in the control group.

Electrophysiological measurements

Ionic currents were recorded in the whole-cell configuration of patch-clamp technique at room temperature essentially as described by Cheng et al. (Cheng et al., 2011) with a few minor modifications. In particular, the resistance of the patch pipettes (R_p) varied from 2 to 4 MΩ when filled with KINT solution. After establishing whole-cell configuration series resistance (R_s>R_p) was compensated to an effective value of ~1-3 MΩ. Currents were filtered at 2 kHz. During recordings, the myocytes were continuously superfused with Tyr solution using a flow chamber. Membrane capacitance (C_M) was

measured with the aid of Clampex (Molecular Devices, Sunnyvale, CA, USA) built-in algorithm using 5 mV depolarizing voltage steps from a holding potential of -75 mV.

The current at the end of depolarizing voltage step ($I_{K,\ end}$) and following inward rectifier tail current ($I_{K1,\ tail}$) were analyzed essentially as described by Cheng et al. (Cheng et al., 2011). Briefly, ionic currents were recorded in response to a 400 ms voltage step to +50 mV followed by repolarization back to a holding potential of -75 mV. The $I_{K1,\ tail}$ current was fitted using a single-exponential function $A*\exp(-t/\tau)+C$. In a fitting procedure approximately 15 ms of the current traces was excluded from the fit to minimize a contribution from capacitative currents. The amplitude of exponential component (A) was then recalculated to zero time using measured time constant. Finally, the ratio $I_{K1,\ tail}/I_{K,\ end}$ was calculated and presented as normalized tail current $I^{N}_{K1,\ tail}$.

Measurements of myocytes dimensions

Myocytes were placed in a flow chamber and imaged using Nikon TE2000-S inverted microscope at 5 sec intervals with the aid of CoolSnap EZ camera (Photometrics, Tucson, AZ, USA) and NIS-Elements D 3.00 software (Laboratory Imaging, Prague, Czech Republic). Time series of images were then analyzed using custom made application (programmed in Delphi 2009, Embarcadero Technologies, San Francisco, CA USA) to measure changes in length and width of the myocytes.

In a subset of cardiomyocytes (n = 3 hearts), the cells were imaged and patched to simultaneously record cell size, C_M, and $I_{K1,\ tail}$ current. Imaging was performed using a MD500 microscope eyepiece camera and the AmScope 3.7 software (AmScope, Irvine, CA, USA). The images were imported into ImageJ and the myocyte outline was manually traced to measure the cross sectional area.

Importantly, in all experiments (electrophysiological and imaging) DMSO and other agents were completely washed out using normal Tyrode or C solution after completion of the stress protocol (e.g. 5-10 minutes after removal of hyposmotic 0.6 Na solution).

Statistics

The data (mean ± standard error) in each experimental series are from at least two heart preparations. Statistical significance was determined using a two-sample t-test assuming equal variances and considered significant if $p < 0.05$. In figures *, **, and *** correspond to p values of <0.05, <0.01 and <0.001, respectively. NS – not statistically significant ($p > 0.05$).

4.5 Results

DMSO prevents stress-induced trapping of extracellular dextran in t-tubules

In the course of the study aimed to understand the mechanisms underlying sealing of t-tubules in response to osmotic challenges (Moench et al., 2013), we have found that DMSO, present in the washing Tyr solution as a result of addition of a number of DMSO soluble agents, displays a strong and nearly instant protective effect (**Fig. 4.1A&B**). The magnitude of t-tubule sealing was quantified using a fluorescent dextran trapping assay as previously described (Moench et al., 2013). Briefly, in this assay t-tubules are first prefilled with fluorescent dextran molecules during cell swelling (by hyposmotic solution), which is then followed by washout of the hyposmotic solution, leading to sealing of t-tubules and thereby trapping the dextran within the cell. Detailed analysis of the action of DMSO (when it is present only in the washout solution) shows that the protective effect displays a clear biphasic dose-response relationship with 1% DMSO being the most effective (**Fig. 4.1C**). At this concentration, there is a ~4 fold reduction ($p < 0.001$) in the

intensity of t-tubular fluorescence compared to that in the absence of DMSO, suggesting that most of t-tubules remain open after resolution of hyposmotic stress. Further increases in DMSO concentration led to an increase in trapped dextran (**Fig. 4.1C**).

Surprisingly, DMSO was significantly less effective in protecting t-tubules when present continuously during both swelling and shrinking phases. Specifically, in a separate set of experiments (**Fig. 4.2**) dextran trapping was reduced only by ~36% in the continuous presence of DMSO *vs* ~69% when applied only upon resolution of stress (see Discussion for a likely explanation).

T-tubules in DMSO protected cells display altered electrophysiological properties

It has been shown that the integrity of t-tubule system can be quantitatively assessed by an electrophysiological approach using measurements of $I_{K1,\ tail}$ current (Cheng et al., 2011; Clark et al., 2001). Therefore, we have applied this technique to quantify the protective effects of DMSO described above (**Fig. 4.3**). Prior to patching, cardiomyocytes were treated as in the dextran trapping experiments and stored in DMSO-free C solution. The cells were subsequently plated onto the glass bottom of the recording chamber continuously perfused with normal Tyrode solution to further ensure washout of any residual DMSO and to exclude any direct effects that DMSO may have on ionic currents (Ogura et al., 1995).

As it has been shown before (Moench et al., 2013) the amplitude of $I_{K1,\ tail}$ current is significantly reduced in mouse ventricular myocytes that were acutely stressed with hyposmotic 0.6 Na solution (**Fig. 4.3A&B**; 0.6 Na), consistent with most t-tubules being sealed and not contributing to the measured current. In this study, the amplitude of normalized $I^{N}_{K1,\ tail}$ current was reduced >3.5 fold from 0.332 ± 0.027 in control myocytes

to 0.095 ± 0.016 after treatment with 0.6 Na solution ($p < 0.001$). Unexpectedly, $I^{N}_{K1,\ tail}$ current was reduced even further, by ~6 fold to 0.056 ± 0.010 when 1% DMSO was present during the whole hyposmotic stress procedure (**Fig. 4.3A&B**; DMSO-A). However, $I^{N}_{K1,\ tail}$ current was reduced only ~2 fold, to 0.184 ± 0.016 ($p < 0.001$), when 1% DMSO was applied only during resolution phase of the stress (**Fig. 4.3A&B**; DMSO-W), suggesting that a significantly larger portion of the t-tubules remains electrically accessible compared to that in two other (0.6 Na and DMSO-A) test groups.

One of the other important features of $I_{K1,\ tail}$ current is its kinetics as it also reflects the magnitude of t-tubule remodeling (Cheng et al., 2011). Inspection of current traces in **Fig. 4.3A** shows that myocytes treated with 1% DMSO applied upon resolution of stress display slower decline of $I_{K1,\ tail}$ current. Accordingly, quantification of the data (**Fig. 4.3C**) shows that the time constant of $I_{K1,\ tail}$ current is increased nearly 2-fold, from 74.0 ± 2.5 ms to 144.0 ± 8.0 ms ($p < 0.001$), in control and 1% DMSO-W treated myocytes, respectively. Combined with the partial preservation of $I^{N}_{K1,\ tail}$ current amplitude described above, the data provide further evidence that DMSO-W treated cells still have electrophysiological defects that are consistent with partial t-tubule constrictions. It is tempting to suggest that the time constants of $I_{K1,\ tail}$ currents in other test groups, 0.6 Na and DMSO-A, are significantly larger than that observed in DMSO-W treated cells but unfortunately, the smaller amplitude of $I_{K1,\ tail}$ currents in those test groups makes estimation of the time constant unreliable (data not presented).

The membrane capacitance, C_M, was also measured to further characterize t-tubule remodeling. In order to minimize potential bias in measured average C_M between various data sets which may arise due to the large dependence of C_M on cell size (Satoh

et al., 1996), cardiomyocytes were also imaged and the cross sectional area (CSA) measured. There was a broad spread of cardiomyocyte CSA ranging from ~2200 to ~8000 μm^2 with average CSA of 4545 ± 346 μm^2 (n = 17) in control cells. Prior exposure of cardiac myocytes to hyposmotic solutions, with or without added DMSO, had no effect on the average CSA: 4165 ± 304 μm^2 (n = 17), 4086 ± 338 μm^2 (n = 18), 4450 ± 302 μm^2 (n = 19), for 0.6 Na, DMSO-W and DMSO-A conditions, respectively.

Measured values of C_M and CSA for individual myocytes as well as corresponding linear regression fits for all groups are shown in **Fig. 4.3D**. The data show significant reduction in measured C_M in myocytes treated with 0.6 Na solution compared to that in control cells. However, the expected restoration of C_M in DMSO-W group towards control values is less evident, in particular, due to the large scatter in the individual data. In order to take advantage of known cell size, individual C_M data were normalized to the corresponding CSAs and averaged normalized C_M (C^N_M) for each group compared (**Fig. 4.3E**).

Control cells show a C^N_M value of 0.047 ± 0.005 pF/μm^2 that is nearly identical to the value reported by Pavlovic et al. (Pavlovic et al., 2010) for isolated mouse ventricular myocytes (**Fig. 4.3E**). Furthermore, cells treated with 0.6 Na solution show a ~27% reduction in C^N_M compared to control cells, 0.034 ± 0.004 pF/μm^2 ($p < 0.01$), similar to the reduction in C_M that we observed previously (Moench et al., 2013). In line with the measurements of $I_{K1,\,tail}$ currents, C^N_M was significantly preserved to 0.038 ± 0.005 pF/μm^2 ($p < 0.05$) and 0.038 ± 0.004 pF/μm^2 ($p < 0.01$), for DMSO-W and DMSO-A groups, respectively, when compared to cells treated with 0.6 Na solution. Again, the data are consistent with DMSO preserving the integrity of t-tubular system.

Evidence against osmotic effects of 1% DMSO in t-tubule protection

Despite the seemingly low concentration, 1% DMSO increases the osmolarity of Tyr solution by ~130 mOsm/L. Therefore, we examined if this increased osmolarity could account for the protective effects of DMSO described above. **Fig. 4.4 A** shows a representative time course of changes in the cell width highlighting quick swelling and shrinking phases as well as a characteristic response to withdrawal of 1% DMSO (**Fig. 4.4A**; arrow). Consistent with the previous findings, the change in the dimensions of the myocytes was primarily due to changes in the width (~14%) of the cells (**Fig. 4.4 B**) (Boyett et al., 1991; Brette et al., 2000; Moench et al., 2013; Roos, 1986). Importantly, the cell width returned to its pre-stretched value in both control and DMSO treated myocytes: 99.7 ± 0.3% and 100.0 ± 0.3% (p ~ 0.2) in the absence and presence of 1% DMSO, respectively. The focus of this study, however, was largely on the kinetics of cell shrinking. The data in **Fig. 4.4C** show that the rate of shrinking (τ_{off}) was slightly faster (but not statistically significant; p ~ 0.12) in the presence of 1% DMSO, consistent with increased osmolarity of washing solution. In order to confirm that this small increase in the rate of shrinking is not due to differences in cell size of the corresponding populations (i.e. the rates of osmotic response may correlate with the cell size) we have also compared swelling rates in both DMSO treated and non-treated cells. The data in **Fig. 4.4C** indicate the absence of this correlation. Also, the minor effect of 1% DMSO on the rate of shrinking is in striking contrast to significant protective changes in the level of dextran trapping (**Fig. 4.1C**) and the amplitude of $I^{N}_{K1,\,tail}$ current (**Fig. 4.3B**).

It should be noted that an increased rate of shrinking in the presence of 1% DMSO would be predicted to increase t-tubule sealing. To confirm that the protection by DMSO-

W (404 ± 13 mOsm/L) is not due to the increased osmolarity of the washout solution, a series of dextran trapping experiments was performed using Tyr solutions with added 60 mM NaCl (362 ± 1 mOsm/L) and 120 mM sucrose (354 ± 3 mOsm/L) instead of DMSO. As shown in **Fig. 4.4D** (*left*), washout with either hyperosmotic solutions did not reduction dextran trapping. Rather, in both conditions a trend towards increased dextran trapping (p = 0.08 and p = 0.07, respectively) is observed, confirming that the mechanism of protection by DMSO is not due to its bulk osmotic effects.

It remained possible that the low level of dextran trapping in the presence of 1% DMSO (**Fig. 4.1C**) could be explained by transient reopening of constricted t-tubules upon DMSO withdrawal which is associated with transient swelling of the cells due to diffusion of accumulated DMSO out of the cells. However, additional experiments (**Fig. 4.5**) designed to test this hypothesis argue strongly against this possibility. In particular, if t-tubules transiently reopen and close again upon DMSO withdrawal then adding dextran prior to this step (but not at the time of washout of hyposmotic stress) should lead to its trapping. However, this effect was not observed (**Fig. 4.5**; protocol 4). Alternatively, applying and removing DMSO to cells that already have dextran trapped in sealed t-tubules does not lead to its release (**Fig. 4.5**; protocol 5). Consistent with this data, postponing DMSO withdrawal does not affect dextran trapping as well (**Fig. 4.5**; protocol 3). Collectively, the data confirm that the protective effect of 1% DMSO occurs during the trapping process, within the first few minutes following resolution of hyposmotic stress, and the reduced level of dextran trapping is not associated with the following removal of DMSO.

Efficacy of osmolites against hyposmotic stress is correlated with their membrane permeability

In order to elucidate the mechanism of t-tubule protection by DMSO, the effects of several other osmolites on t-tubular integrity were tested (**Fig. 4.6**). Each osmolite was added to the washout solution at the concentration matching the osmolarity of Tyrode solution containing 1% DMSO (solution osmolarity: 410 ± 3 mOsm/L). Interestingly, highly membrane permeable formamide (solution osmolarity: 376 ± 2 mOsm/L) and acetamide (solution osmolarity: 398 ± 4 mosM/L) showed a significant protective effect similar to that observed with DMSO (**Fig. 4.6A**). In contrast, structurally similar urea (solution osmolarity: 385 ± 4 mOsm/L) showed no significant protective effects. The results in **Fig. 4.4D** demonstrated that application of relatively membrane impermeable NaCl and sucrose also showed no significant protection, suggesting that the high membrane permeability of the osmolites may underlie the protection against hyposmotic stress. In order to compare relative membrane permeabilities of DMSO, formamide, acetamide and urea, we measured the changes in the width of the myocytes in response to the application of high concentrations (~700 mM) of each agent (**Fig. 4.6C**). As expected, application of highly permeable DMSO (solution osmolarity: 966.7 ± 7 mOsm/L), formamide (solution osmolarity: 794 ± 10 mOsm/L) and acetamide (solution osmolarity: 912 ± 6 mOsm/L) led to fast but transient shrinking of the cells and thus is characterized by relatively small amplitude of the changes in the cell width. A clear feature of the formamide effect was that the steady state width of the cell in the continuous presence of the agent was measurably larger than the original value, consistent with observations made by Kawai et al. (Kawai et al., 1999). In contrast, application of urea (solution osmolarity: 926 ± 8 mOsm/L) led to significant and quasi steady-state shrinking of the

cells which was quickly (within few minutes) followed by cell death. These data are consistent with significantly lower membrane permeability of urea compared to that of DMSO, formamide and acetamide. Similar results were also observed with n=3-9 more cells in each group (the data were not quantified).

At high concentrations DMSO acts as a detubulating agent

A loss of protective effect of DMSO at high concentration (10%, which corresponds to ~1.4 M; **Fig. 4.1**) suggests an additional mechanism of its action on the integrity of t-tubular system. Formamide at ~1.4 M (5.6%) concentration has been used as a tool to detubulate cardiomyocytes for many years (Kawai et al., 1999). Accordingly, we hypothesized that in the experiments presented in **Fig. 4.1**, the increase in trapped dextran at 10% DMSO may be due to a secondary (to that induced by washout of 0.6 Na hyposmotic solution) detubulation that occurs when DMSO is finally withdrawn. To test this hypothesis, we first compared the efficacy of DMSO (10%) and formamide (5.6%) in inducing t-tubule sealing using the classical protocol (a brief application of the drug followed by its withdrawal (Kawai et al., 1999); **Fig. 4.7A**). Indeed, the data show that DMSO seals t-tubules as effectively as formamide, and the magnitude of dextran tapping induced by both agents is similar to that produced by application of 0.6 Na solution alone (**Fig. 4.7A**). This data strongly support the above hypothesis. Specifically, even if t-tubules were to be fully protected by DMSO at the time of washout of hyposmotic 0.6 Na solution they would become sealed and dextran trapped since it is still present in t-tubules at the time of withdrawal of 10% DMSO (**Fig. 4.1A**). In order to further confirm this suggestion, we performed experiments similar to those described in **Fig. 4.5** where we studied similar effects of DMSO but at lower concentration (1%). In this regard, the data in **Fig. 4.7B**

show that if extracellular dextran is removed before withdrawal of 10% DMSO the amount of trapped dextran becomes even lower than that observed in experiments using 1% DMSO (**Fig. 4.1C; Fig. 4.5B**). Altogether, these data reveal a truly strong protective effect of DMSO at the time of removal of hyposmotic 0.6 Na solution and explain the biphasic concentration dependence of DMSO effects on t-tubular sealing presented in **Fig. 4.1C**.

Experiments with formamide (5.6%) showed similar results (**Fig. 4.7B**) suggesting that it likely protects t-tubules by the same mechanisms as DMSO.

To further illustrate the true magnitude of protection against hyposmotically-induced t-tubule sealing, the data from experiments using protocols 2 and 3 (**Fig. 4.7B**) as well as the data obtained at lower concentrations of DMSO and formamide were plotted against the osmolarity of the washout solution (instead of %). In particular, the data show that most of the protection is observed at <500 mOsm/L of DMSO or formamide containing solutions, and the effects of the secondary t-tubule sealing are minimal at these doses.

4.6 Discussion

In this paper, we show that significant protection against t-tubular sealing in response to hyposmotically-induced membrane stretch can be achieved by application of DMSO, one of the most common solvents in biological research, as well as other SMPM such as formamide and acetamide.

Proposed mechanism of protection by SMPM

DMSO and other SMPM may have a variety of targets that can potentially modulate t-tubule integrity. In particular, SMPM could act on targets located at both the plasma membrane and within the cardiomyocyte. However, a number of key observations

in this study put significant constraints on the potential mechanisms of their action. For example, the protection by DMSO against hyposmotically-induced sealing of t-tubules is strongest when it is applied at the time of cell shrinkage (**Fig. 4.2**) and the effect is fast. This would be more consistent with DMSO acting directly on a membrane target or the lipid bilayer itself rather than through activation of some intracellular pathway ultimately leading to t-tubule protection. Also, despite very similar structures, the chemical nature of the tested SMPM is quite different (**Fig. 4.6B**) which would likely translate to differential effects due to different specificity to the key target. However, the data in **Fig. 4.7** show that DMSO, formamide and acetamide produce nearly identical level of protection.

DMSO has been used as a cryoprotectant, which stems partly from its ability to counteract the freezing-induced osmotic stress (Yu and Quinn, 1994). However, the mode of action of DMSO in t-tubule protection is unlikely to be simply through counteracting changes in the osmotic pressure. For example, the increase in the rate of cell shrinkage due to added DMSO (**Fig. 4.4C**) is expected to trend towards increased rather that decreased t-tubular sealing. Consistent with this prediction, the data in **Fig. 4.4D** indeed show a trend towards an increase in the amount of dextran trapping when osmolarity of washout solutions is increased by adding NaCl or sucrose instead of DMSO. The osmotic effects of DMSO and formamide at higher concentrations are indeed strong and in fact do lead to sealing of t-tubules (**Fig. 4.7A**) but only upon withdrawal of the agents, not at the critical time of resolution of hyposmotic stress. In this regard, the data in **Fig. 4.7** reveal strong protective effects of SMPM at high concentrations when the data are corrected for secondary detubulation caused by their withdrawal. Clearly, increased osmolarity of washout solution does not explain the protective effects of SMPM.

It follows from above that the most unifying property of the agents displaying protection is their membrane permeability, which would translate to their ability to intercalate into the lipid bilayer of the membrane. In this regard, the ability of DMSO to influence membrane fluidity may explain its protective effects when this agent is present throughout the experiment (**Fig. 4.2**). For example, Gurtovenko and Anwar (Gurtovenko and Anwar, 2007) have demonstrated using molecular dynamics simulations that DMSO penetrates into the membrane and acts as a spacer between lipids, ultimately leading to membrane thinning. In addition to the *in silico* findings, work by Hochmuth et al. (Hochmuth et al., 1996) using laser tweezer pulled membrane tethers has demonstrated that high concentrations of DMSO have significant effects on membrane tension. In particular, DMSO at concentrations 1% and 5% reduced the apparent surface tension and the bending modulus for the membrane, which would be expected if membrane expansion occurs. These observations demonstrate that DMSO directly affects the biomechanical properties of the plasma membrane in a way that the membrane becomes more flexible, which is in agreement with the *in silico* results (Gurtovenko and Anwar, 2007). With this in mind, it is tempting to speculate that the enhanced membrane fluidity may minimize its misfolding in the spatially restricted space of t-tubules after the relief of membrane stretch to limit t-tubule sealing.

T-tubules are significantly more protected against sealing when DMSO is applied during washout of hyposmotic stress rather than when being constantly present. This important finding suggests that the concentration gradient of the SMPM plays a significant role. In this regard, the bilayer couple model may explain these results (Sheetz and Singer, 1974, 1976). This model posits that each leaflet of the bilayer can be modified

independently of the other leaflet and this asymmetric modification of the membrane can lead to significant structural changes of the membrane (Sheetz and Singer, 1974). In particular, if SMPM expand the outer side of the membrane bilayer relative to the inner side, for example due to the existence of a concentration gradient of SMPM, then the bilayer would protrude outward, and *vice versa*. According to this model, SMPM should produce an outward protruding force on the membrane bilayer during their application which would then counteract some of the inwardly-directed osmotic forces produced by the removal of hyposmotic solution. It has been shown that inwardly-directed osmotic forces may induce invaginated plasma membrane vacuoles in other cell types (Kosmalska et al., 2015; Krolenko and Lucy, 2002; Reuzeau et al., 1995), and it is tempting to speculate that the same osmotic forces underlie t-tubule sealing in cardiomyocytes.

The data in this study show that SMPM can act as both detubulating and protective agents against hyposmotic stress (**Fig. 4.7**). These seemingly contradictory findings can again be easily explained by the bilayer couple model described above. Specifically, it is known that in the classical formamide-induced detubulation (Kawai et al., 1999) t-tubule sealing occurs at the time of washout of formamide. At this time, formamide concentration is greater inside the cell which in turn would produce an invaginating force upon the membrane according to bilayer couple model. This is also consistent with a recently discovered phenomenon of detubulation of cardiac myocytes in the presence of a number of cationic amphiphilic drugs (CADs) (Osman et al., 2016). CADs selectively accumulate in the inner leaflet due to their high affinity for anionic phosphoinositides and thus may

induce a similar invaginating force. However, further experiments would be necessary to test this model.

Additional important information about the mechanism of DMSO protection can be gleaned from the analysis of $I_{K1,\ tail}$ currents and membrane capacitance. For example, the data in **Fig. 4.3** show that in myocytes protected by 1% DMSO the amplitude of $I^{N}_{K1,\ tail}$ currents is still significantly reduced compared to normal cells and the time constant of $I^{N}_{K1,\ tail}$ current decline is significantly increased. This suggests the presence of a significant number of partially (weakly) constricted t-tubules. However, these t-tubule constrictions are likely large enough (in diameter) to allow most of the initially trapped dextran to escape to the extracellular space before myocytes are imaged. The significantly smaller protective effect of 1% DMSO on membrane capacitance (**Fig. 4.3D&E**) when compared to that on dextran trapping or amplitude of $I^{N}_{K1,\ tail}$ currents is likely a reflection of the differences in the measured parameters used to estimate the magnitude of t-tubular constrictions. In particular, it should be noted that the measurements of C_M used in this study (performed using the algorithm provided in Clampex software) in principle depend on the length of the analyzed current traces. Specifically, it is clear that partially constricted t-tubules are still connected to the outside solution and contribute the same capacitance as normal t-tubules. However, the time constant of the capacitative current originating from constricted t-tubules may be significantly longer than the analyzed segment of the current ultimately leading to reduced measured C_M. Therefore, measured C_M should be treated as apparent C_M and the data interpreted accordingly.

Physiological connections

The results of this study have important physiological implications since the hyposmotic swelling applied in this study is likely relevant in a number of pathological conditions including ischemic stress. For example, it has been estimated that during ischemia, accumulation of metabolic byproducts can increase the intracellular osmolarity by as much as 69 mOsm/L relative to the extracellular fluid (Jennings et al., 1986). This estimate is very close to the ~90 mOsm/L gradient between the Tyr and 0.6 Na solutions used in this study. This ischemic swelling has been validated *in vitro* using isolated adult ventricular cardiomyocytes (Diaz et al., 2003). Cardiomyocytes swell in volume by as much as 40% after 30 minutes of simulated ischemia, a magnitude similar to the that observed in cardiomyocytes exposed to 200 mOsm/L hyposmotic solutions (Diaz et al., 2003). This massive cell swelling is rapidly reversed upon reperfusion. Thus, the volume changes a cell experiences during ischemia-reperfusion may be mimicked by the hyposmotic stress used in our current study. Accordingly, our findings suggest that DMSO may protect against ischemia-reperfusion stress by attenuating constriction of t-tubules but whether the volume changes during ischemic stress can lead to sealing of t-tubules in the first place still remains unknown. In this regard, an alternative hypothesis has been suggested that t-tubule remodeling following ischemic-reperfusion may be mediated by calpain-mediated degradation of the t-tubular structural protein, junctophilin-2 (Wu et al., 2014a). However, further experiments would be necessary to test the above hypotheses and to confirm the t-tubular protective action of SMPM in ischemic conditions.

Cellular dysfunction consistent with constricted t-tubules has also been observed in cardiac myocytes isolated from failing hearts. For example, Sacconi et al. (Sacconi et al., 2012) reported AP propagation failure in t-tubules that were still accessible by

extracellular membrane specific dye di-8-ANEPPS. Importantly, these findings highlight the limitations of using di-8 ANEPPS alone to characterize t-tubule remodeling as this assay is not well suited for characterization of the functional defects that arise from partial constriction of t-tubules. Constriction of t-tubules in failing myocytes was also associated with altered Ca^{2+} release (Crocini et al., 2014), which is consistent with our previous finding of aberrant t-tubular Ca^{2+} handling in myocytes exposed to hyposmotic stress (Moench and Lopatin, 2014).

In conclusion, the results of this study show that sealing of cardiac t-tubules in response to hyposmotic stress in cardiac ventricular myocytes can be significantly attenuated by a brief application of various SMPM which likely exert their protective effect through direct action on the cellular membrane. However, further work is required to determine the specific properties of SMPM contributing to their protection against hyposmotically induced t-tubule sealing. Furthermore, understanding the mechanisms of SMPM action on cardiac t-tubules could be important in identifying novel agents and protocols for their application with strong protective effects against t-tubular sealing in various disease conditions.

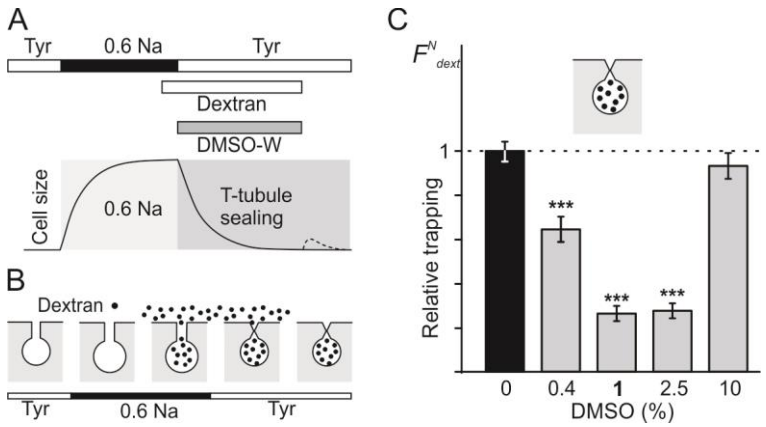

Figure 4.1 Effects of post-shock acute application of DMSO on t-tubular sealing.

(A) Timing of the application of fluorescent dextran and DMSO relative to the timing of hyposmotic challenge induced by application of 0.6 Na solution for ~7 min. Extracellular fluorescent dextran is applied ~2 min before removal of 0.6 Na solution and DMSO is applied exactly at the time of its washout by normal Tyr solution. After ~5 min myocytes are transferred to Tyr solution and the amount of trapped dextran measured using confocal microscopy. ***(B)*** Proposed mechanism of trapping of extracellular dextran. T-tubules become sealed (lumens are highly constricted) at the time of cell shrinking thus trapping previously added extracellular dextran. ***(C)*** Quantification of the amount of fluorescent dextran trapped in sealed t-tubules in the presence of varying concentrations of DMSO during cell-shrinking phase. T-tubules are most protected against sealing at 1% DMSO. n = 40, 40, 33, 38, and 38 for 0% to 10% DMSO groups, respectively. ***P < 0.001.

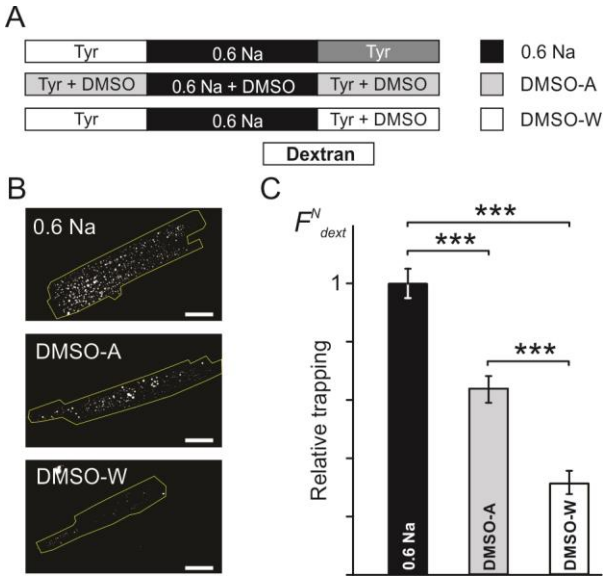

Figure 4.2 Effect of timing of DMSO application on dextran trapping.

(A) Protocols describing the application of 1% DMSO. 0.6 Na: protocol is characterized by maximum dextran trapping. DMSO-A: in this protocol 1% DMSO was present all the time, i.e., before, during and after hyposmotic challenge with 0.6 Na solution. DMSO-W: in this protocol 1% DMSO was present only during the washing phase of the hyposmotic challenge with 0.6 Na solution. ***(B)*** Representative confocal images of ventricular myocytes (from the groups described in A) containing trapped dextran. The cell border is outlined for clarity. Scale bars = 20 µm. ***(C)*** Quantification of the amount of trapped dextran in the three groups as in A using fluorescent confocal microscopy. Myocytes were imaged identically and the measured fluorescence is presented in arbitrary units for relative comparison. n = 31, 26, 25, and 24 for 0.6 Na, DMSO-A, DMSO-W, and control myocytes (used for background correction), respectively. ***$P < 0.001$.

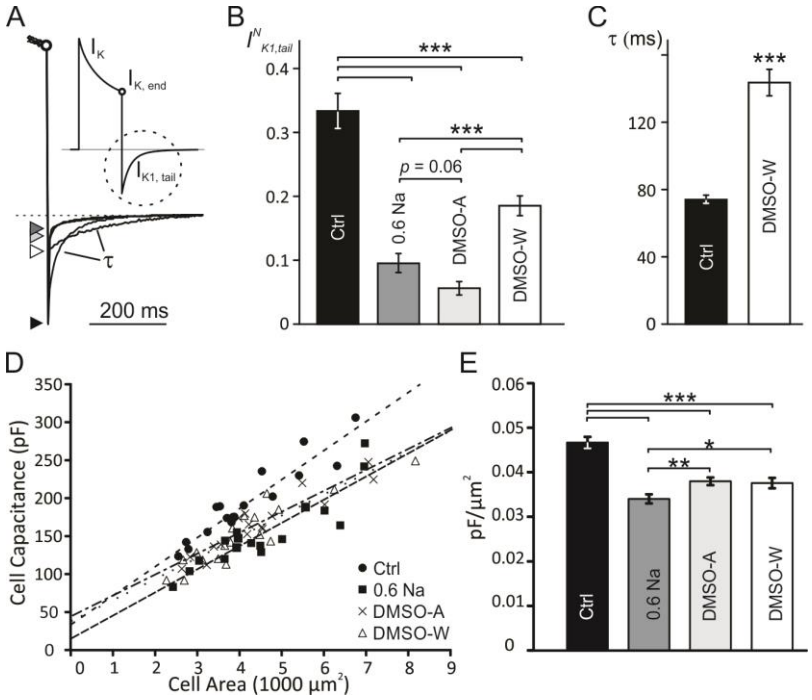

Figure 4.3 Electrophysiological effects of DMSO application.

(A) Integrity of t-tubules was assessed using so-called $I_{K1,\ tail}$ current (*Inset;* Methods). Whole-cell currents recorded from different groups of myocytes were normalized at the end of depolarizing voltage step (Insert; o) in order to highlight the differences in the magnitude and kinetics of the $I_{K1,\ tail}$ current. Zero current is indicated by the horizontal dashed line. Ctrl - control myocytes; 0.6 Na - myocytes treated with 0.6 Na hyposmotic solution; DMSO-A - myocytes were exposed to 1 % DMSO All time, before, during, and after hyposmotic challenge with 0.6 Na solution; DMSO-W- myocytes were exposed to 1 % DMSO only during the Washing phase of the hyposmotic challenge with 0.6 Na solution. ***(B)*** Quantification of normalized $I_{K1,\ tail}$ currents in myocytes treated as described above. n = 34, 34, 35, and 24 for Ctrl, 0.6 Na, DMSO-A and DMSO-W myocytes, respectively. ***(C)*** Quantification of the time constant (τ) of $I_{K1,\ tail}$ current in Ctrl and DMSO-W treated myocytes above. n = 34 and 35 myocytes, respectively. ***(D)*** Relationship between cell cross sectional area (CSA) and membrane capacitance (C_M). The regression lines are as follows: C_M = 0.0385*CSA + 32.7, R^2 = 0.846 for Ctrl (n = 17), C_M = 0.0306*CSA + 14.6, R^2 = 0.809 for 0.6 Na (n = 17), C_M = 0.0277 * CSA + 43.9, R^2 = 0.883 for DMSO-A (n = 19), C_M = 0.028*CSA + 37.2, R^2 = 0.826 for DMSO-W (n = 18). ***(E)*** Averages of individual C_M normalized by the CSA (C^N_M).

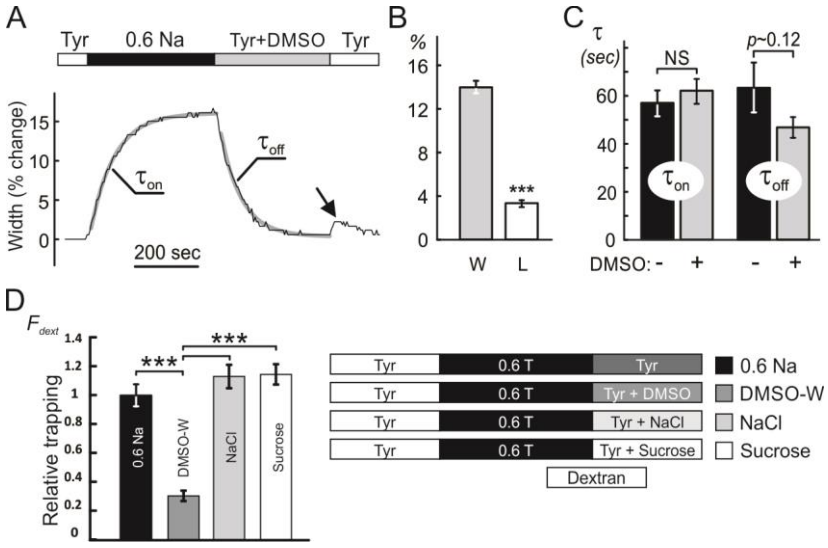

Figure 4.4 Effects of DMSO on myocyte dimensions.

(A) Representative time course of changes in the width of myocytes during application of hyposmotic 0.6 Na solution and its washout with normal Tyrode solution (Tyr) containing 1% DMSO. Orange arrow indicates the transient swelling of the myocytes as 1% DMSO is being removed from the extracellular solution. ***(B)*** Quantification of the extent of swelling. 'W' and 'L' are width and length of myocytes, respectively. ***(C)*** Effect of 1% DMSO on the rate of swelling (τ_{on}) and shrinking (τ_{off}) of myocytes. DMSO was applied as indicated in A. While DMSO was only applied upon washout of 0.6 Na solution, the data for the rate of swelling (τ_{on}) were split into two groups (DMSO - and +) which correspond to those for the rate of shrinking (τ_{off}). The data show that the decrease in τ_{off} in the presence of DMSO does not correlate with τ_{on}. n = 10 and 11 myocytes, for 0% and 1% DMSO, respectively. ***(D)*** The effect of hyperosmotic solutions on dextran trapping. (*left*) Quantification of the relative amount of dextran trapping after application of various (*right*) test solutions. n = 29 for 0.6 Na, n = 30 for DMSO-W, NaCl, and sucrose groups.

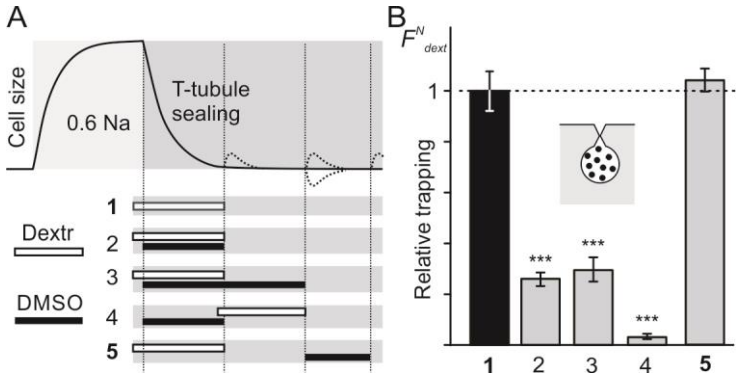

Figure 4.5 Protective action of DMSO occurs exclusively upon removal of osmotic stress.

(A) Various protocols designed to test whether the reduced trapping of extracellular dextran (a measure of presumed protection) is not due to transient swelling upon withdrawal of 1% DMSO. ***(B)*** Quantification of relative dextran trapping following the experiments described in A. Dextran fluorescence was normalized (F^N_{dext}) to that measured in protocol 1**.** The data show, in particular, that dextran is neither trapped in nor released from sealed t-tubules during transient swelling upon DMSO withdrawal (protocols 4 and 5, respectively). n = 40, 36, 18, 20, 20, and 20 for control cells and cells in protocols 1-5, respectively.

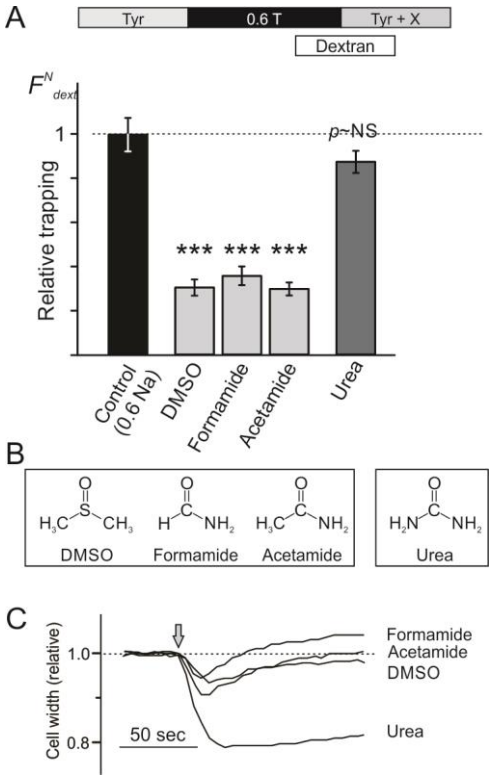

Figure 4.6 SMPM reduce dextran trapping when present upon washout of hyposmotic 0.6 Na solution.

(A) Quantification of relative dextran trapping in cardiomyocytes following washout of hyposmotic 0.6 Na solution with Tyrode solution containing 1% DMSO (~140 mM) or similar concentrations of other osmolites (X). n = 29, 30, 30, 20, 30, 30, 30 for Control (0.6 Na) cells and osmolite X (from left to right, respectively). ***(B)*** Chemical structures of selected osmolites. ***(C)*** Representative examples of the changes in the relative width of the myocytes in response to the application (indicated by arrow) of indicated osmolites at ~700 mM concentration.

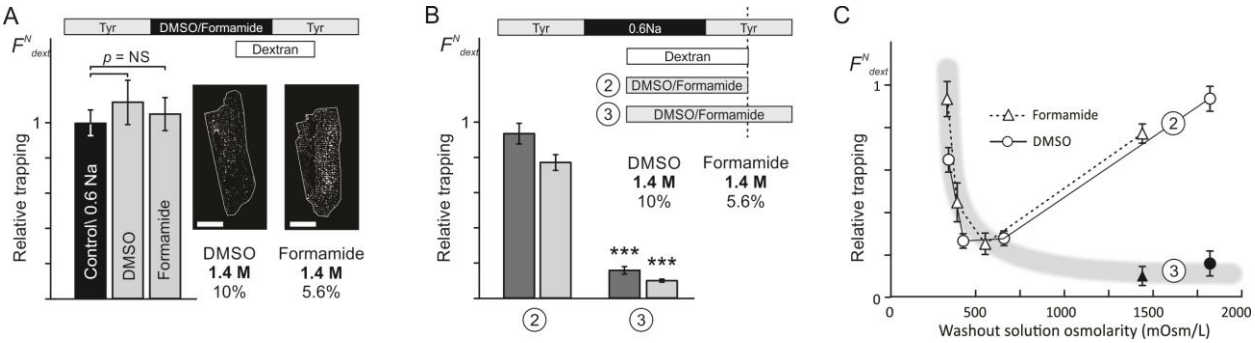

Figure 4.7 Effects of high concentration of DMSO and formamide on hyposmotically- induced sealing of t-tubules.

(A) Quantification of dextran trapping following 7 minutes application and removal of control 0.6 Na hyposmotic solution, 10% DMSO or 5.6% formamide. n = 20, 15, and 20 for Control/0.6 Na, DMSO and formamide, respectively. *(Right)* Representative confocal images of fluorescent dextran trapped in t-tubules following DMSO or formamide treatment. Scale bars = 20 µm. ***(B)*** 10% DMSO or 5.6% formamide were applied during washout of hyposmotic 0.6 Na solution according to indicated protocols (2 and 3) and the amount of trapped dextran compared to that obtained with protocol 1. In protocol 2 the removal of fluorescent dextran coincided with the removal of DMSO or formamide. Alternatively, in protocol 3 the removal of fluorescent dextran preceded removal of DMSO or formamide. (n = 15 and 20 for DMSO and formamide, respectively). The extent of dextran trapping with these two protocols is depicted for DMSO (dark gray) and Formamide (light gray). ***(C)*** Amount of relative dextran trapping for DMSO and formamide experiments in B are plotted along with the data at lower concentrations against the osmolarity of washout solutions (instead of % or concentration). Thin lines connect data points (open markers) collected using protocol 2 and filled markers indicate data collected using protocol 3. The shaded thick line depicts the true protective effect of DMSO and formamide against hyposmotically-induced detubulation. n = 20, 20, 20, 19 and 20 for 0% to 5.6% formamide groups using protocol 2. DMSO data at concentrations <10% are from Fig. 4.1.

CHAPTER 5 CONCLUSIONS, ONGOING PROJECTS, AND FUTURE DIRECTIONS

5.1 Summary of key findings

Cardiac t-tubules are complex structures containing a series of nanoscale constrictions and dilations. These structures have largely been ignored resulting in t-tubules being abstracted as cylindrical tubes. However, the preceding three chapters have demonstrated that the physical structure of t-tubules can have significant effects on their function. In Chapter 2, I described the development of a novel diffusional assay to detect subtle changes in the diffusional properties of the t-tubular lumen. The quantitative experimental data along with computational modeling allowed us to infer that sub-microscopic structures within t-tubules strongly determine the t-tubular diffusional property. Furthermore, I demonstrated that t-tubular constrictions can develop during hyposmotic swelling. Next, in Chapter 3, I used this diffusion assay along with quantitative detubulation measurements to determine that t-tubular constrictions/dilations promote detubulation and the formation of t-tubular vacuoles. The data suggest that during cell shrinking, dilated t-tubules will likely expand to form a vacuole and by drawing nearby membrane to support the growth of the vacuole, will further constrict narrow t-tubules to the point of sealing. Finally, in Chapter 4, I described how SMPMs can modulate the propensity of t-tubules to undergo sealing, possibly by affecting the t-tubular membrane curvature. Overall, the data suggests that nanoscale t-tubular structures have an important role in maintaining t-tubular integrity in response to osmotic stress.

5.2 Mechanisms of detubulation

The findings in this dissertation provide additional detail into the mechanisms of osmotic detubulation discussed below. The distinction between the forces that cause t-tubular disruption (Chapter 5.2) and the factors that stabilize t-tubules in response to these forces (Chapter 5.3) are discussed separately.

This dissertation introduced osmotic forces that induced or protected against detubulation. Detubulation can be induced by chemical modifications that also result in forces developing within the bilayer. Regardless of the origin, all known mechanisms of detubulation and related models of endocytosis are hypothesized to be closely associated with the imposition of an inwardly directed force and negative curvature on the t-tubular membrane.

5.2.1 Hyper- and hypo- osmotic detubulation

Chapter 3 demonstrated cell shrinking in response to hyperosmotic stress is sufficient to cause t-tubule sealing and the hypothetical mechanism of osmotic detubulation was discussed in section 3.4. Briefly, negative pressure develops within the cell during cell shrinking, which will pull on membranes differently depending on their geometry. Based on Laplace's law, dilated t-tubules will develop greater membrane tension than constricted t-tubules, resulting in the preferential expansion of t-tubule dilations. Expansion of these t-tubule vacuoles will draw in the reserve membrane that becomes available when the cell shrinks. Further expansion of the vacuole may pull membrane from nearby constricted t-tubules which results in further constrictions. Thus, the variable geometry of sub-microscopic structures within t-tubules allows for the vacuolation of certain regions within the t-tubular network and constriction in others.

Hyposmotic detubulation is conceptually similar to hyperosmotic detubulation. The major difference between hyper- and hyposmotic detubulation lies in the structure of the t-tubules prior to the detubulating stress. Cell swelling promotes t-tubules to seal during cell shrinking by introducing more t-tubular constrictions and exacerbating the size difference between constricted and dilated t-tubules. During cell shrinking, these constricted t-tubules develop less membrane tension and may promote the redistribution of membrane to the growing vacuoles. Ultimately, the development of negative intracellular pressure that pulls in susceptible membrane is a key driver of osmotic detubulation.

5.2.2 Chemical detubulation

Recent work by Osman et al. demonstrated that simple application of cationic amphiphilic drugs (CADs) can induce detubulation in cardiomyocytes (Osman et al., 2016). Preliminary work by Azadeh Nikouee in our lab confirmed that application of the CAD, Verapamil, can rapidly trap dextran in a dose-dependent manner (data not shown). However, the mechanism by which CADs induce detubulation is unknown. Osman et al. presented a hypothetical mechanism suggesting that CADs permeate the membrane and bind to anionic phospholipids (PI(3,4)P2, PI(3,4,5)P3, and PI(4,5)P2) predominant in the inner leaflet of the bilayer (Osman et al., 2016). These phospholipids, which are essential for binding to cytoskeletal proteins containing PH domains, may be sequestered by competitive binding to CADs and the disruption of scaffolding and cytoskeletal proteins on the t-tubular membrane was speculated to disrupt t-tubules. However, as mentioned in the outset of this section, a distinction must be made between factors that modulate t-tubule stability and the forces that cause detubulation. Osman's hypothetical model of

cytoskeletal disruption details a modulation of t-tubule stability but fails to describe the force that causes detubulation.

The Hilgemann group have found that multiple amphipathic molecules, along with a variety of other stimuli, induce massive endocytosis (MEND) in multiple cell types including cardiomyocytes (Hilgemann et al., 2018). Membrane capacitance can decline by > 50% in cultured cells and by > 30% in adult rodent cardiomyocytes following MEND, demonstrating that MEND is one of the largest endocytic events observed in live cells (Hilgemann and Fine, 2011; Lariccia et al., 2011). Surprisingly, pharmacological inhibition of classical endocytosis pathways has little to no effect on MEND (Lariccia et al., 2011). Rather, MEND depends critically on membrane properties, specifically on nanoscale liquid ordered (Lo) and liquid disordered (Ld) domains within the outer leaflet of biological membranes since MEND preferentially internalizes Lo membranes (i.e. lipid rafts rich in cholesterol and sphingomyelin) (Fine et al., 2011). A wide range of amphipathic molecules including the detergent NP-40, tamoxifen, edelfosine, or the phospholipase C inhibitor, U73122 can induce MEND (Fine et al., 2011). The authors initially speculated that application of amphipathic molecules may strip away lipids from the outer leaflet, generating a mismatch in the monolayer surface area to generate negative curvature. However, the lack of membrane shedding or formation of outward vesicles when amphipathic molecules were introduced in the intracellular solution quickly discounted this idea (Fine et al., 2011). Instead, the current hypothetical model (summarized below) proposes that lipidic forces are driving the formation of endocytic vesicles (Hilgemann et al., 2018). The model suggests that amphipathic molecules promote the coalescence of Lo domains. Due to differences in lipid compositions, Lo domains tend to be thicker than

Ld domains. The difference in bilayer thickness at the boundary of Lo and Ld domains is theoretically expected to expose the hydrophobic fatty acid tails of the lipids in the thicker Lo domains to the aqueous solution. This highly energetically unfavorable boundary forms a force called line tension, which drives the membrane to distort. As a result, the aggregated Lo domain will curve inward and form vesicles to reduce the length and the thickness mismatch at the boundary between Lo and Ld domains.

Other alternative upstream mechanisms can also drive domain coalescence in the absence of amphipathic drugs in cardiomyocytes. Large Ca^{2+} transients can also induce MEND by extensively palmitoylating integral membrane proteins, which segregate into Lo domains and potentially drive domain coalescence (Hilgemann et al., 2013; Levental et al., 2010). This form of Ca^{2+}-activated MEND is also observed in the myocardium following anoxia-reoxygenation stress (Lin et al., 2013). The similarity in the membrane capacitance decline (~30%) following detubulation (Kawai et al., 1999) and MEND (Lariccia et al., 2011) and the fact that CADs induce detubulation (Osman et al., 2016) suggest that MEND likely reflects t-tubular loss. However, whether MEND in cardiomyocytes specifically occurs in t-tubular membranes or throughout the sarcolemmal membrane has not been specifically tested. Additionally, the necessity of lipid domain coalescence for osmotic or chemical detubulation remains unclear.

Other mechanisms of endocytosis have also been proposed to be driven primarily by lipidic forces. Ben-Dov and Korenstein observed the prolific formation of surface membrane invaginations and endocytic vesicles following exposure to strong acidosis—a phenomenon they coined “Proton-Induced Uptake (PIU)” (Ben-Dov and Korenstein, 2012). PIU is conserved across a variety of culture cells, insensitive to pharmacological

inhibition of known endocytic pathways, and is strongly pH-dependent, displaying a threshold for uptake at pH≤6.5 that increases linearly until saturating at pH ~3. In response to extracellular acidosis, the intracellular pH will also become acidotic but will not equilibrate with the extracellular pH, resulting in the formation of a proton gradient across the surface membrane. Follow-up studies demonstrated that pharmacological disruption of the underlying cortical actin cytoskeleton can promote PIU (Ben-Dov and Korenstein, 2013a). Furthermore, PIU is augmented by increasing membrane fluidity while treatments that reduce membrane fluidity inhibit PIU (Ben-Dov and Korenstein, 2013b). The data overall led the authors to suggest that charge imbalance across the membrane may drive fluid, unsupported membranes to curve inward through electrostatic repulsion. Although it is unclear whether PIU will also be observed in cardiomyocytes and the pH necessary to observe this phenomenon is well beyond physiological range, the proposed mechanism is consistent with a general notion that the formation of inward membrane curvature results in membrane invagination and potentially endocytosis. The global nature of inward membrane curvature in inducing endocytosis across a variety of cell types raises the possibility that detubulation may simply be a specific manifestation of these endocytic processes in myocytes with t-tubules. Further experiments are necessary to link these endocytosis mechanisms with detubulation.

5.2.3 Formamide detubulation

Formamide detubulation was the first detubulation method described for cardiomyocytes and, of the osmotic detubulation protocols, 1.5 M formamide remains the most effective method of detubulating cardiomyocytes (Moench et al., 2013). During this treatment, cardiomyocyte volume undergoes complex changes. First, myocytes shrink

~20% upon application of formamide as the hyperosmotic stress extracts intracellular water (Kawai et al., 1999). Next, formamide will slowly permeate into the cell along with corresponding water and slowly swell the cell. During incubation with formamide, the volume will return to its initial value but the cell width will preferentially increase while cell length correspondingly decreases (Kawai et al., 1999). Upon removal of extracellular formamide, the intracellular osmolarity is transiently hyperosmotic relative to the extracellular solution. This results in rapid cell swelling of ~18% followed by cell shrinking back to the initial cell volume as intracellular formamide and water slowly effluxes out of the cell (Kawai et al., 1999). T-tubule sealing is observed during this second cell shrinking process.

Several factors likely contribute to the efficacy of formamide in sealing t-tubules. First, cardiomyocytes shrink rapidly upon removal of formamide and, as demonstrated in Chapter 3, shrinking alone is sufficient to induce t-tubule sealing. Second, the increase in cell width during formamide incubation may constrict t-tubules, although experiments will need to be performed to confirm this suspicion. Hyposmotic swelling in 0.6 Na solution, which increases cell width by ~14% increases the time constant for dextran diffusion by ~2-3 fold over 7 min (Chapter 2 and 3). Kawai et al. observed that cardiomyocyte width increases gradually during the 15 min formamide treatment reaching a peak increase of ~17% (Kawai et al., 1999). These observations suggest formamide treated cells match conditions necessary for the development of t-tubule constrictions. Lastly, the accumulated intracellular formamide forms a concentration gradient of formamide permeating out of the cell through the bilayer upon formamide washout. This gradient may induce an inward curvature in the membrane based on the “bilayer couple hypothesis”

(Chapter 4) and potentially promote detubulation. Note, t-tubule sealing is not observed during the initial cell shrinking upon formamide application (Figure 4.7). In this situation, the formamide gradient is greater outside the cell than inside, and may impose an outwardly directed membrane curvature and counteract t-tubule sealing. It is worth noting that many other SMPMs will similarly exhibit potential as a detubulating agent and formamide is mentioned solely for historical purposes. Thus, these SMPMs present as a hybrid detubulation method that combines osmotic forces and chemical modulation of the membrane to drive the formation of inwardly directed membrane curvature and promote t-tubule sealing.

5.3 T-tubular structural stability

The forces discussed in section 5.2 can disrupt t-tubular structure of normal isolated cardiomyocytes but the impact of these forces depends critically on the stability of the t-tubular membrane. The lipid bilayer itself can have different properties depending on its composition and is supported on either side by an extracellular matrix and the cortical cytoskeleton. Thus, disruption of any of these physical structures will play a strong modulating role in t-tubule remodeling.

5.3.1 Membrane composition: cholesterol

Cholesterol is highly enriched within t-tubular membranes (Sumnicht and Sabbadini, 1982) and may explain why t-tubular membranes are stiffer than other biological membranes (Hidalgo, 1985). Recent work has led to surprising insights into the stabilizing role that cholesterol plays in cardiac t-tubules. Cholesterol depletion using methyl-β-cyclodextrin (MβCD) was shown to disrupt t-tubules in a concentration and time-dependent manner (Zhu et al., 2016). However, this effect of MβCD is somewhat

controversial as more recent work demonstrated that cholesterol depletion by itself does not appear to directly disrupt the t-tubular network organization or reduce membrane capacitance of the cardiomyocyte (Gadeberg et al., 2017a). These two seemingly contradictory findings may be reconciled by determining the effect of cholesterol on t-tubular stability instead of t-tubular integrity. Recent work in our lab by Azadeh Nikouee demonstrated that cholesterol depletion promotes dextran trapping following both hyposmotic and chemical detubulation (data not shown), suggesting that cholesterol depleted t-tubules are indeed less stable. These recent data may indicate that Zhu et al. observed the combined effects of MβCD treatment and long-term culture, a condition known to cause t-tubule loss (Guo et al., 2018; Louch et al., 2004; Zhu et al., 2016). Furthermore, t-tubules may be remodeled by cholesterol depletion in subtle ways. Preliminary experiments suggest that t-tubular diffusion time constant may be increased in MβCD treated cardiomyocytes (data not shown). The above data are consistent with the findings from Chapter 3 that t-tubular diffusion time constant strongly correlates with the magnitude of t-tubular sealing during detubulation. However, the mechanism by which cholesterol depletion results in restricted t-tubular diffusion remains unclear and further experiments will be necessary to understand how t-tubular structure is affected with MβCD treatment.

5.3.2. Cytoskeletal proteins

A variety of cytoskeletal proteins including Junctophilin 2 (Guo et al., 2013), Bin 1 (Hong et al., 2014), and telethonin (Ibrahim et al., 2013) regulate the stability of t-tubule membranes. The correlation between t-tubule remodeling and Junctophilin 2 (JP2), a transmembrane protein located in the junctional SR membrane that spans across the

dyad to bind to the t-tubular membrane (Guo et al., 2013), has been extensively studied and will be the focus of this discussion. The loss of JP2 is linked to a decline in structural integrity of t-tubules and an exacerbation of t-tubule remodeling in disease states (Wei et al., 2010; Wu et al., 2014b; Wu et al., 2011; Zhang et al., 2014). However, the cause-and-effect relationship between JP2 loss and t-tubular remodeling is difficult to ascertain because both occur in the context of heart failure, which has many other factors that must be taken into account. A recent study using an AAV9 based delivery method of CRISPR-Cas9 targeted downregulation of JP2 produced hearts with some mosaic expression of JP2 (Guo et al., 2017). Heart failure developed spontaneously in hearts with greater number of JP2 depleted cells and displayed t-tubule disorganization in both transduced and non-transduced cells, suggesting that the t-tubule loss is driven not by JP2 loss but by the disease condition. However, greater t-tubular disruptions were observed in JP2 depleted myocytes than JP2 expressing myocytes, suggesting that these cardiomyocytes display a difference in the stability of the t-tubular structure. Here, the specific roles of the extracellular membrane in regulating t-tubular stability will be discussed in detail.

5.4.3 Extracellular matrix

T-tubule membranes are lined with an extensive basement membrane and a complex extracellular matrix extends into the t-tubular lumen from the interstitial space. Many of the proteins in the extracellular matrix are glycosylated and the interconnected mesh of proteins and sugars provide structural support for cardiomyocytes. The extracellular matrix undergoes continual remodeling and can dramatically change in composition in pathophysiological conditions, resulting in changes in the physical and electrical properties of the myocardium. Extensive fibrosis in response to cardiac injury is

known to increase the myocardial stiffness and can block electrical conduction to certain parts of the heart.

There is increasing evidence suggesting that the extracellular matrix plays an important role in maintaining t-tubular stability. During the isolation procedure, much of the extracellular matrix is digested to release individual cardiomyocytes. It has been suggested that this loss of the extracellular matrix may underlie the disruption of cardiac t-tubules *in vitro* although direct evidence for this is unavailable. We found that t-tubule diffusion is slow in cardiomyocytes treated with Neuraminidase A, an enzyme that cleaves sialic acid residues from glycosylated proteins (Chapter 2). These cells are, in a sense, overdigested. With further removal of the extracellular matrix, the t-tubule integrity appears to be compromised although overt changes in the t-tubule network were not observed (although this was not extensively quantified).

Surprisingly, cross-linking sialic acid and N-acetyl glucosamine residues with the lectin, WGA, also causes a significant increase in the time constant of t-tubular diffusion (Chapter 3). However, the mechanism for this action remains unclear. One potential explanation may be that WGA binding forms a denser sponge-like lattice that restricts diffusion within t-tubules. This hypothesis is confounded by the fact that the Neuraminidase A treatment, which would be expected to reduce the dense extracellular matrix, also results in slower t-tubular diffusion. Furthermore, the changes in the density of the extracellular matrix would not fully explain why t-tubule structural integrity is compromised in response to hyposmotic stress. Alternatively, WGA treatment may preferentially stiffen the surface membrane more than the t-tubular membrane, resulting

in a differential response to osmotic stress. Additional experiments are necessary to elucidate the mechanism by which WGA treatment restricts diffusion.

There is a clear correlation between t-tubule remodeling and fibrosis *in vivo*. Following myocardial infarction, both t-tubule remodeling and fibrosis are observed. The location of t-tubule disruption appears to correlate with the amount of nearby fibrosis (Seidel et al., 2017b). Furthermore, Ivabradine treatment following MI abolished the development of fibrosis and similarly prevent t-tubule loss (Navaratnarajah et al., 2013). In addition to these studies in HF models, tissue samples collected from human patients with HF also show increased WGA labeling within dilated t-tubule lumens suggesting an increase in the extracellular matrix along with t-tubular remodeling (Crossman et al., 2011). More recently, it was found that these dilated t-tubules also show increased labeling for collagen VI, an isoform typically not found in t-tubules, in patients with idiopathic dilated cardiomyopathy (Crossman et al., 2017; Speiser et al., 1991). The unexpected colocalization of a fibroblast filopodia within dilated t-tubule lumens have led to the proposal that fibroblasts may directly remodel t-tubules by depositing collagen VI in disease conditions (Crossman et al., 2017).

However, given the strong link between t-tubule remodeling and fibroblast activation with mechanical stress, the correlation between t-tubule remodeling and fibrosis may be a foregone conclusion. Fibrosis is associated with stiffening of the myocardium and others have suggested that the surrounding fibrotic tissue may affect the mechanical forces acting on a cell (Seidel et al., 2017b). Shearing was suggested to develop if a cell is adjacent to an essentially static fibrotic mass while connected to a contracting cell on the other side. Excessive mechanical stress created in this situation

would likely result in t-tubule disruption. The effect of fibrosis on the mechanical properties of the myocardium may be heterogeneous. Maron observed that some cells were completely separated from other cells by large amounts of fibrotic tissue (Maron et al., 1975). These cells appeared atrophied and displayed severe t-tubule loss and vacuolations. In this situation, it appears that part of the myocardium was electrically and mechanically isolated from the rest of the tissue, resulting in local mechanical unloading and t-tubule remodeling. Further studies are necessary to determine how fibrosis modifies the local mechanical environment surrounding the cardiomyocyte and how the mechanical stimuli modulate t-tubular structure.

5.4 Physiological Implications

5.4.1 Pathophysiological osmotic swelling

Plasma osmolarity is strictly controlled and the heart rarely encounters strong osmotic stresses such as those used to detubulate cardiomyocytes *in vitro*. However, certain conditions are expected to cause milder osmotic stresses.

Metabolically stressed muscle cells can accumulate metabolites and display significant cell swelling (Jennings et al., 1986; Peeze Binkhorst et al., 1990; Raja et al., 2006). This suggests that situations of extreme metabolic stress such as myocardial ischemia may provide the necessary conditions for cardiomyocyte volume changes to occur. Indeed, tissue swelling has been observed in Langendorff perfused hearts during global ischemia (Askenasy and Navon, 2005). Isolated cardiomyocytes have been reported to increase in volume by as much as 40% after 30 min exposure to simulated ischemia (Diaz et al., 2003). The ischemic cell swelling is rapidly reversed upon reperfusion. Therefore, the cell volume response observed during ischemia-reperfusion

would qualitatively mimic the volume changes observed during hyposmotic detubulation. Preliminary work in our lab showed that global IR of Langendorff perfused whole hearts leads to significant sealing of t-tubules, evidenced by trapping of extracellularly applied fluorescent dextran. Furthermore, $I_{K1,tail}$ currents measured in cardiomyocytes isolated from Langendorff perfused hearts exposed to 30 min ischemia/ 30 min reperfusion showed a significant decrease compared to those in control perfused hearts. These studies indicated that t-tubule sealing following IR injury may be driven by a mechanism similar to hyposmotic detubulation.

However, when cell volume measurements were performed in isolated cardiomyocytes perfused with simulated ischemia solutions at room temperature, very little change in cell width was observed (~2% increase in cell width after 20 min perfusion). Unsurprisingly, the t-tubular diffusion time constant was not significantly different from that in control cells after perfusion with simulated ischemia solution. Unfortunately, the diffusion time constant could not be reliably measured following reperfusion due to the high mortality of individual myocytes. Future experiments may attempt to measure dextran diffusion, cell volume changes, and t-tubular remodeling in multicellular preparations, which may tolerate ischemia-reperfusion stress better than isolated cardiomyocytes.

5.4.2 Mechanical modulation of t-tubular diffusion

Chapter 2 and 3 demonstrated that the diffusional mobility within t-tubules can be restricted by osmotic stress. However, as mentioned above, osmotic stress is rarely encountered *in vivo*. As discussed in the Physiological Implications section of Chapter 3.5, it remains unknown how physiological or pathophysiological mechanical stretch

affects t-tubular structure. Determining the relationship between mechanical stress and t-tubular diffusion remains a critical open question that needs to be addressed in future studies. In this regard, Scardigli et al. has demonstrated that cardiomyocytes from failing rat hearts display restricted t-tubular diffusion (Scardigli et al., 2017), suggesting that there is some correlation between diffusional mobility in t-tubules and mechanical stress. However, heart failure is a complex disorder and a variety of other factors may contribute to the slow diffusion rate including overt t-tubular loss. One approach to study this link between mechanical stress and t-tubular diffusion is to take advantage of the inherent heterogeneity in mechanical stress within a single heart. There is a strong transmural gradient of mechanical stress across the ventricular wall with greater mechanical stress in endocardial (endo) cells than in epicardial (epi) cells (Streeter et al., 1970). The *in vivo* heterogeneity in mechanical stress may partially explain the broad distribution of t-tubular diffusion observed in mouse cardiomyocytes (Fig 2.5). However, separation of endo/epi cells in mouse ventricles is difficult due to the thin ventricular wall. The magnitude of the transient outward current (I_{TO}) also demonstrates a transmural gradient with greater levels of I_{TO} observed in epicardial cells and less in endo cells (Clark et al., 1993). A weak negative correlation was observed in a preliminary analysis between the peak I_{TO} amplitude and the time constant of the decline of $I_{K1,tail}$ current, suggesting that perhaps t-tubular diffusion is more restricted in endo than in epi cells. However, further studies are necessary to rigorously test this hypothesis. Dual measurements of I_{TO} and dextran diffusion may be a better direct method to address this question. Ultimately, this hypothesis can be more easily tested in larger mammals (canine for example) and future studies could measure t-tubular diffusion across myocytes isolated from different sections

across the ventricular wall to correlate t-tubular structure with transmural mechanical stress. Furthermore, isolated cardiomyocytes can be exposed to varying levels of mechanical stretch and the diffusional mobility can be measured before and after the stretch as a proof-of-concept experiment to demonstrate the link between t-tubular structure and mechanical stretch. Finally, rapid cryofixation methods may be optimized in ventricular myocytes to minimize potential fixation artifacts (e.g. due to strong osmotic effects of fixatives) that arise during sample preparation for electron microscopy. Proper fixation may allow for the direct visualization and quantitative characterization of t-tubular constrictions and dilations in three dimensional reconstructions from serial block face scanning EM or focused ion beam scanning EM in stretched and unloaded myocytes. Overall, these future studies would add strong support to a hypothetical mechanism directly linking mechanical stress and the formation of t-tubular constrictions and dilations.

If future experiments support the notion that t-tubular diffusion is stretch regulated, then mechanical control of t-tubular diffusion may be a mechanotransduction mechanism that has significant effects on various signaling pathways. The electrical properties of cardiomyocytes are also heterogeneous across the ventricular wall and are correlated with the magnitude of mechanical stress (Gao et al., 2014). Endo cells typically have longer action potentials than epi cells, largely due to the differential expression levels of voltage gated potassium channels (Clark et al., 1993; Cohen and Mathias, 2016; Kim et al., 2015). The pump current (I_{pump}) produced by the electrogenic Na^+/K^+ ATPase has also been reported to display a transmural gradient (Gao et al., 2014). Recent work by Gao et al proposed the hypothetical model that angiotensin II (Ang II), which is secreted from cardiomyocytes in response to mechanical stretch (Sadoshima et al., 1993), may

underlie this transmural gradient (Gao et al., 2014). Ang II acts on Angiotensin II Type 1 receptors (AT1R) that are expressed on the t-tubular membrane (Gao et al., 2014). These authors demonstrated that the electrical properties of canine endo and epi cells can be induced by application of exogenous Ang II or specific blockade of AT1R, respectively (Gao et al., 2014), demonstrating that the t-tubular AT1R activation dynamically regulates the expression of various ion channels and transporters. Similar effects were observed in mouse ventricular myocytes (Kim et al., 2015). Importantly, the concentration of Ang II necessary to cause these changes in ion channel expression levels are folds greater than the plasma concentration of Ang II (van Kats et al., 1998). These observations led the authors to hypothesize that a transmural gradient of mechanical stress causes differential release of Ang II across the myocardium, which down regulates I_{TO} and I_{pump} by activation of AT1R signaling (Cohen and Mathias, 2016). However, the mechanism that transduces the differential mechanical stress to the magnitude of AT1R activation remains unknown.

Based on the above literature, the key parameter is the concentration of t-tubular Ang II, which is estimated to be in the low micromolar range in the endocardium (Gao et al., 2014). The effective concentration of t-tubular Ang II is dependent on 1) secretion rate into the t-tubule lumen and 2) the diffusion rate of the ligand out of the t-tubule. As demonstrated in Chapter 2, this latter factor is critically dependent on the sub-microscopic structure of t-tubules and will certainly affect the local Ang II concentration. However, to date, direct measurements of Ang II concentration in t-tubules and the secretion rate of Ang II into the t-tubular lumen remain unavailable. Future studies could measure the diffusion rate of fluorescently tagged Ang II to get a quantitative understanding of the

magnitude of the effect that t-tubular constrictions may have on Ang II diffusion and the effective Ang II concentration.

Furthermore, if one may make the radical assumption that the previous hypotheses that diffusion in t-tubules is mechanically regulated and displays a transmural gradient are in fact supported by future experiments, then these sub-microscopic structures may dynamically regulate the t-tubular Ang II concentration and the magnitude of AT1R activation in response to mechanical load. In this way, t-tubular constrictions and dilations may directly regulate electrical remodeling of the t-tubular ion channels and may have potential implications for ventricular repolarization and the generation of arrhythmogenic substrates. This hypothetical regulation of signaling pathways by t-tubular diffusion may extend to other signaling pathways as well. Similar to Ang II, Endothelin I (ET1) has been reported to be secreted in a stretch-dependent manner (Yamazaki et al., 1996), the plasma concentrations of ET1 are too low for activation of ET1 receptors, and ET1 receptors are also concentrated on the t-tubular membrane (Robu et al., 2003). Both pathways (ET1 and AngII) have been implicated in activation of hypertrophic signaling pathways (Sadoshima and Izumo, 1993; Sadoshima et al., 1993; Yamazaki et al., 1996), so sustained t-tubular constrictions or dilations may represent the initial step in the development of cardiac hypertrophy. However, these are merely plausible speculations at the moment and further studies on the mechanical regulation of t-tubular diffusion are necessary to test these hypotheses. Overall, the t-tubular system represents an exciting model to study the interaction between mechanical and biochemical signals and the transition from physiologic to pathophysiologic remodeling.

BIBLIOGRAPHY

Askenasy, N., and Navon, G. (2005). Measurements of intracellular volumes by 59Co and 2H/1H NMR and their physiological applications. NMR Biomed *18*, 104-110.

Ben-Dov, N., and Korenstein, R. (2012). Enhancement of cell membrane invaginations, vesiculation and uptake of macromolecules by protonation of the cell surface. PloS one *7*, e35204.

Ben-Dov, N., and Korenstein, R. (2013a). Actin-cytoskeleton rearrangement modulates proton-induced uptake. Experimental cell research *319*, 946-954.

Ben-Dov, N., and Korenstein, R. (2013b). Proton-induced endocytosis is dependent on cell membrane fluidity, lipid-phase order and the membrane resting potential. Biochimica et biophysica acta *1828*, 2672-2681.

Bers, D.M. (2001). Excitation-Contraction Coupling and Cardiac Contractile Force. In Developments in Cardiovascular Medicine, (Dordrecht: Springer Netherlands), pp. 1 online resource (452 pages).

Bers, D.M. (2002). Cardiac excitation-contraction coupling. Nature *415*, 198-205.

Bers, D.M., and Peskoff, A. (1991). Diffusion around a cardiac calcium channel and the role of surface bound calcium. Biophys J *59*, 703-721.

Boyett, M.R., Frampton, J.E., and Kirby, M.S. (1991). The length, width and volume of isolated rat and ferret ventricular myocytes during twitch contractions and changes in osmotic strength. Experimental physiology *76*, 259-270.

Brette, F., Calaghan, S.C., Lappin, S., White, E., Colyer, J., and Le Guennec, J.Y. (2000). Biphasic effects of hyposmotic challenge on excitation-contraction coupling in rat ventricular myocytes. American journal of physiology Heart and circulatory physiology *279*, H1963-1971.

Brette, F., Komukai, K., and Orchard, C.H. (2002). Validation of formamide as a detubulation agent in isolated rat cardiac cells. American journal of physiology Heart and circulatory physiology *283*, H1720-1728.

Brette, F., and Orchard, C. (2007). Resurgence of cardiac t-tubule research. Physiology *22*, 167-173.

Cannell, M.B., Crossman, D.J., and Soeller, C. (2006). Effect of changes in action potential spike configuration, junctional sarcoplasmic reticulum micro-architecture and altered t-tubule structure in human heart failure. J Muscle Res Cell Motil *27*, 297-306.

Charras, G.T., Yarrow, J.C., Horton, M.A., Mahadevan, L., and Mitchison, T.J. (2005). Non-equilibration of hydrostatic pressure in blebbing cells. Nature *435*, 365-369.

Cheng, L.F., Wang, F., and Lopatin, A.N. (2011). Metabolic stress in isolated mouse ventricular myocytes leads to remodeling of t tubules. American journal of physiology Heart and circulatory physiology *301*, H1984-1995.

Christe, G. (1999). Localization of K(+) channels in the tubules of cardiomyocytes as suggested by the parallel decay of membrane capacitance, IK(1) and IK(ATP) during culture and by delayed IK(1) response to barium. J Mol Cell Cardiol *31*, 2207-2213.

Clark, R.B., Bouchard, R.A., Salinas-Stefanon, E., Sanchez-Chapula, J., and Giles, W.R. (1993). Heterogeneity of action potential waveforms and potassium currents in rat ventricle. Cardiovascular research *27*, 1795-1799.

Clark, R.B., Tremblay, A., Melnyk, P., Allen, B.G., Giles, W.R., and Fiset, C. (2001). T-tubule localization of the inward-rectifier K(+) channel in mouse ventricular myocytes: a role in K(+) accumulation. The Journal of physiology *537*, 979-992.

Cohen, I.S., and Mathias, R.T. (2016). The renin-angiotensin system regulates transmural electrical remodeling in response to mechanical load. Progress in biophysics and molecular biology *122*, 187-201.

Crocini, C., Coppini, R., Ferrantini, C., Yan, P., Loew, L.M., Tesi, C., Cerbai, E., Poggesi, C., Pavone, F.S., and Sacconi, L. (2014). Defects in T-tubular electrical activity underlie local alterations of calcium release in heart failure. Proceedings of the National Academy of Sciences of the United States of America *111*, 15196-15201.

Crossman, D.J., Ruygrok, P.N., Soeller, C., and Cannell, M.B. (2011). Changes in the organization of excitation-contraction coupling structures in failing human heart. PloS one *6*, e17901.

Crossman, D.J., Shen, X., Jullig, M., Munro, M., Hou, Y., Middleditch, M., Shrestha, D., Li, A., Lal, S., Dos Remedios, C.G*., et al.* (2017). Increased collagen within the transverse tubules in human heart failure. Cardiovascular research.

Despa, S., Brette, F., Orchard, C.H., and Bers, D.M. (2003). Na/Ca exchange and Na/K-ATPase function are equally concentrated in transverse tubules of rat ventricular myocytes. Biophysical journal *85*, 3388-3396.

Diaz, R.J., Armstrong, S.C., Batthish, M., Backx, P.H., Ganote, C.E., and Wilson, G.J. (2003). Enhanced cell volume regulation: a key protective mechanism of ischemic preconditioning in rabbit ventricular myocytes. Journal of molecular and cellular cardiology *35*, 45-58.

Diz-Munoz, A., Fletcher, D.A., and Weiner, O.D. (2013). Use the force: membrane tension as an organizer of cell shape and motility. Trends Cell Biol *23*, 47-53.

Drewnowska, K., and Baumgarten, C.M. (1991). Regulation of cellular volume in rabbit ventricular myocytes: bumetanide, chlorothiazide, and ouabain. The American journal of physiology *260*, C122-131.

Dulhunty, A.F., and Franzini-Armstrong, C. (1975). The relative contributions of the folds and caveolae to the surface membrane of frog skeletal muscle fibres at different sarcomere lengths. The Journal of physiology *250*, 513-539.

Edwards, J.N., and Launikonis, B.S. (2008). The accessibility and interconnectivity of the tubular system network in toad skeletal muscle. The Journal of physiology *586*, 5077-5089.

Endo, M. (1964). Entry of a Dye into the Sarcotubular System of Muscle. Nature *202*, 1115-1116.

Endo, M. (1966). Entry of fluorescent dyes into the sarcotubular system of the frog muscle. The Journal of physiology *185*, 224-238.

Evans, E., and Leung, A. (1984). Adhesivity and rigidity of erythrocyte membrane in relation to wheat germ agglutinin binding. The Journal of cell biology *98*, 1201-1208.

Fawcett, D.W., and McNutt, N.S. (1969). The ultrastructure of the cat myocardium. I. Ventricular papillary muscle. The Journal of cell biology *42*, 1-45.

Ferrantini, C., Coppini, R., Sacconi, L., Tosi, B., Zhang, M.L., Wang, G.L., de Vries, E., Hoppenbrouwers, E., Pavone, F., Cerbai, E.*, et al.* (2014). Impact of detubulation on force and kinetics of cardiac muscle contraction. The Journal of general physiology *143*, 783-797.

Ferrantini, C., Crocini, C., Coppini, R., Vanzi, F., Tesi, C., Cerbai, E., Poggesi, C., Pavone, F.S., and Sacconi, L. (2013). The transverse-axial tubular system of cardiomyocytes. Cellular and molecular life sciences : CMLS *70*, 4695-4710.

Fine, M., Llaguno, M.C., Lariccia, V., Lin, M.J., Yaradanakul, A., and Hilgemann, D.W. (2011). Massive endocytosis driven by lipidic forces originating in the outer plasmalemmal monolayer: a new approach to membrane recycling and lipid domains. The Journal of general physiology *137*, 137-154.

Forbes, M.S., Hawkey, L.A., and Sperelakis, N. (1984). The transverse-axial tubular system (TATS) of mouse myocardium: its morphology in the developing and adult animal. Am J Anat *170*, 143-162.

Friedman, A.M., and Kennedy, J.W. (1955). The self-diffusion coefficients of potassium, cesium, iodide and chloride ions in aqueous solutions. Journal of the American Chemical Society *77*, 4499-4501.

Frisk, M., Ruud, M., Espe, E.K., Aronsen, J.M., Roe, A.T., Zhang, L., Norseng, P.A., Sejersted, O.M., Christensen, G., Sjaastad, I.*, et al.* (2016). Elevated ventricular wall stress disrupts cardiomyocyte t-tubule structure and calcium homeostasis. Cardiovascular research.

Gadeberg, H.C., Kong, C.H.T., Bryant, S.M., James, A.F., and Orchard, C.H. (2017a). Cholesterol depletion does not alter the capacitance or Ca handling of the surface or t-tubule membranes in mouse ventricular myocytes. Physiol Rep *5*.

Gadeberg, H.C., Kong, C.H.T., Bryant, S.M., James, A.F., and Orchard, C.H. (2017b). Sarcolemmal distribution of ICa and INCX and Ca autoregulation in mouse ventricular myocytes. American journal of physiology Heart and circulatory physiology, ajpheart 00117 02017.

Gallagher, F.A., and Huang, C.L. (1997). Osmotic 'detubulation' in frog muscle arises from a reversible vacuolation process. J Muscle Res Cell Motil *18*, 305-321.

Gao, J., Sun, X., Potapova, I.A., Cohen, I.S., Mathias, R.T., and Kim, J.H. (2014). Autocrine A2 in the T-system of ventricular myocytes creates transmural gradients in ion transport: a mechanism to match contraction with load? Biophysical journal *106*, 2364-2374.

Gauthier, N.C., Fardin, M.A., Roca-Cusachs, P., and Sheetz, M.P. (2011). Temporary increase in plasma membrane tension coordinates the activation of exocytosis and contraction during cell spreading. Proceedings of the National Academy of Sciences of the United States of America *108*, 14467-14472.

Gerdes, A.M., Kellerman, S.E., Malec, K.B., and Schocken, D.D. (1994). Transverse shape characteristics of cardiac myocytes from rats and humans. Cardioscience *5*, 31-36.

Gomez, A.M. (1997). Defective Excitation-Contraction Coupling in Experimental Cardiac Hypertrophy and Heart Failure. Science *276*, 800-806.

Gomez, A.M., Guatimosim, S., Dilly, K.W., Vassort, G., and Lederer, W.J. (2001). Heart failure after myocardial infarction: altered excitation-contraction coupling. Circulation *104*, 688-693.

Guo, A., Chen, R., Wang, Y., Huang, C.K., Chen, B., Kutschke, W., Hong, J., and Song, L.S. (2018). Transient activation of PKC results in long-lasting detrimental effects on systolic [Ca(2+)]i in cardiomyocytes by altering actin cytoskeletal dynamics and T-tubule integrity. Journal of molecular and cellular cardiology *115*, 104-114.

Guo, A., Zhang, C., Wei, S., Chen, B., and Song, L.S. (2013). Emerging mechanisms of T-tubule remodelling in heart failure. Cardiovascular research *98*, 204-215.

Guo, A., Zhang, X., Iyer, V.R., Chen, B., Zhang, C., Kutschke, W.J., Weiss, R.M., Franzini-Armstrong, C., and Song, L.S. (2014). Overexpression of junctophilin-2 does not

enhance baseline function but attenuates heart failure development after cardiac stress. Proceedings of the National Academy of Sciences of the United States of America *111*, 12240-12245.

Guo, Y., VanDusen, N.J., Zhang, L., Gu, W., Sethi, I., Guatimosim, S., Ma, Q., Jardin, B.D., Ai, Y., Zhang, D.*, et al.* (2017). Analysis of Cardiac Myocyte Maturation Using CASAAV, a Platform for Rapid Dissection of Cardiac Myocyte Gene Function In Vivo. Circ Res *120*, 1874-1888.

Gurtovenko, A.A., and Anwar, J. (2007). Modulating the structure and properties of cell membranes: the molecular mechanism of action of dimethyl sulfoxide. The journal of physical chemistry B *111*, 10453-10460.

Heinzel, F.R., Bito, V., Biesmans, L., Wu, M., Detre, E., von Wegner, F., Claus, P., Dymarkowski, S., Maes, F., Bogaert, J.*, et al.* (2008). Remodeling of T-tubules and reduced synchrony of Ca2+ release in myocytes from chronically ischemic myocardium. Circ Res *102*, 338-346.

Heinzel, F.R., Bito, V., Volders, P.G., Antoons, G., Mubagwa, K., and Sipido, K.R. (2002). Spatial and temporal inhomogeneities during Ca2+ release from the sarcoplasmic reticulum in pig ventricular myocytes. Circ Res *91*, 1023-1030.

Hidalgo, C. (1985). Lipid phase of transverse tubule membranes from skeletal muscle. An electron paramagnetic resonance study. Biophysical journal *47*, 757-764.

Hilgemann, D.W., Dai, G., Collins, A., Larricia, V., Magi, S., Deisl, C., and Fine, M. (2018). Lipid signaling to membrane proteins: From second messengers to membrane domains and adapter-free endocytosis. The Journal of general physiology *150*, 211-224.

Hilgemann, D.W., and Fine, M. (2011). Mechanistic analysis of massive endocytosis in relation to functionally defined surface membrane domains. The Journal of general physiology *137*, 155-172.

Hilgemann, D.W., Fine, M., Linder, M.E., Jennings, B.C., and Lin, M.J. (2013). Massive endocytosis triggered by surface membrane palmitoylation under mitochondrial control in BHK fibroblasts. eLife *2*, e01293.

Hochmuth, F.M., Shao, J.Y., Dai, J., and Sheetz, M.P. (1996). Deformation and flow of membrane into tethers extracted from neuronal growth cones. Biophysical journal *70*, 358-369.

Hochmuth, R.M., Mohandas, N., and Blackshear, P.L., Jr. (1973). Measurement of the elastic modulus for red cell membrane using a fluid mechanical technique. Biophysical journal *13*, 747-762.

Hong, T., Yang, H., Zhang, S.S., Cho, H.C., Kalashnikova, M., Sun, B., Zhang, H., Bhargava, A., Grabe, M., Olgin, J.*, et al.* (2014). Cardiac BIN1 folds T-tubule membrane, controlling ion flux and limiting arrhythmia. Nature medicine *20*, 624-632.

Ibrahim, M., Al Masri, A., Navaratnarajah, M., Siedlecka, U., Soppa, G.K., Moshkov, A., Al-Saud, S.A., Gorelik, J., Yacoub, M.H., and Terracciano, C.M. (2010). Prolonged mechanical unloading affects cardiomyocyte excitation-contraction coupling, transverse-tubule structure, and the cell surface. FASEB J *24*, 3321-3329.

Ibrahim, M., Kukadia, P., Siedlecka, U., Cartledge, J.E., Navaratnarajah, M., Tokar, S., Van Doorn, C., Tsang, V.T., Gorelik, J., Yacoub, M.H.*, et al.* (2012a). Cardiomyocyte Ca2+ handling and structure is regulated by degree and duration of mechanical load variation. Journal of cellular and molecular medicine *16*, 2910-2918.

Ibrahim, M., Navaratnarajah, M., Siedlecka, U., Rao, C., Dias, P., Moshkov, A.V., Gorelik, J., Yacoub, M.H., and Terracciano, C.M. (2012b). Mechanical unloading reverses transverse tubule remodelling and normalizes local Ca(2+)-induced Ca(2+)release in a rodent model of heart failure. Eur J Heart Fail *14*, 571-580.

Ibrahim, M., Siedlecka, U., Buyandelger, B., Harada, M., Rao, C., Moshkov, A., Bhargava, A., Schneider, M., Yacoub, M.H., Gorelik, J.*, et al.* (2013). A critical role for Telethonin in regulating t-tubule structure and function in the mammalian heart. Hum Mol Genet *22*, 372-383.

Ibrahim, M., and Terracciano, C.M. (2013). Reversibility of T-tubule remodelling in heart failure: mechanical load as a dynamic regulator of the T-tubules. Cardiovascular research *98*, 225-232.

Jayasinghe, I., Crossman, D., Soeller, C., and Cannell, M. (2012). Comparison of the organization of T-tubules, sarcoplasmic reticulum and ryanodine receptors in rat and human ventricular myocardium. Clin Exp Pharmacol Physiol *39*, 469-476.

Jayasinghe, I.D., Cannell, M.B., and Soeller, C. (2009). Organization of ryanodine receptors, transverse tubules, and sodium-calcium exchanger in rat myocytes. Biophysical journal *97*, 2664-2673.

Jennings, R.B., Reimer, K.A., and Steenbergen, C. (1986). Myocardial ischemia revisited. The osmolar load, membrane damage, and reperfusion. Journal of molecular and cellular cardiology *18*, 769-780.

Jian, Z., Han, H., Zhang, T., Puglisi, J., Izu, L.T., Shaw, J.A., Onofiok, E., Erickson, J.R., Chen, Y.J., Horvath, B.*, et al.* (2014). Mechanochemotransduction during cardiomyocyte contraction is mediated by localized nitric oxide signaling. Science signaling *7*, ra27.

Katz, A.M. (2010). Physiology of the heart, 5th edn (Philadelphia, Pa. ; London: Lippincott Williams & Wilkins).

Kawai, M., Hussain, M., and Orchard, C.H. (1999). Excitation-contraction coupling in rat ventricular myocytes after formamide-induced detubulation. The American journal of physiology *277*, H603-609.

Kerr, J.P., Ziman, A.P., Mueller, A.L., Muriel, J.M., Kleinhans-Welte, E., Gumerson, J.D., Vogel, S.S., Ward, C.W., Roche, J.A., and Bloch, R.J. (2013). Dysferlin stabilizes stress-induced Ca2+ signaling in the transverse tubule membrane. Proceedings of the National Academy of Sciences of the United States of America *110*, 20831-20836.

Kihara, T., Ito, J., and Miyake, J. (2013). Measurement of biomolecular diffusion in extracellular matrix condensed by fibroblasts using fluorescence correlation spectroscopy. PLoS One *8*, e82382.

Kim, J., Gao, J., Cohen, I.S., and Mathias, R.T. (2015). Angiotensin II Type 1 Receptor-Mediated Electrical Remodeling in Mouse Cardiac Myocytes. PloS one *10*, e0138711.

Kohl, P., Cooper, P.J., and Holloway, H. (2003). Effects of acute ventricular volume manipulation on in situ cardiomyocyte cell membrane configuration. Progress in biophysics and molecular biology *82*, 221-227.

Kong, C.H.T., Rog-Zielinska, E.A., Orchard, C.H., Kohl, P., and Cannell, M.B. (2017). Sub-microscopic analysis of t-tubule geometry in living cardiac ventricular myocytes using a shape-based analysis method. Journal of molecular and cellular cardiology *108*, 1-7.

Kosmalska, A.J., Casares, L., Elosegui-Artola, A., Thottacherry, J.J., Moreno-Vicente, R., Gonzalez-Tarrago, V., Del Pozo, M.A., Mayor, S., Arroyo, M., Navajas, D*., et al.* (2015). Physical principles of membrane remodelling during cell mechanoadaptation. Nat Commun *6*, 7292.

Kostin, S., Scholz, D., Shimada, T., Maeno, Y., Mollnau, H., Hein, S., and Schaper, J. (1998). The internal and external protein scaffold of the T-tubular system in cardiomyocytes. Cell Tissue Res *294*, 449-460.

Krolenko, S.A., and Lucy, J.A. (2001). Reversible vacuolation of T-tubules in skeletal muscle: mechanisms and implications for cell biology. Int Rev Cytol *202*, 243-298.

Krolenko, S.A., and Lucy, J.A. (2002). Vacuolation in T-tubules as a model for tubular-vesicular transformations in biomembrane systems. Cell biology international *26*, 893-904.

Lande, M.B., Donovan, J.M., and Zeidel, M.L. (1995). The relationship between membrane fluidity and permeabilities to water, solutes, ammonia, and protons. The Journal of general physiology *106*, 67-84.

Lariccia, V., Fine, M., Magi, S., Lin, M.J., Yaradanakul, A., Llaguno, M.C., and Hilgemann, D.W. (2011). Massive calcium-activated endocytosis without involvement of classical endocytic proteins. The Journal of general physiology *137*, 111-132.

Levental, I., Lingwood, D., Grzybek, M., Coskun, U., and Simons, K. (2010). Palmitoylation regulates raft affinity for the majority of integral raft proteins. Proceedings of the National Academy of Sciences of the United States of America *107*, 22050-22054.

Levin, K.R., and Page, E. (1980). Quantitative studies on plasmalemmal folds and caveolae of rabbit ventricular myocardial cells. Circ Res *46*, 244-255.

Li, H., Lichter, J.G., Seidel, T., Tomaselli, G.F., Bridge, J.H., and Sachse, F.B. (2015). Cardiac Resynchronization Therapy Reduces Subcellular Heterogeneity of Ryanodine Receptors, T-Tubules, and Ca2+ Sparks Produced by Dyssynchronous Heart Failure. Circulation Heart failure *8*, 1105-1114.

Lin, M.J., Fine, M., Lu, J.Y., Hofmann, S.L., Frazier, G., and Hilgemann, D.W. (2013). Massive palmitoylation-dependent endocytosis during reoxygenation of anoxic cardiac muscle. eLife *2*, e01295.

Louch, W.E., Bito, V., Heinzel, F.R., Macianskiene, R., Vanhaecke, J., Flameng, W., Mubagwa, K., and Sipido, K.R. (2004). Reduced synchrony of Ca2+ release with loss of T-tubules-a comparison to Ca2+ release in human failing cardiomyocytes. Cardiovascular research *62*, 63-73.

Louch, W.E., Mork, H.K., Sexton, J., Stromme, T.A., Laake, P., Sjaastad, I., and Sejersted, O.M. (2006). T-tubule disorganization and reduced synchrony of Ca2+ release in murine cardiomyocytes following myocardial infarction. The Journal of physiology *574*, 519-533.

Louch, W.E., Sejersted, O.M., and Swift, F. (2010). There goes the neighborhood: pathological alterations in T-tubule morphology and consequences for cardiomyocyte Ca2+ handling. Journal of biomedicine & biotechnology *2010*, 503906.

Lyon, A.R., MacLeod, K.T., Zhang, Y., Garcia, E., Kanda, G.K., Lab, M.J., Korchev, Y.E., Harding, S.E., and Gorelik, J. (2009). Loss of T-tubules and other changes to surface topography in ventricular myocytes from failing human and rat heart. Proceedings of the National Academy of Sciences of the United States of America *106*, 6854-6859.

Maron, B.J., Ferrans, V.J., and Roberts, W.C. (1975). Ultrastructural features of degenerated cardiac muscle cells in patients with cardiac hypertrophy. The American journal of pathology *79*, 387-434.

Mathai, J.C., Tristram-Nagle, S., Nagle, J.F., and Zeidel, M.L. (2008). Structural determinants of water permeability through the lipid membrane. The Journal of general physiology *131*, 69-76.

McNary, T.G., Bridge, J.H., and Sachse, F.B. (2011). Strain transfer in ventricular cardiomyocytes to their transverse tubular system revealed by scanning confocal microscopy. Biophysical journal *100*, L53-55.

McNary, T.G., Spitzer, K.W., Holloway, H., Bridge, J.H., Kohl, P., and Sachse, F.B. (2012). Mechanical modulation of the transverse tubular system of ventricular cardiomyocytes. Progress in biophysics and molecular biology *110*, 218-225.

Moench, I., and Lopatin, A.N. (2014). Ca homeostasis in sealed t-tubules of mouse ventricular myocytes. J Mol Cell Cardiol *72C*, 374-383.

Moench, I., Meekhof, K.E., Cheng, L.F., and Lopatin, A.N. (2013). Resolution of hyposmotic stress in isolated mouse ventricular myocytes causes sealing of t-tubules. Experimental physiology *98*, 1164-1177.

Morris, C.E., and Homann, U. (2001). Cell surface area regulation and membrane tension. J Membr Biol *179*, 79-102.

Navaratnarajah, M., Ibrahim, M., Siedlecka, U., van Doorn, C., Shah, A., Gandhi, A., Dias, P., Sarathchandra, P., Yacoub, M.H., and Terracciano, C.M. (2013). Influence of ivabradine on reverse remodelling during mechanical unloading. Cardiovascular research *97*, 230-239.

Nichol, J.A., and Hutter, O.F. (1996). Tensile strength and dilatational elasticity of giant sarcolemmal vesicles shed from rabbit muscle. The Journal of physiology *493 (Pt 1)*, 187-198.

Nikolaev, V.O., Moshkov, A., Lyon, A.R., Miragoli, M., Novak, P., Paur, H., Lohse, M.J., Korchev, Y.E., Harding, S.E., and Gorelik, J. (2010). Beta2-adrenergic receptor redistribution in heart failure changes cAMP compartmentation. Science *327*, 1653-1657.

Ogata, T., and Yamasaki, Y. (1990). High-resolution scanning electron microscopic studies on the three-dimensional structure of the transverse-axial tubular system, sarcoplasmic reticulum and intercalated disc of the rat myocardium. Anat Rec *228*, 277-287.

Ogura, T., Imanishi, S., and Shibamoto, T. (2002). Osmometric and water-transporting properties of guinea pig cardiac myocytes. Jpn J Physiol *52*, 333-342.

Ogura, T., Shuba, L.M., and McDonald, T.F. (1995). Action potentials, ionic currents and cell water in guinea pig ventricular preparations exposed to dimethyl sulfoxide. The Journal of pharmacology and experimental therapeutics *273*, 1273-1286.

Ohler, A., Weisser-Thomas, J., Piacentino, V., Houser, S.R., Tomaselli, G.F., and O'Rourke, B. (2009). Two-photon laser scanning microscopy of the transverse-axial tubule system in ventricular cardiomyocytes from failing and non-failing human hearts. Cardiol Res Pract *2009*, 802373.

Osman, S., Taylor, K.A., Allcock, N., Rainbow, R.D., and Mahaut-Smith, M.P. (2016). Detachment of surface membrane invagination systems by cationic amphiphilic drugs. Sci Rep *6*, 18536.

Oyehaug, L., Loose, K.O., Jolle, G.F., Roe, A.T., Sjaastad, I., Christensen, G., Sejersted, O.M., and Louch, W.E. (2013). Synchrony of cardiomyocyte Ca(2+) release is controlled by T-tubule organization, SR Ca(2+) content, and ryanodine receptor Ca(2+) sensitivity. Biophysical journal *104*, 1685-1697.

Page, E., and Upshaw-Earley, J. (1977). Volume changes in sarcoplasmic reticulum of rat hearts perfused with hypertonic solutions. Circ Res *40*, 355-366.

Parfenov, A.S., Salnikov, V., Lederer, W.J., and Lukyanenko, V. (2006). Aqueous diffusion pathways as a part of the ventricular cell ultrastructure. Biophysical journal *90*, 1107-1119.

Pasek, M., Brette, F., Nelson, A., Pearce, C., Qaiser, A., Christe, G., and Orchard, C.H. (2008). Quantification of t-tubule area and protein distribution in rat cardiac ventricular myocytes. Progress in biophysics and molecular biology *96*, 244-257.

Pavlovic, D., McLatchie, L.M., and Shattock, M.J. (2010). The rate of loss of T-tubules in cultured adult ventricular myocytes is species dependent. Experimental physiology *95*, 518-527.

Peachey, L.D. (1965). The sarcoplasmic reticulum and transverse tubules of the frog's sartorius. The Journal of cell biology *25*, Suppl:209-231.

Peeze Binkhorst, F.M., Slaaf, D.W., Kuipers, H., Tangelder, G.J., and Reneman, R.S. (1990). Exercise-induced swelling of rat soleus muscle: its relationship with intramuscular pressure. J Appl Physiol (1985) *69*, 67-73.

Pinali, C., Bennett, H., Davenport, J.B., Trafford, A.W., and Kitmitto, A. (2013). Three-dimensional reconstruction of cardiac sarcoplasmic reticulum reveals a continuous network linking transverse-tubules: this organization is perturbed in heart failure. Circ Res *113*, 1219-1230.

Pinali, C., and Kitmitto, A. (2014). Serial block face scanning electron microscopy for the study of cardiac muscle ultrastructure at nanoscale resolutions. Journal of molecular and cellular cardiology *76*, 1-11.

Porter, K.R., and Palade, G.E. (1957). Studies on the endoplasmic reticulum. III. Its form and distribution in striated muscle cells. J Biophys Biochem Cytol *3*, 269-300.

Prosser, B.L., Ward, C.W., and Lederer, W.J. (2011). X-ROS signaling: rapid mechano-chemo transduction in heart. Science *333*, 1440-1445.

Rabbany, S.Y., Funai, J.T., and Noordergraaf, A. (1994). Pressure generation in a contracting myocyte. Heart Vessels *9*, 169-174.

Raja, M.K., Raymer, G.H., Moran, G.R., Marsh, G., and Thompson, R.T. (2006). Changes in tissue water content measured with multiple-frequency bioimpedance and metabolism measured with 31P-MRS during progressive forearm exercise. J Appl Physiol (1985) *101*, 1070-1075.

Reddy, A.S., Warshaviak, D.T., and Chachisvilis, M. (2012). Effect of membrane tension on the physical properties of DOPC lipid bilayer membrane. Biochimica et biophysica acta *1818*, 2271-2281.

Reuzeau, C., Mills, L.R., Harris, J.A., and Morris, C.E. (1995). Discrete and reversible vacuole-like dilations induced by osmomechanical perturbation of neurons. J Membr Biol *145*, 33-47.

Robu, V.G., Pfeiffer, E.S., Robia, S.L., Balijepalli, R.C., Pi, Y., Kamp, T.J., and Walker, J.W. (2003). Localization of functional endothelin receptor signaling complexes in cardiac transverse tubules. The Journal of biological chemistry *278*, 48154-48161.

Roos, K.P. (1986). Length, width, and volume changes in osmotically stressed myocytes. The American journal of physiology *251*, H1373-1378.

Sacconi, L., Ferrantini, C., Lotti, J., Coppini, R., Yan, P., Loew, L.M., Tesi, C., Cerbai, E., Poggesi, C., and Pavone, F.S. (2012). Action potential propagation in transverse-axial tubular system is impaired in heart failure. Proceedings of the National Academy of Sciences of the United States of America *109*, 5815-5819.

Sachse, F.B., Torres, N.S., Savio-Galimberti, E., Aiba, T., Kass, D.A., Tomaselli, G.F., and Bridge, J.H. (2012). Subcellular structures and function of myocytes impaired during heart failure are restored by cardiac resynchronization therapy. Circ Res *110*, 588-597.

Sadoshima, J., and Izumo, S. (1993). Molecular characterization of angiotensin II--induced hypertrophy of cardiac myocytes and hyperplasia of cardiac fibroblasts. Critical role of the AT1 receptor subtype. Circ Res *73*, 413-423.

Sadoshima, J., Xu, Y., Slayter, H.S., and Izumo, S. (1993). Autocrine release of angiotensin II mediates stretch-induced hypertrophy of cardiac myocytes in vitro. Cell *75*, 977-984.

Sandrin, D., Wagner, D., Sitta, C.E., Thoma, R., Felekyan, S., Hermes, H.E., Janiak, C., de Sousa Amadeu, N., Kuhnemuth, R., Lowen, H.*, et al.* (2016). Diffusion of macromolecules in a polymer hydrogel: from microscopic to macroscopic scales. Phys Chem Chem Phys *18*, 12860-12876.

Satoh, H., Delbridge, L.M., Blatter, L.A., and Bers, D.M. (1996). Surface:volume relationship in cardiac myocytes studied with confocal microscopy and membrane capacitance measurements: species-dependence and developmental effects. Biophysical journal *70*, 1494-1504.

Savio-Galimberti, E., Frank, J., Inoue, M., Goldhaber, J.I., Cannell, M.B., Bridge, J.H., and Sachse, F.B. (2008). Novel features of the rabbit transverse tubular system revealed by quantitative analysis of three-dimensional reconstructions from confocal images. Biophysical journal *95*, 2053-2062.

Scardigli, M., Crocini, C., Ferrantini, C., Gabbrielli, T., Silvestri, L., Coppini, R., Tesi, C., Rog-Zielinska, E.A., Kohl, P., Cerbai, E.*, et al.* (2017). Quantitative assessment of passive electrical properties of the cardiac T-tubular system by FRAP microscopy. Proceedings of the National Academy of Sciences of the United States of America.

Schaper, J., Froede, R., Hein, S., Buck, A., Hashizume, H., Speiser, B., Friedl, A., and Bleese, N. (1991). Impairment of the myocardial ultrastructure and changes of the cytoskeleton in dilated cardiomyopathy. Circulation *83*, 504-514.

Schneider, M.F. (1970). Linear electrical properties of the transverse tubules and surface membrane of skeletal muscle fibers. The Journal of general physiology *56*, 640-671.

Scriven, D.R., Klimek, A., Asghari, P., Bellve, K., and Moore, E.D. (2005). Caveolin-3 is adjacent to a group of extradyadic ryanodine receptors. Biophysical journal *89*, 1893-1901.

Seidel, T., Navankasattusas, S., Ahmad, A., Diakos, N.A., Xu, W.D., Tristani-Firouzi, M., Bonios, M.J., Taleb, I., Li, D.Y., Selzman, C.H.*, et al.* (2017a). Sheet-Like Remodeling of the Transverse Tubular System in Human Heart Failure Impairs Excitation-Contraction Coupling and Functional Recovery by Mechanical Unloading. Circulation *135*, 1632-1645.

Seidel, T., Sankarankutty, A.C., and Sachse, F.B. (2017b). Remodeling of the transverse tubular system after myocardial infarction in rabbit correlates with local fibrosis: A potential role of biomechanics. Progress in biophysics and molecular biology *130*, 302-314.

Sheetz, M.P., and Singer, S.J. (1974). Biological membranes as bilayer couples. A molecular mechanism of drug-erythrocyte interactions. Proceedings of the National Academy of Sciences of the United States of America *71*, 4457-4461.

Sheetz, M.P., and Singer, S.J. (1976). Equilibrium and kinetic effects of drugs on the shapes of human erythrocytes. The Journal of cell biology *70*, 247-251.

Shepherd, N., and McDonough, H.B. (1998). Ionic diffusion in transverse tubules of cardiac ventricular myocytes. The American journal of physiology *275*, H852-860.

Sinha, B., Koster, D., Ruez, R., Gonnord, P., Bastiani, M., Abankwa, D., Stan, R.V., Butler-Browne, G., Vedie, B., Johannes, L.*, et al.* (2011). Cells respond to mechanical stress by rapid disassembly of caveolae. Cell *144*, 402-413.

Smyrnias, I., Mair, W., Harzheim, D., Walker, S.A., Roderick, H.L., and Bootman, M.D. (2010). Comparison of the T-tubule system in adult rat ventricular and atrial myocytes, and its role in excitation-contraction coupling and inotropic stimulation. Cell calcium *47*, 210-223.

Soeller, C., and Cannell, M.B. (1999). Examination of the Transverse Tubular System in Living Cardiac Rat Myocytes by 2-Photon Microscopy and Digital Image Processing Techniques. Circulation Research *84*, 266-275.

Song, L.S., Sobie, E.A., McCulle, S., Lederer, W.J., Balke, C.W., and Cheng, H. (2006). Orphaned ryanodine receptors in the failing heart. Proceedings of the National Academy of Sciences of the United States of America *103*, 4305-4310.

Speiser, B., Riess, C.F., and Schaper, J. (1991). The extracellular matrix in human myocardium: Part I: Collagens I, III, IV, and VI. Cardioscience *2*, 225-232.

Staykova, M., Arroyo, M., Rahimi, M., and Stone, H.A. (2013). Confined bilayers passively regulate shape and stress. Phys Rev Lett *110*, 028101.

Staykova, M., Holmes, D.P., Read, C., and Stone, H.A. (2011). Mechanics of surface area regulation in cells examined with confined lipid membranes. Proceedings of the National Academy of Sciences of the United States of America *108*, 9084-9088.

Streeter, D.D., Jr., Vaishnav, R.N., Patel, D.J., Spotnitz, H.M., Ross, J., Jr., and Sonnenblick, E.H. (1970). Stress distribution in the canine left ventricle during diastole and systole. Biophysical journal *10*, 345-363.

Suleymanian, M.A., and Baumgarten, C.M. (1996). Osmotic gradient-induced water permeation across the sarcolemma of rabbit ventricular myocytes. The Journal of general physiology *107*, 503-514.

Sumnicht, G.E., and Sabbadini, R.A. (1982). Lipid composition of transverse tubular membranes from normal and dystrophic skeletal muscle. Archives of biochemistry and biophysics *215*, 628-637.

Swift, F., Stromme, T.A., Amundsen, B., Sejersted, O.M., and Sjaastad, I. (2006). Slow diffusion of K+ in the T tubules of rat cardiomyocytes. J Appl Physiol *101*, 1170-1176.

Uchida, K., and Lopatin, A.N. (2016). Fluorescent Dextran Diffusion Assay to Study Cardiac T-Tubules. Biophysical Journal *110*, 597A-598A.

Uchida, K., and Lopatin, A.N. (2018). Diffusional and Electrical Properties of T-Tubules Are Governed by Their Constrictions and Dilations. Biophysical journal *114*, 437-449.

Uchida, K., Moench, I., Tamkus, G., and Lopatin, A.N. (2016). Small membrane permeable molecules protect against osmotically-induced sealing of t-tubules in mouse ventricular myocytes. American journal of physiology Heart and circulatory physiology, ajpheart 00836 02015.

van Kats, J.P., Danser, A.H., van Meegen, J.R., Sassen, L.M., Verdouw, P.D., and Schalekamp, M.A. (1998). Angiotensin production by the heart: a quantitative study in pigs with the use of radiolabeled angiotensin infusions. Circulation *98*, 73-81.

Venturoli, D., and Rippe, B. (2005). Ficoll and dextran vs. globular proteins as probes for testing glomerular permselectivity: effects of molecular size, shape, charge, and deformability. Am J Physiol Renal Physiol *288*, F605-613.

Wagner, E., Lauterbach, M.A., Kohl, T., Westphal, V., Williams, G.S., Steinbrecher, J.H., Streich, J.H., Korff, B., Tuan, H.T., Hagen, B.*, et al.* (2012). Stimulated emission depletion live-cell super-resolution imaging shows proliferative remodeling of T-tubule membrane structures after myocardial infarction. Circ Res *111*, 402-414.

Wei, S., Guo, A., Chen, B., Kutschke, W., Xie, Y.P., Zimmerman, K., Weiss, R.M., Anderson, M.E., Cheng, H., and Song, L.S. (2010). T-tubule remodeling during transition from hypertrophy to heart failure. Circ Res *107*, 520-531.

Wong, J., Baddeley, D., Bushong, E.A., Yu, Z., Ellisman, M.H., Hoshijima, M., and Soeller, C. (2013). Nanoscale distribution of ryanodine receptors and caveolin-3 in mouse ventricular myocytes: dilation of t-tubules near junctions. Biophysical journal *104*, L22-24.

Wu, C.Y., Chen, B., Jiang, Y.P., Jia, Z., Martin, D.W., Liu, S., Entcheva, E., Song, L.S., and Lin, R.Z. (2014a). Calpain-dependent cleavage of junctophilin-2 and T-tubule remodeling in a mouse model of reversible heart failure. Journal of the American Heart Association *3: e000527*, 1-18.

Wu, C.Y., Chen, B., Jiang, Y.P., Jia, Z., Martin, D.W., Liu, S., Entcheva, E., Song, L.S., and Lin, R.Z. (2014b). Calpain-dependent cleavage of junctophilin-2 and T-tubule remodeling in a mouse model of reversible heart failure. Journal of the American Heart Association *3*, e000527.

Wu, C.Y., Jia, Z., Wang, W., Ballou, L.M., Jiang, Y.P., Chen, B., Mathias, R.T., Cohen, I.S., Song, L.S., Entcheva, E.*, et al.* (2011). PI3Ks maintain the structural integrity of T-tubules in cardiac myocytes. PloS one *6*, e24404.

Yamazaki, T., Komuro, I., Kudoh, S., Zou, Y., Shiojima, I., Hiroi, Y., Mizuno, T., Maemura, K., Kurihara, H., Aikawa, R.*, et al.* (1996). Endothelin-1 is involved in mechanical stress-induced cardiomyocyte hypertrophy. The Journal of biological chemistry *271*, 3221-3228.

Yao, A., Spitzer, K.W., Ito, N., Zaniboni, M., Lorell, B.H., and Barry, W.H. (1997). The restriction of diffusion of cations at the external surface of cardiac myocytes varies between species. Cell calcium *22*, 431-438.

Yeung, E.W., Balnave, C.D., Ballard, H.J., Bourreau, J.P., and Allen, D.G. (2002). Development of T-tubular vacuoles in eccentrically damaged mouse muscle fibres. The Journal of physiology *540*, 581-592.

Yu, Z.W., and Quinn, P.J. (1994). Dimethyl sulphoxide: a review of its applications in cell biology. Biosci Rep *14*, 259-281.

Zhang, C., Chen, B., Guo, A., Zhu, Y., Miller, J.D., Gao, S., Yuan, C., Kutschke, W., Zimmerman, K., Weiss, R.M.*, et al.* (2014). Microtubule-mediated defects in junctophilin-2 trafficking contribute to myocyte transverse-tubule remodeling and Ca2+ handling dysfunction in heart failure. Circulation *129*, 1742-1750.

Zhu, Y., Zhang, C., Chen, B., Chen, R., Guo, A., Hong, J., and Song, L.S. (2016). Cholesterol is required for maintaining T-tubule integrity and intercellular connections at intercalated discs in cardiomyocytes. Journal of molecular and cellular cardiology *97*, 204-212.